Heterogeneous internal fabric of the Mount Barcroft pluton, White Mountains, of eastern California: an anisotropy of magnetic susceptibility study

Karen J. Michelsen

Thesis submitted to the Faculty of Virginia Polytechnic Institute and State University in partial fulfillment of the requirements for the degree of

Master of Science

in

Geological Sciences

Committee
Richard D. Law, Chair
James A. Spotila
Allen F. Glazner
Sven S. Morgan

December 16, 2003

Blacksburg, Virginia

Keywords: anisotropy of magnetic susceptibility, heterogeneous magnetic fabric, Mount Barcroft pluton, northern White Mountains

Heterogeneous Internal Fabric of the Mount Barcroft Pluton, White Mountains, eastern California: an Anisotropy of Magnetic Susceptibility Study

Karen J. Michelsen

ABSTRACT

Anisotropy of magnetic susceptibility (AMS) have been used with great success for determining the internal structure and fabrics of Jurassic and Cretaceous plutons of felsic-intermediate compositions in the White-Inyo Range of eastern California. However, application of the AMS techniques to the Mount Barcroft pluton, located in the northern White Mountains, has yielded anomalous scalar and directional AMS data indicative of unprecedented heterogeneity on the meter-kilometer scale. The 165 Ma Mount Barcroft pluton is primarily of granodiorite composition and was intruded into the Barcroft Structural Break, a northeast striking, steeply dipping structure that juxtaposes Mesozoic metavolcanic rocks to the north against Proterozoic-Paleozoic metasedimentary rocks to the south.

Two oriented hand samples (A and B) were collected at each of 78 sites distributed on a 1 kilometer grid pattern across the 5 by 15 kilometer Mount Barcroft pluton and oriented cores were prepared from these hand samples for AMS analysis. Microstructure identification of single thin sections prepared for each sample site yielded primarily magmatic with minor solid-state structures. A highly heterogeneous distribution of scalar parameters (Km, P%, F%, L%, T) was documented both between sample sites and between the A and B cores at individual sites. The heterogeneity may be the result of complex mineral assemblages and the interaction between different magnetic mineral species ranging from single domain to pseudo-single domain to multidomain magnetite. More problematic are the directional parameters between A and B cores in orientation and fabric type (e.g. prolate and oblate susceptibility ellipsoids) which cannot be readily explained by a complex mineral assemblage. Different fabric types in A and B cores at individual sample sites could be the result of discrete, temporally unrelated, magma pulses of variable composition and viscosity. Heterogeneity of scalar and directional AMS parameters in the Mount Barcroft pluton, and its contrast with the homogeneous AMS signatures within similar age plutons to the south, may provide evidence for a previously unrecognized magma source beneath the northern White Mountains.

ACKNOWLEDGEMENTS

First of all I would like to thank my parents Barbara and Don Michelsen, without which this project would not have been completed. Their consistent support, in terms of providing finances, housing, kennel services, and in their capacity as cheerleaders and "motivators" have been the primary force behind the completion of this work.

Heartfelt thanks go to Rick Law as he put a tremendous amount of energy and time into this endeavor. His effort are certainly not limited to dealing with the tedium of running AMS samples in Toulouse, France, picking up the ball repeatedly, when I was ready to throw my hands up in defeat and forget the project entirely, and having faith that I could handle the rigors of the field work in a difficult/remote area…alone. Additionally, without Rick I never would have been introduced to the White Mountains, granites and the wonderful folks at WMRS. Thank you. I appreciate Allen Glazner's tutorial in the not so subtle science of contouring data. Brooks Hanson assisted in understanding the nature of the northern fault contact of the pluton. Having the opportunity to meet, rub elbows, and discuss the most puzzling Mount Barcroft pluton with the likes of Gary Ernst has been a delight. He truly is a great man and I am thankful to have had the opportunity to work with him. A great deal of thanks must go to Eric Ferre, who in the last year has provided me with gentle nudge towards an alternative perspective on the Mount Barcroft pluton AMS study and a plausible mechanism as to the cause of the problematic data set.

White Mountain Research Station, in a number of respects, provided me with the opportunity to make the acquaintance of a number of absolutely incredible individuals, co-workers and scientists. Cecil Patrick, the former head cook at WMRS, with a passion for natural history, good food, Airedales and baseball, introduced me to the landscape of the Barcroft in the winter 2000, was instrumental in landing me a job at the station and has become and remains a dear friend. Hat's off to you Cecil, in more ways than one! Other WMRS staff members (past and present) who provided friendship, support, comfort, conversation and laughter were the likes of Bird Bob, Will Stenzel, Dori Cann, Murray Clay, Kathy Anderson, Scotty Hetzler and Dave Trydahl. I particularly recognize Chris Kobyashi for schlepping 100's of kilos of my cached rocks up the final 2000-3000 feet to the range summit when I couldn't. Thanks to Chris Libby for his route finding and assistance sample collecting in the precipitous Perry Aiken Canyon. I still find it difficult to "scamper" with a forty-pound pack full of rocks, up steep slopes, at 11,000 feet in altitude, after a long day in the field. Discussions with the likes of Tim Welch and the residing, grand geologist, Dr. Clem Nelson concerning mapping and field relations in the northern Whites provided ample food for thought. The friendship and conversations concerning granodiorites, publishing, politics and life in general with Dr. Angela Jayko and Dr. Jen Wenner were inspirational and great fun.

Digit, my energetic, able-bodied field assistant (Australian Shepherd), was a constant companion while collecting samples on the remote, difficult terrain of the Mount Barcroft pluton. She provided a source of constant entertainment and diversion with her

antics of keeping the outcrops clear of marmots, attempts to extract rocks for fetching purposes, and production of "doggie angels" in the lingering snow fields. She definitely worked well in her capacity to ward off the mountain lions. We never saw a single one!

Paul Bartholomew and Rebecca Kavage-Adams, my GIS Jedi knights, helped immensely with learning just enough ArcView to get by for this project and bailed me out of numerous system crashes and laptop freak-outs. Hal Pendrak made a valiant effort to retrieve my final thesis draft when my laptop sent it off into oblivion, and was always very helpful when the Macs went down in the Structure lab. 6-packs of doughnuts and "beverages" always seemed like fair payment for services rendered.

Within the department, the assistance and wisdom of the "ladies" eased the navigation of the labyrinth of departmental and university paper work and protocol. Thanks to Connie Lowe, Mary McMurray, Linda Bland, Carolyn Williams and Ellen Mathena for always being there and positive.

Ed Robinson assisted with understanding the formation of epidote from magnetite and Ca rich plagioclase. Jim Craig helped with the initial identification of oxides in the Mount Barcroft pluton. Time at the microscope with Bob Tracey, Bill Henika and Victor Liogys greatly helped me with my petrography and mineral identification. Thanks to Ken Erikkson for simply listening.

Ports in the storm that allowed the space, quiet and place for the various stages of the writing phase of the project include: Camp Altamons, Joanne Underwood, Guy and Jean Hammond, my parent's sunroom, and the "bunker". Brian Cook, (fellow office mate) provided ample computer assistance and engaging conversations on a number of occasions. Through out the process Jeb Rawnsley, put me back together when things fell apart.

This project was funded by grants from the Va. Tech Geological Sciences Department David Wones award, Geological Society of America, White Mountain Research Station, and Sigma Xi.

I dedicate this work to my dad, Dr. Don Michelsen, who applauds my efforts; listens and provides support in times of defeat; but never accepts quitting as an option in the face of adversity.

TABLE OF CONTENTS

INTRODUCTION

The mechanisms by which plutons are emplaced into the upper levels of the crust have been the source of debate for decades. One of the avenues available for helping to determine the method of emplacement is to study the internal fabric of plutons. The orientation of the internal fabric of plutons is controlled by a variety of factors, including: 1) wall rock geometries, which may control the mode of initial pluton emplacement, 2) presence or absence of local feeder conduits as either linear or planar sources, 3) magma flow within the evolving pluton chamber, 4) deformation of solidified or more viscous magmas by forcible emplacement by younger magma pulses, and 5) overprinting by later stages of tectonic strain (Bouchez and Gleizes, 1995; Tobisch and Cruden, 1995; Saint Blanquat and Tikoff, 1997; Saint Blanquat et al., 2001). The anisotropy of magnetic susceptibility (AMS) technique has been used extensively as an efficient, effective way to map the microscopic internal fabric of plutons. The internal fabric is determined by calculating the magnitudes and orientations of the principal axes (k1, k2, k3) of the magnetic susceptibility ellipsoid, reflecting the iron-bearing minerals in the rock.

The White-Inyo Range of eastern California provides an excellent opportunity to study pluton emplacement methods. Many of the Jurassic and Cretaceous age plutons have well-constrained U/Pb dates. The White-Inyo Range is dominantly composed of a well-mapped sedimentary section of folded and faulted late Precambrian to lower Middle Cambrian and, locally, Mississippian rocks (Nelson, 1962; Nelson et al., 1991) in which the dominant regional shortening preceded pluton emplacement (Morgan and Law, 1988). Additionally, Cenozoic uplift and extreme topographic relief, results in excellent exposures of the plutons at various structural levels (Fig. 1). The past 15-25 years have seen extensive analysis and study of the wall rock petrology and internal fabric of the Jurassic and Cretaceous plutons in the White-Inyo Range.

Previous AMS work, in conjunction with wall rock, petrographic and microstructural analysis in the White-Inyo Range, has addressed the question of forcible versus passive emplacement. The Cretaceous Papoose Flat and Birch Creek plutons and the Jurassic Eureka

Valley-Joshua Flats-Beer Creek composite pluton provide examples of forcible emplacement (Morgan, 1998a; Saint Blanquat et al., 2001). Forcibly emplaced plutons are characterized by wall rock attenuation and most are discordant with the original structural orientation of the country rock; they also exhibit identifiable internal fabrics, and solid-state deformation. In contrast, the Late Jurassic Sage Hen Flat pluton provides an example of a cookie-cutter type of emplacement style that punched up through the country rock with little attenuation and metamorphism of the wall rocks (Nelson et al., 1991; Morgan, 1998a). The Jurassic, Santa Rita Flat pluton has been cited as an example of passive emplacement in a saddle reef structure (Vines, 1999; Vines and Law, 2000, 2001).

In the northern White Mountains, Mesozoic metavolcanic and metasedimentary rocks are juxtaposed against the Proterozoic-Paleozoic section, along a planar, subvertical, locally faulted and intruded discontinuity called the Barcroft Structural Break (Fig. 1). The Mount Barcroft pluton is significant as it discretely separates Mesozoic rocks, to the north, from the Proterozoic-Paleozoic section, to the south, and was the first pluton to be emplaced along the Barcroft Structural Break (Hanson, 1986a).

The purpose of this study was to analyze the Mount Barcroft pluton using AMS data and microstructural analysis to determine the internal fabric of the pluton. To a large extent, all the previous AMS studies in the White-Inyo Range are of plutons that exclusively intruded into folded Proterozoic-Paleozoic sedimentary rock, rather than between juxtaposed fault blocks. Initially, we hoped to ascertain the extent that the Barcroft Structural Break controlled emplacement of the Mount Barcroft pluton. Unfortunately, the AMS data has proven to be very heterogeneous, with unprecedented variation in scalar and directional parameters on the kilometer and meter scale. The lack of interpretable magnetic systematics is probably the result of a complex mineral content and interaction of different magnetite species. The anomalous results may be the result of the unique emplacement setting associated with the Barcroft Structural

Break, a magma source associated with the northern White Mountains, not been previously identified in the White-Inyo Range, or discrete, magma batch pulses during emplacement.

GEOLOGIC BACKGROUND

The White-Inyo Range lies in the transition zone between the Sierra Nevada and Basin and Range provinces. The White Mountains are located at the north end of the White-Inyo Range and are bounded to the west by Owens and Chalfant valleys, the range front being controlled by the Cenozoic Owens Valley fault (Stockli et al., 2003) and the Cretaceous White Mountain Shear Zone (Sullivan, 2003). To the east, the White Mountains are bounded by Fish Lake Valley, associated with the Furnace Creek fault. The White Mountains lie entirely within the westernmost jog of the 87Sr/86Sr = 0.706 line (Fig. 1b) which reflects the Precambrian continental basement edge at depth (Kistler and Peterman, 1983; Stevens and Greene, 1999).

The geology of the Mount Barcroft pluton and the northern White Mountains have been studied by numerous investigators (Emerson, 1966; Krauskopf, 1971; Crowder and Sheridan, 1972; Crowder et al., 1973; Hanson et al., 1987; Ernst and Hall, 1987; Bateman, 1992; Ernst et al., 1993; Nelson and Ernst, 1994; McKee and Conrad, 1996; Ernst, 1996; Ernst et al., 2002; Ernst et al, 2003). The northeast-trending Mount Barcroft pluton is an approximately 15 X 5 kilometer tabular plutonic body that cuts the north-northwest regional trend of the White-Inyo Range. The pluton is Jurassic (165 Ma) (Ernst et al., 2003) and varies in composition from granodiorite, gabbro/diorite, metadiorite to rare alaskite aplite. The pluton was emplaced at a depth of 10-12 kilometers at approximately 3 kbars pressure (Ernst et al., 1993; Ernst, 1996). Exposures of the Mount Barcroft pluton range from 4,900 feet in altitude (1,500 meters) to the west in Chalfant Valley, up to 13,000 feet (approximately 4,000 meters) at the crest of the White Mountain Range.

Proterozoic to Mesozoic history of the White-Inyo Range

Precambrian to Mississippian rocks of the White-Inyo Range were deposited in a passive margin setting along the western margin of the North American plate (Nelson et al., 1991). Starting in the Late Devonian to Early Mississippian, the Antler orogeny produced northeast

trending folds and associated cleavage (Sylvester and Babcock, 1975; Dunne et al., 1978; Stevens et al., 1997; Morgan and Law, 1998). During the Sonoman orogeny (Early Permian to Early Triassic) the large north to northwest-trending White Mountain and Inyo anticlines were formed. These large anticlines have been interpreted as thrust fault related ramp structures, possibly associated with the Last Chance Thrust system (Corbett et al., 1988; Morgan and Law, 1998). The Nevadan orogeny from Late Jurassic has been identified as the final major period of deformation. The East Sierra thrust system has also been included in this last episode of contraction and has been recognized along the western edge of the White Mountains southward to the Mojave Desert (Dunne et al., 1983; Walker et al., 1990; Dunne and Walker, 1993; Coleman et al., 2003).

Mesozoic magmatism began in the Late Triassic with subduction (Stevens et al., 1997) related to the Sonoman orogeny and the development of a magmatic arc. Extensive volcanism in a marine environment continued and occurred through the Jurassic and continued intermittently until Early Cretaceous time (Stevens et al., 1997). According to Dunne et al., (1998) volcanic eruption and deposition occurred at ca. 170 Ma and a less voluminous event occurred at around 148 Ma or earlier. Plutonism occurred in two distinct periods during Jurassic and Cretaceous times (Coleman et al., 2003).

Mesozoic history of the northern White Mountains

The geology of the northern White Mountains provides a unique record of events following the Sonoman orogeny. Evidence of bimodal volcanic rocks being deposited on top of, and contemporaneous with, carbonates of marine origin is present in the northern White Mountains. These rocks are assumed to be Late Triassic in age and were probably deposited nonconformably on the folded Proterozoic-Paleozoic section (Hanson, 1986a, b; Hanson et al., 1987). Problematic U/Pb zircon ages of 137 Ma and 154 Ma for a hypabyssal rock and an ash flow tuff, respectively, may be the result of entrainment of older zircons in Cretaceous magmas or

associated with the ~ 148 Ma volcanic event. Apparently, the problematic samples intrude and/or overlie the bimodal metavolcanic section (Hanson et al., 1987).

Faulting in the northern White Mountains probably resulted in the formation of several fault blocks and initial establishment of the Barcroft Structural Break. Faulting post-dated deposition of the Mesozoic volcanic rocks but predated Jurassic plutonism (Ernst et al, 2002). Down-dropped blocks may have provided accommodation space for deposition of sediments, volcanic rocks and hypabyssal material to the north of the Barcroft Structural Break.

The style of Jurassic plutonism throughout the White-Inyo Range was controlled in most cases, by emplacement of magmas into synclines within the Proterozoic-Paleozoic section for the Santa Rita, Eureka Valley-Joshua Flats-Beer Creek, and Cottonwood. However it remains unclear if this influenced the emplacement of the Jurassic plutons along the Barcroft Structural Break.

Hanson (1986a) and Hanson et al. (1986) identified two distinct periods of deformation which post-dated Jurassic plutonism and predated Cretaceous plutonism. The first period of deformation was east-directed thrusting, possibly associated with development of the East Sierra thrust system. The second period of deformation was associated with west-directed motion, resulting in westward-vergent folding of the Mesozoic metavolcanic and metasedimentary rocks, and transformation of the Barcroft Structural Break into a west directed high-angle reverse fault. Cretaceous plutonism in the northern White Mountains is indicated by: 1) intrusion of the Pellisier pluton, and resultant further doming the Mesozoic rocks to the north; 2) intrusion of smaller plutonic masses into the Barcroft Structural Break from the south and east; 3) final emplacement of the Boundary Peak pluton on both sides of the Break.

Upper Precambrian to Lower Cambrian strata

Bedded carbonate and siliciclastic rocks of the White-Inyo Range bound the Mount Barcroft pluton to the south. The rocks consist of conformable, mature, well-sorted cyclical

stable-margin sediments ranging in age from latest Precambrian to Early Cambrian (Nelson, 1962; Nelson et al., 1991; Stevens and Greene, 1999). These rocks are metamorphosed to greenschist facies, and deformed into open, north-south trending, gently north-, and south-plunging folds (Roubigou, 1986; Ernst, 1996).

Mid-Mesozoic metavolcanic and metasedimentary rocks

An approximately 3 kilometer thick pile of intercalated, bimodal metavolcanic, metavolcaniclastic and hypabyssal rock is exposed to the northwest of the Mount Barcroft pluton (Crowdcr and Sheridan, 1972; Dunne et al., 1978; Fates and Hanson, 1985, Hanson, 1986). These rocks generally dip west, with an apparent westward-vergent system of fold structures. The rocks are most strongly sheared in the west, south along strike, to the White Mountain Shear Zone and metamorphosed to greenschist facies.

Hanson (1986a) and Hanson and Fates (1987) described four major rock units within the Mesozoic age rock sequence. The oldest rocks crop out within the northeast section of the Mount Barcroft pluton as indicated on the Mount Barcroft geologic map (Krauskopf, 1971) and are marbles interbedded with felsic metavolcanic rocks. A ~2-3 kilometer thick pile of interbedded mafic andesite, to rhyodacite volcanics are intruded locally by the Mount Barcroft pluton. Hypabyssal rocks and an ash flow tuff with U/Pb zircon ages of 137 Ma and 154 Ma, respectively, intrude and overlie the metavolcanic section (Hanson et al., 1987). Metasedimentary, volcanogenic rocks, inclusive of the ash flow tuff and hypabyssal rocks that overlie the metavolcanic rocks were probably deposited during or following emplacement of the Mount Barcroft pluton (165 Ma).

The Inyo Mountain Volcanic Complex (Dunne and Walker, 1993; Dunne et al., 1998; Sorensen et al., 1998) is part of a widespread apron of volcaniclastic and volcanic arc units of Mesozoic age identified and mapped throughout east-central California. According to Dunne et al. (1998) two periods of volcanic eruption and deposition occurred at ca. 170 Ma and a less

voluminous event occurred at around 148 Ma. The Mesozoic metavolcanic and metasedimentary rocks to the north of the Barcroft Structural Break are considered to be the northern-most expression of the Inyo Mountain Volcanic Complex (Dunne and Walker, 1993; Dunne et al., 1998; Sorensen et al., 1998).

Timing of metamorphism

Jurassic and Cretaceous age intrusions are considered to have supplied the heat necessary for metamorphism of the country rocks to the north and south of the Barcroft Structural Break (Barton and Hanson, 1989; Dollase, 1994; Ernst, 1996). Contact metamorphism is retrograded to the south of the Barcroft Structural Break (Ernst, 1996). Contact metamorphism minerals generated in the wall rocks indicate maximum temperatures of 500°-600° C at pressures of 3 kbars at time of emplacement (Dollase, 1994; Ernst, 1996). The southern pluton margin is regionally metamorphosed to greenschist facies and contact metamorphism is to andalusite-sillmanite grade (Roubigou, 1984).

The andalusite isograd to the south parallels the Mount Barcroft pluton and then veers south to parallel the Cottonwood pluton (Ribigou, 1984) of Jurassic age, consistent with the highest regional metamorphic temperatures achieved in Jurassic time. It is doubtful that Cretaceous magmatism could have raised regional metamorphic temperatures back to the greenschist (~375-475° C) to epidote-amphibolite (475-525° C) facies within the Mount Barcroft pluton.

The northwest pluton margin is metamorphosed to hornblende-hornfels grade (450°C) up to 1 kilometer from the intrusion (i.e. greenschist-amphibolite transition) (Hanson, 1986a). To the north, retrograde recrystallization and advective metamorphic processes also occurred along with hydrothermal alteration. Hydrothermal alteration was the result of post-emplacement

deformational events associated with development of the White Mountain Shear Zone and alkali metasomatism resulting from final emplacement of the Pellisier granite (Hanson, 1986a).

Jurassic and Cretaceous age plutons

Granitoids ranging in composition from gabbro/diorite to granite invade the adjacent country rocks in the White-Inyo Range. Earlier geochronological studies distinguished between Jurassic and Cretaceous plutons in both the White-Inyo and Sierra Nevada Mountains (Curtis et al., 1958; Kistler et al., 1965*)*. Recent high-resolution U/Pb geochronological studies in the White-Inyo and the central Sierra Nevada (Ratajeski et al., 2001; Coleman et al., 2003) have more tightly resolved the magmatic periods of Mesozoic plutonism into two discrete periods during the Late Jurassic ca. 180-165 Ma and Early Cretaceous ca. 102-86 Ma (Coleman et al., 2003).

The Late Jurassic period of plutonism in the White-Inyo Range spans the period from 180-165 Ma. The oldest composite Jurassic age pluton is the Eureka Valley-Joshua Flats-Beer Creek pluton with U/Pb zircon ages including: Eureka Valley- 179-180 Ma (Gillespie, 1979); Beer Creek – 179 Ma (Coleman et al., 2003); Joshua Flats – 160-175 Ma (Gillespie, 1979). Intrusion continued with Sage Hen Flat at 175 Ma (Coleman et al., 2003), Cottonwood 168-172 Ma (Stern et al., 1981) and Redding Canyon at 164 ± 5 Ma (Coleman et al., 2003). The Mount Barcroft pluton is dated at 165 Ma (Ernst et al., 2003). The Santa Rita Flat pluton in the Inyo Mountains (Fig. 1) is dated at 164 Ma (Chen, 1977). This restricts the potential Jurassic age pluton without U/Pb dates in the White Mountains to the Cabin Creek and Indian Garden plutons.

Many of the Jurassic age plutons in the White-Inyo Range were emplaced into Proterozoic-Paleozoic sedimentary rock synclines (Krauskopf, 1965, 1971; Nelson et al., 1991; Morgan, 1998a; Vines, 1999; Vines and Law, 2000). Specific to the Mount Barcroft pluton, Krauskopf (1965, 1971) contends that the assumed eastern extension of the pluton was clearly

intruded into a syncline, although it remains unclear if this is the case for the Mount Barcroft pluton in general.

Early Cretaceous McAfee Creek pluton dated 102-86 Ma (U/Pb) (Hanson, 1986a), cross-cut the Mount Barcroft pluton to the east and intrude into the Barcroft Structural Break. The Pellisier Flat pluton, dated at 82-100 Ma (U/Pb) (Stern et al., 1981) intruded into the folded and faulted Mesozoic section. The Boundary Peak pluton, has a mis-reported U/Pb of 72 Ma by McKee and Conrad (1996) referenced to Crowdcr et al. (1973). However, dates attained by Crowder et al., (1973) were originally based on K/Ar dating of biotite, not U/Pb. Nonetheless, the Boundary Peak pluton is considered younger than the Pellisier Flat pluton due to cross-cutting relationships. The Leidy Creek pluton, of assumed Cretaceous age, also intrudes the metavolcanics and the Barcroft Structural Break, but so far is undated.

Barcroft Structural Break

The Barcroft Structural Break juxtaposes mid-Mesozoic metavolcanic and metasedimentary rocks to the north, against the uppermost Proterozoic to lowermost Paleozoic carbonate and siliciclastic metasedimentary platform rocks to the south. The Break is intruded by Jurassic and Cretaceous age plutons or locally faulted. The Barcroft Structural Break has been interpreted as a thrust fault with 7 kilometers of throw, with the Mesozoic rocks to the north being exposed as a window beneath the Proterozoic to lower Paleozoic section (Crowder and Ross, 1972; Stevens and Olson, 1972; Dunne et al., 1978). Alternatively, the structural break has been described as a northern extension of the Last Chance thrust fault hypothesized to underlie most of the pre-Mesozoic rocks in the White-Inyo Range (Stewart et al., 1966). Finally, McKee et al. (1982) and Diggles et al. (1983) proposed that the Mesozoic rocks are allochthonous and have been juxtaposed against the Proterozoic-Paleozoic sections by faulting.

Pluton geometry

The Mount Barcroft pluton is large and tabular, with east-northeast-trending margins that are predominantly vertical to southeast-dipping (see Ernst et al., 2003). The northwest and southeast margins are intrusive, with narrow contact aureoles and are locally reverse faulted. The northwest margin is partially defined by the Barcroft and Sabies faults (Hanson, 1986a). The long-axis of the Mount Barcroft pluton trends east-northeast, at right angles to the north-northwest structural trend of the White-Inyo Range. Structural contour mapping by Ernst et al. (2003, their Fig. 3), indicates that the northwest and southeast margins dip steeply to the southeast. The northeast margin of the Mount Barcroft pluton is cut by the Cretaceous (100 Ma – U/Pb) McAfee pluton (Hanson, 1986a). Cenozoic alluvial cover obscures the west pluton margin.

Possible pluton emplacement models

Given the geometry, orientation, and probable emplacement location along a fault, a number of emplacement models may be applicable. Earlier investigators considered the Barcroft Structural Break to be a steep reverse fault. However, Andersonian mechanics require that reverse faults rarely achieve dips greater than 35°. Steeper dips can be achieved in reverse faults if pore fluid pressures are high, and differential stresses are low (Sibson, 1985), which could be caused by repeated magma injections at the time of emplacement, coincident with fault motion.

A second hypothesis involves normal, strike-slip or combination wrench style motion. Andersonian mechanics require that normal dip-slip faults dip at approximately 60° whereas, strike-slip faults are vertical to sub-vertical. Given that the existing pluton margins are very steep to vertical, and that this steep orientation continues to the northeast along the Barcroft Structural Break, it seems unlikely that a pre-existing thrust fault could have initially formed the Break unless faulting occurred coincident with Jurassic plutonism. Further support for a normal, strike-

slip or wrench style fault origin for the Break, is evidenced on USGS geological maps; whereby the northern White Mountains are composed of three distinct, crustal blocks (Krauskopf, 1971; Crowder and Sheridan, 1972; Crowder et al., 1972; Robinson and Crowder, 1973) which formed prior to or during Jurassic plutonism (see later discussion).

The Mount Barcroft pluton is not visibly, texturally or petrographically zoned and with few exceptions, lacks a macroscopic foliation. Pluton wall geometry, lack of visible fabric or zonation, and local field relationships support a pre-existing normal, strike-slip or wrench type faulting scenario prior to emplacement. The Barcroft Structural Break probably was formed prior to Jurassic plutonism and provided a conduit for magma to move into the upper crust.

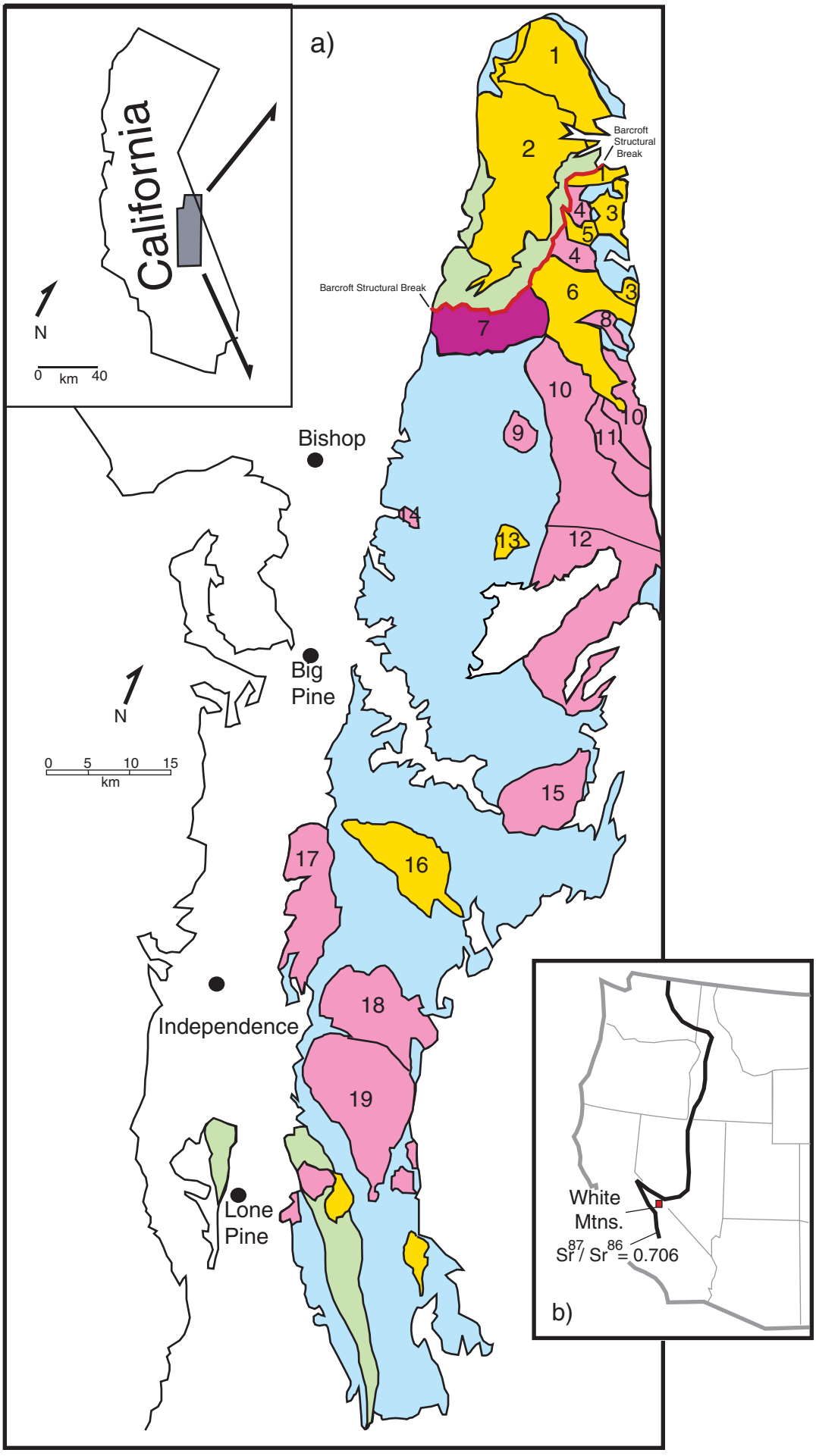

Figure 1: a) Regional Map (adapted from Dunne et al., 1978); b) Sr 0.706 line (adapted from Ernst et al, 2003)

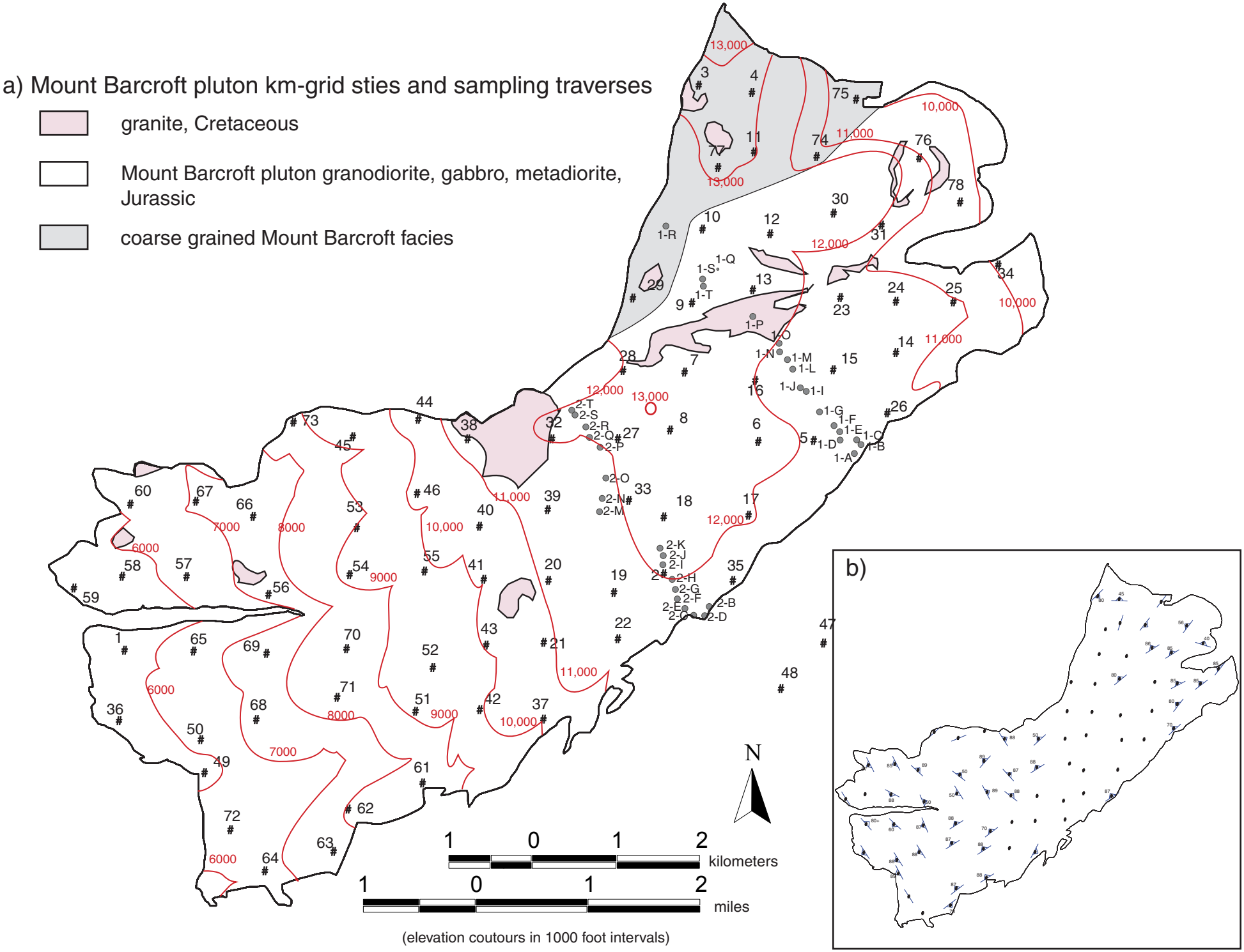

Figure 2 - Mount Barcroft pluton: a) sample and traverse sites and rock types; b) macroscopic foliation

MACROSCOPIC STRUCTURES WITHIN THE PLUTON

Equigranular and medium grained crystals generally characterize rocks of the Mount Barcroft pluton. Toward the northern part of the pluton, a distinctive coarse-grained fabric is mapped (Fig. 2a). The pluton generally does not display macroscopic lineation, although foliation of variable strength is locally visible (Fig. 2b). Macroscopic foliation tends is visible along the immediate northwest and southeast pluton margins and the east and west portions of the pluton (Fig. 2b). Foliation is most obvious on vertical joint faces and is defined by alignment of hornblende, biotite and other mafic minerals. Foliation of the coarser-grained facies located in the northern part of the pluton is most clearly expressed by alignment of the plagioclase laths together with mafic silicate and opaque minerals. In contrast, the obvious macroscopic fabric in the western part of the pluton (near the Chalfant Valley floor) is due to pervasive vertical-subvertical brittle faulting along the range front.

Within the western part of the pluton, a number of magmatic mixing zones, corresponding to lower relief topography, like staircase treads, were identified. These zones strike ~150°, are vertical to subvertical, approximately 100 meters wide, and at assumed deeper structural levels within the pluton. Magmatic mixing zones are characterized by apparently swirled felsic and mafic magmas mixed to varying degrees. Dikes of felsic granitoids, quartz and fine-grained mafic rock, both planar and folded, are common. These magmatic mixing zones seem to be similar to the Barcroft border facies described by Hanson (1986a) and migmatites mapped along the northwestern pluton margin by Crowder and Ross (1972).

PETROLOGY

The Mount Barcroft pluton has been the subject of a number of petrological studies (Emerson, 1966; Crowder and Ross, 1973; Ernst et al., 2002, 2003). Commonly the pluton composition has been classified as granodiorite because of its medium gray coloration, high mafic mineral concentration, and bluish-gray quartz and feldspar (Emerson, 1966). The dark silicate minerals occur as distinct aggregates or clots. The pluton is quartz-poor, and has a high percentage of K-feldspar for rocks of such dark coloration (Crowder and Ross, 1973). Grain size ranges from coarse-grained (4 mm) to fine-grained (1 mm). The pluton is calcalkaline, with ferromagnesian hornblende and clinopyroxene. Ernst et al. (2003) have subdivided the rocks of the pluton into a system referred to as the Mount Barcroft Pluton Intrusive Series. Rock types are designated by their commonly used names ranging from granodiorite, gabbro/diorite, metadiorite to rare alaskite aplite. According to the Stiekensen (1976) classification, the Mount Barcroft granodiorites range from quartz-poor granodiorites to quartz and feldspar poor granites; gabbro/diorites are classified as quartz monzodiorite, quartz diorite, and quartz gabbro; metadiorites are quartz diorites. Rocks of the Mount Barcroft Intrusive Suite are considered members of a broadly varying, mineralogically diverse magmatic continuum resulting from fractional crystallization (Ernst et al., 2003). The Mount Barcroft pluton is not zoned, but is chemically and mineralogically heterogeneous, with lateral variations probably reflecting continuous magma batch injections during emplacement (Ernst et al., 2003). Also present within the Mount Barcroft plutonic complex are small, scattered intrusive bodies of granite of assumed Cretaceous age (McAfee Creek granite), and Tertiary, fine-grained, unmetamorphosed, diabase dikes (Ernst et al., 2002), which are not considered in this study.

Constituent minerals

Silicate minerals tend to be Ca-rich and have variable ferromagnesian and titanium contents. Orthoclase is the primary K-feldspar, whereas plagioclase ranges from sodic albite to

calcic andesine. Clinopyroxenes are diopside-hedenbergite to sub-calcic and have various concentrations of ferromagnesisan and titanium (Ernst et al., 2002). Clino-amphiboles are calcic and lie along a continuum from igneous hornblende to actinolite (Ernst, 2002). Clinoamphibole series members in the magmatic suite probably crystallized semi-continuously from early magmatic to late magmatic stages, through a post-consolidation deuteric-hydrothermal-metamorphic stage. Epidote is ubiquitous, and appears to have crystallized across the pluton at subsolidus temperatures. Biotites are enriched in iron, magnesian, and titanium. Most biotites contain exosolution lamellae of magnetite-ilmenite and/or titanite. White mica is rare in the Mount Barcroft pluton. Chlorite is ferromagnesian-enriched in both granodiorites and metadiorites. Mg-chlorite is present in the gabbro/diorites. Titanite is present across the pluton in all phases and iron oxides consist of magnetite and coexisting ilmenite (Ernst et al, 2002). Tourmaline is present as an accessory phase and is locally abundant (Emerson, 1966: Ernst et al., 2002).

MICROSTRUCTURES WITHIN THE PLUTON

Microstructural analysis of thin sections was carried out to determine the extent of the magmatic to solid-state deformation fabrics within the Mount Barcroft pluton. Microstructural analysis was used in conjunction with anisotropy of magnetic susceptibility to ascertain if fabrics were locked in during the magmatic phase of emplacement or if the fabric was produced in a later solid-state deformation.

Two (labeled A and B) oriented hand samples from each site (78 sites total) were collected on a 1 kilometer grid (Fig. 2a). One of the two samples was selected and prepared for thin section analysis. In addition, two sampling transects perpendicular to the long axis of the pluton from southern pluton margin to northern margin (approximately twenty sites per traverse) were also made, collecting one sample per site (Transects 1 and 2) (Fig. 2a). Samples on the two transects were not oriented inasmuch as they were employed exclusively for identification of microstructures present. Presence or absence of specific microstructures was recorded and their domainal distribution mapped out across the pluton.

Microstructures were mapped based on the presence or absence of the structure in thin section; minerals analyzed included feldspar, plagioclase and quartz. The microstructures are primarily magmatic in origin although, solid-state deformation overprinting to varying degrees occurs across the pluton. Thin sections, for the most part exhibit magmatic structure lacking a grain shape fabric or imbrication. Individual mineral grains exhibit evidence of varying degrees of strain typically associated with intracrystalline plasticity.

The highest temperature solid-state microstructures (>550-500° C) are recorded by the presence of recrystallized quartz and feldspar, and chessboard pattern of extinction in quartz grains. Recrystallized quartz and feldspar is intermittently distributed along the pluton margins and chessboard quartz is ubiquitously recorded across the pluton (Fig. 3a and 3d).

Medium temperature solid-state deformation is recorded by the distribution of myrmekite and lobate boundaries between quartz and feldspar (400-550°C) (Simpson and Wintsch, 1989).

Myrmekite is present across the pluton with the exception of the west and northwest part of the pluton (Fig. 3b). Lobate boundaries of quartz and feldspar produced by grain boundary migration are present in rocks along the northwest margin of the pluton (Fig. 3c).

Indications of low temperature solid-state deformation (300-400°C) include kinking of feldspar and undulose extinction in quartz (Passchier and Trouw, 1996). Kinked feldspar grains (Fig. 4d) are localized along the southwest, northwest and north-northwest boundaries of the pluton with a band cutting across the middle of the pluton. Quartz undulose extinction is present in all thin sections (Fig. 4c).

Brittle deformation at temperatures > 300°C (Passchier and Trouw, 1996) is indicated by intracrystalline microfracturing of feldspar and quartz. Microfractures in feldspars are ubiquitous across the Mount Barcroft pluton (Fig. 4b) and are rarely infilled with secondary quartz, chlorite or epidote. Microfractures in quartz (Fig. 4a) occur in non-systematic zones originating along the northwest and southeast margins of the pluton, and extending into the pluton interior. Most of the microstructures developed during cooling of the pluton through the solidus, as opposed to reheating during intrusion of adjacent Cretaceous age plutons.

Possible exceptions to this pattern are localized along the contact with the McAfee Creek pluton (Fig. 1) and also associated with small felsic intrusions within the Mount Barcroft pluton (Fig. 2a). Specifically, the high to medium temperature solid-state microstructures that may have formed at this time include recrystallized quartz and feldspar along the northeast contact with the later McAfee Creek pluton (Fig. 3d) and domains of the lobate quartz and feldspar (Fig. 3c) possibly formed in association with Cretaceous intrusions within the Mount Barcroft pluton.

Mineral alteration

Domainal variations in degree of feldspar alteration in Figure 5a. Alteration is apparent in all thin sections. Inspection of thin sections (one thin section for each site) for degree of

alteration inclusive of all feldspars was carried out at each sample site and alteration rated from high (>75%) to moderate (75% -25%) to low (<25%) (Fig.5a).

A high degree of alteration was identified in the Ca-rich plagioclase grains where large, felt-like mats of epidote with some zoisite occur within the original mineral, whereas plagioclase rims are less altered. A moderate degree of alteration is characterized by alteration of Ca-plagioclase and feldspar along grain margins and along cracks within the grains, with formation of epidote, zoisite, and locally muscovite and sericite. Minor degree of alteration of feldspar is characterized by alteration of feldspar around grain edges and along microfractures within the original mineral. The greatest degree of alteration is readily apparent along the western portion of the pluton (Fig. 5a). Moderate alteration is defined by three distinct zones, oriented approximately perpendicular to the long axis of the pluton. The least altered feldspars are distributed within a large zone in the northeast-central part of the pluton that cuts across the pluton.

Alteration due to deuteric processes is indicated by the development of epidote from Ca-rich plagioclase, actinolite from hornblende and augite, and muscovite and chlorite from biotite (Ernst et al., 2003). Most of this alteration probably occurred during the initial cooling phases at subsolidus temperatures ~ 545-395° C (Ernst et al., 2003), consistent with progressive development of the solid-state microstructures.

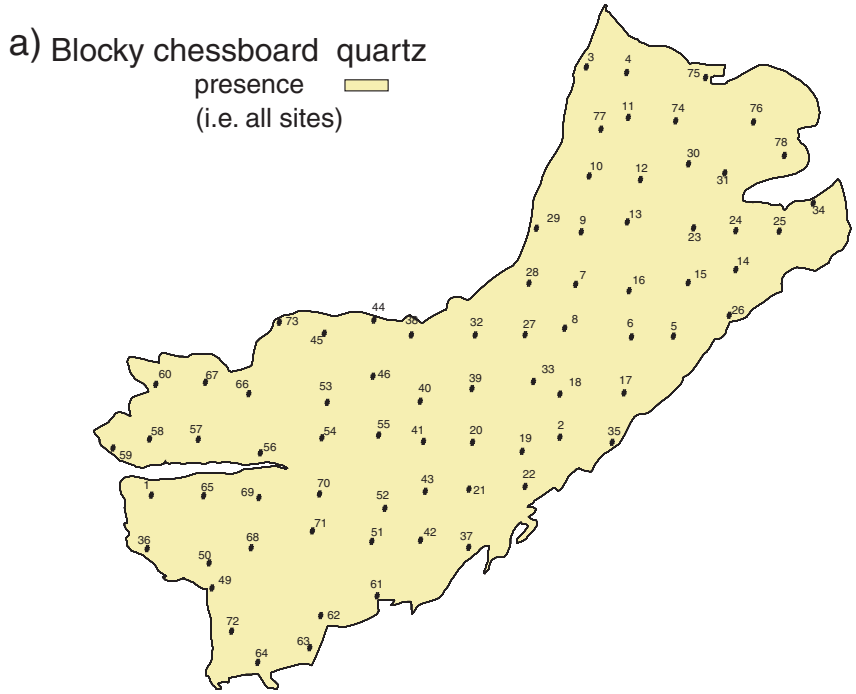

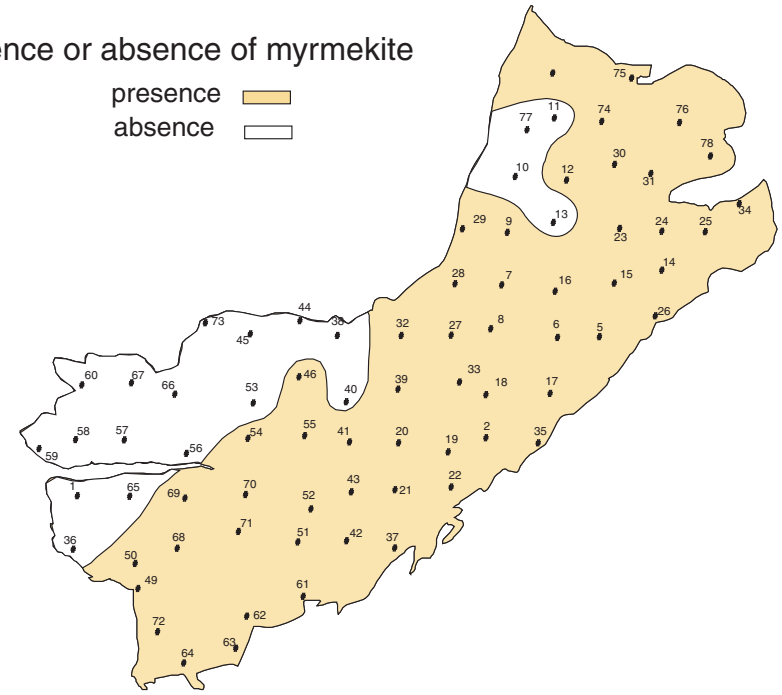

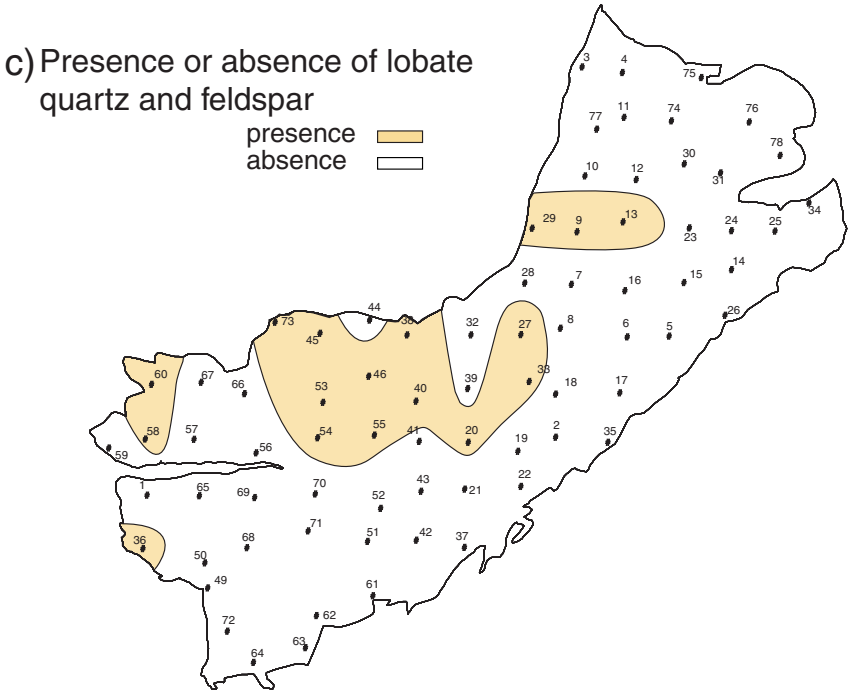

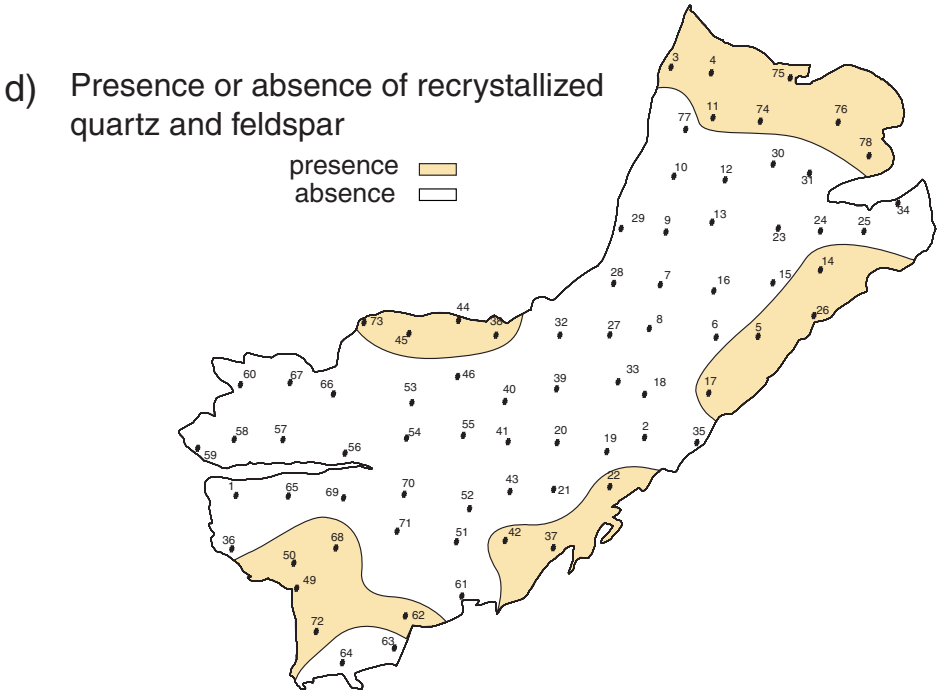

Figure 3: Microstructure distribution maps (high temperature)

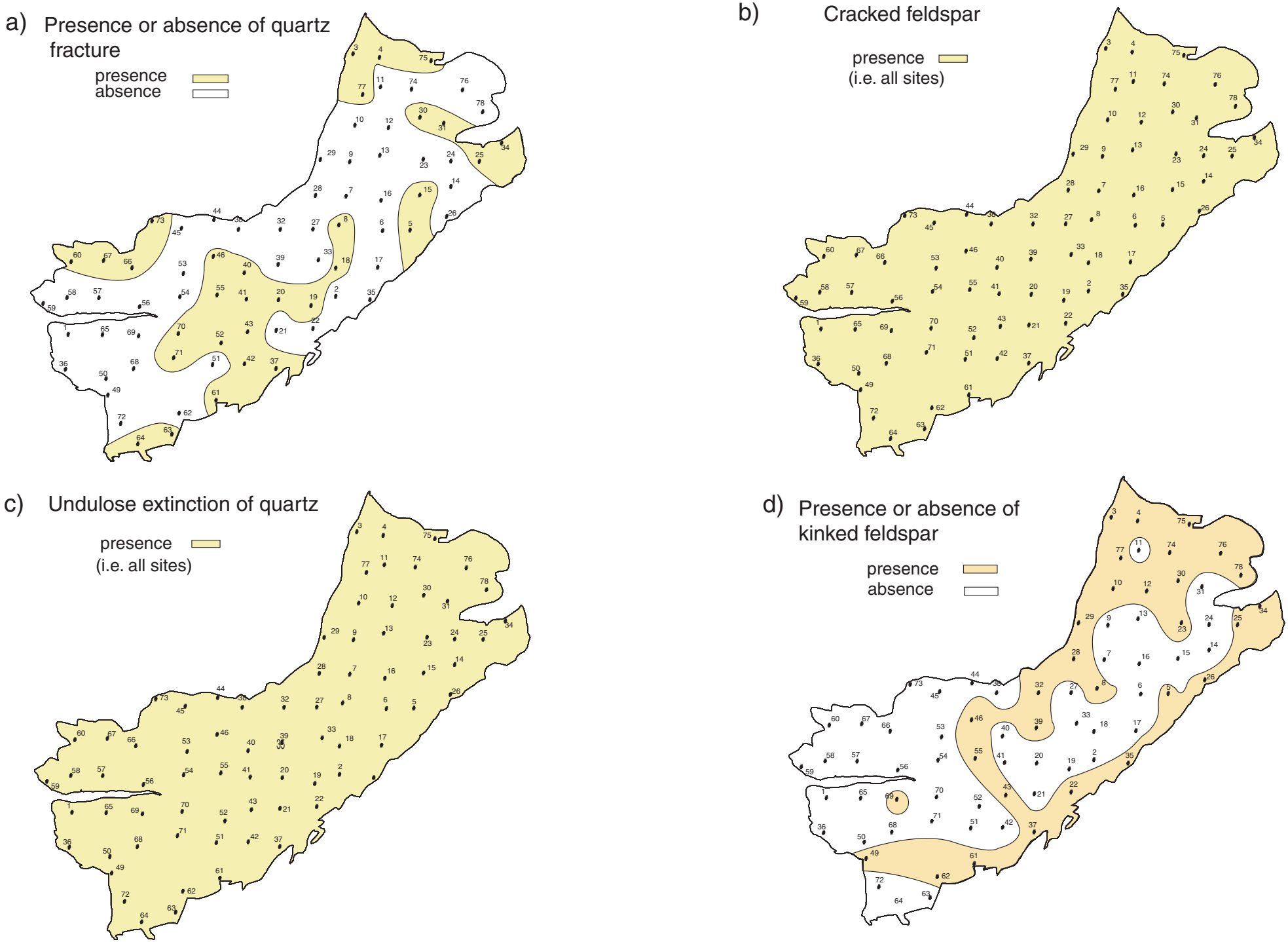

Figure 4: Microstructure distribution maps (low temperature)

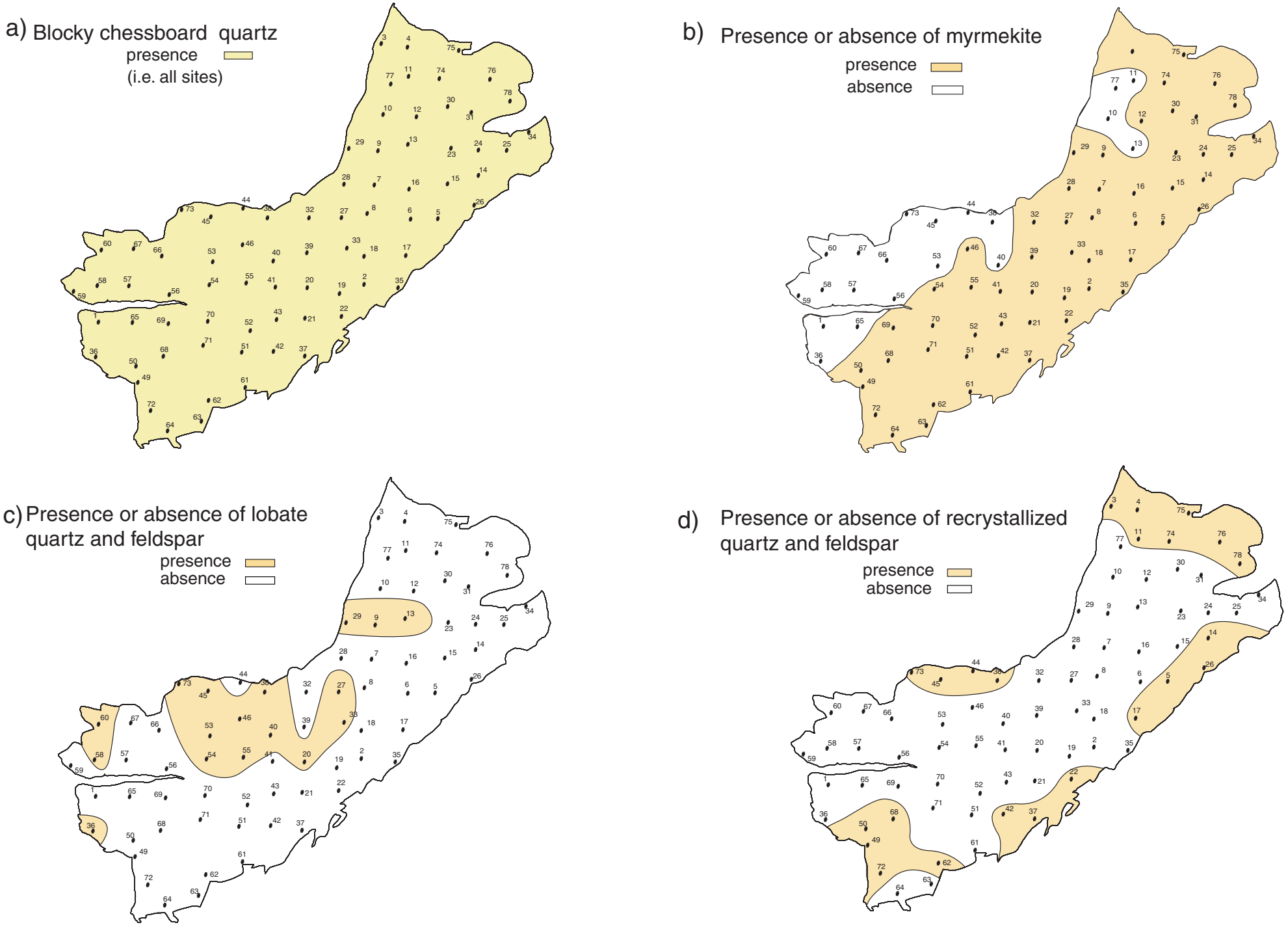

Figure 4: Microstructure distribution maps (high temperature)

OPAQUE MINERALS

Various oxide minerals have been identified in previous studies of the Mount Barcroft pluton. The majority of the pluton is characterized by 1-2% of interstitial opaques associated with mafic silicates (Emerson, 1966). Ernst (2002) identified magnetite and coexisting ilmenite. Unfortunately, no systematic reflective light studies have been conducted to determine the oxides present, their relative concentrations and spatial distribution within the pluton. Additionally, no analysis of the magnetite has been undertaken to ascertain the types present (single, pseudo-single, or multidomain) and their relative concentrations and distribution. Preliminary reflected light observation indicates that magnetite, ilmenite, various titanium oxides and minor hematite are present (J. Craig, personal communication, 7/2002).

Opaque minerals were analyzed in thin section and different grain shape types were distinguished based on their concentration and distribution (isolated versus interstitial of individual crystals. The domainal distribution of grain shape opaque mineral types are shown in Figure 5b. Generally, opaque minerals within the Mount Barcroft pluton occur as interstitial opaques associated with mafic silicates. Low concentrations of the interstitial opaques are sparsely distributed across the eastern and western parts of the pluton, typically along the pluton margins. High concentrations of small, individual opaque mineral grains are located in the western part of the pluton. High concentrations of small individual opaque mineral grains are limited to four sites in the west-central part of the pluton (Fig. 5b).

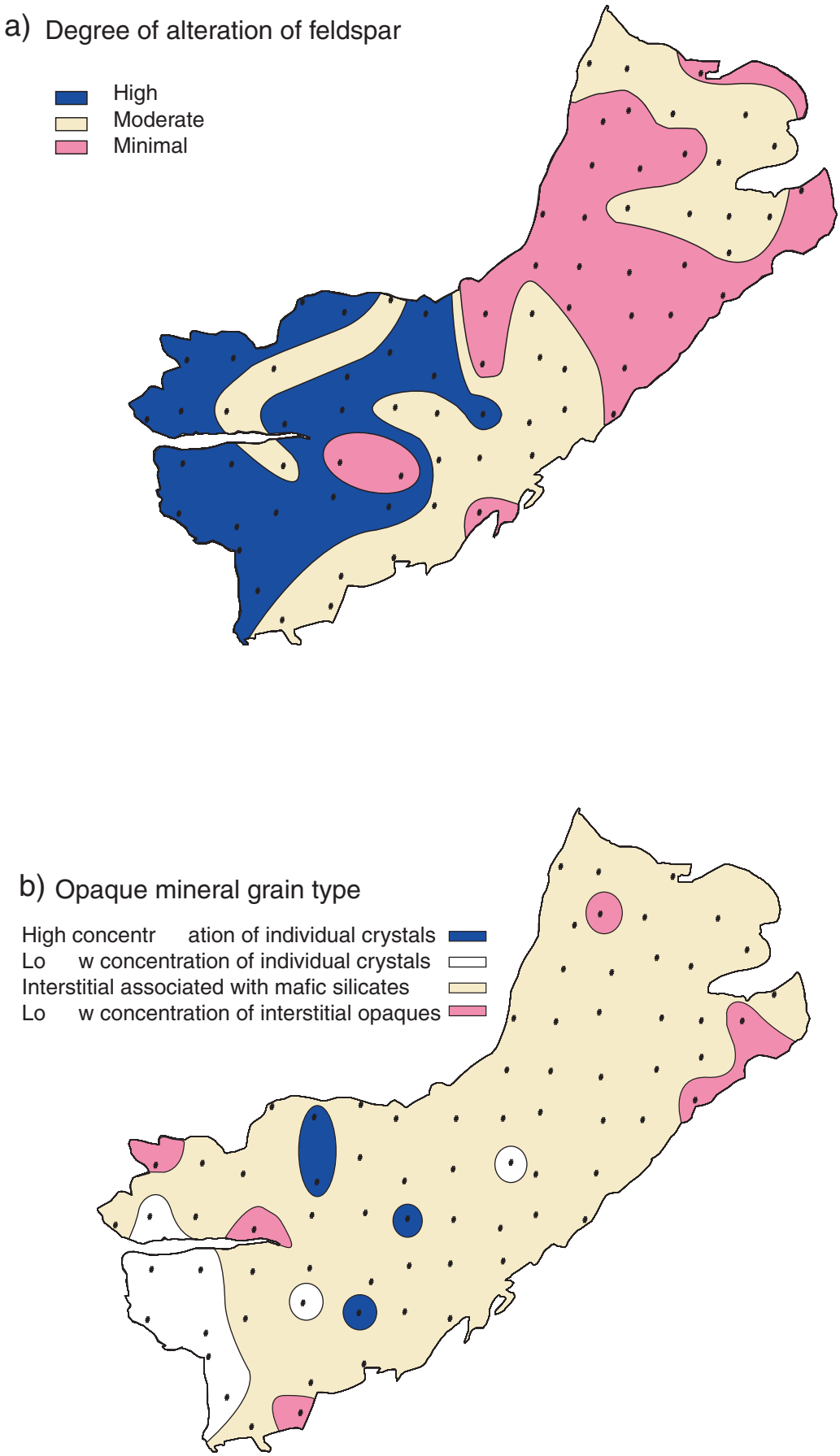

Figure 5: Distribution maps: a) degree of feldspar alteration; b) opaque mineral grain type

ANISOTROPY OF MAGNETIC SUSCEPTIBILITY – ANALYTICAL METHODS AND DATA PRESENTATION

Anisotropy of magnetic susceptibility (AMS), a low-field magnetic fabric measure provides a rapid quantitative description of the crystalline fabric in rocks. AMS is helpful in determining the bulk internal structure of plutons, where macroscopically observed foliation and lineation are weak or absent. Typically, most AMS studies find a strong parallelism between visible grain shape and magnetic fabrics. Relationships between grain shape and magnetic fabric of the rock depends on the nature of the iron-bearing minerals and on the textural relationships between mineral grains (Rochette, 1987; Jover et al., 1989; Borradaile, 1991).

Paramagnetic and ferromagnetic iron-bearing minerals are primarily responsible for the magnetic signal (see review by Bouchez, 1997). Paramagnetic minerals, typically the matrix minerals, are iron-bearing silicates and have a slightly positive magnetic susceptibility (Rochette, 1987). Ferromagnetic minerals have a stronger positive magnetic susceptibility, the primary mineral being magnetite. Magnetite, depending on grain size, may be single-domain, pseudo-single domain or multidomain, and this domainal nature will affect the AMS intensity and direction (Rochette et al., 1992).

Analytical methods

Two oriented granodiorite hand samples (referred to as A and B) were collected at each of the 78 sites located on a 1 kilometer grid pattern with good coverage across the pluton (Fig. 2). Two of these sample sites are from satellites of the Mount Barcroft intrusion, cropping out to the south, outside the main body of the pluton (sites 47 and 48). The data from these two sites were included in consideration of the overall pluton scalar data, but excluded from contouring and directional data analysis. The oriented samples were machine cored in the Department of Mining and Minerals Engineering at Virginia Tech, and each of the 1 inch diameter cores (~2.5 cm) was then oriented in the lab. Oriented cores were cut into 2.2 cm length sections, and the cut surfaces

hand polished to remove any metallic material from the rock saw. An average of 8 core sections were produced for each site. Anisotropy of magnetic susceptibility for all 655 oriented core sections was measured at the Laboratoire de Petrophisique et Tectonique, Universite Paul-Sabatier, by Dr. R. D. Law, using a kappa-bridge KLY-2, manufactured by Agico (Brno, Czech Republic). Fifteen measurements from each core section were taken in different orientations, and the orientation magnitude of the three principle axes of the AMS ellipsoid, k1, k2, k3, for each sample were calculated from the bulk susceptibility data (Km) and orientation of the sample using the ANISOFT package of Jelinek (1981). The working data for each site were computed from the tensor means of the sample data with the programs EXAMS (Saint Blanquat, 1993) giving the bulk magnetic susceptibility magnitude of the site, the orientation and intensity of the three main susceptibility axes k1, k2, k3, and the usual intensity (P%, F%, L%) and shape (T) parameters. Directional data were automatically plotted on equal area stereonets using the EXAMS program. Contoured maps of the magnetic data were produced at Virginia Tech using the ArcView software package using both spline and polynomial functions (3^{rd} and 4^{th} order).

The three axes of the susceptibility ellipsoid $k_{max}>k_{int}>k_{min}$ (k1, k2, k3) are the components of the magnetic parameters discussed below.

$1/3(k1+k2+k3) = Km$, average bulk susceptibility (10^{-3} SI)

$k1/k3 \times 100 = P\%$, percentage of total anisotropy

$k1/k2 \times 100 = L\%$, percentage of linear anisotropy

$k2/k3 \times 100 = F\%$, percentage of foliated anisotropy

$2[(\ln k2 - \ln k3)/(\ln k1 - \ln k3)] - 1 = T$, shape parameter

Magnetic foliation was obtained by determining the orientation of the plane that contains the k1 and k2 axes, and the magnetic lineation is parallel to the k1 axes. Values of scalar magnetic parameters, Km, P%, L%, F%, T, and the orientation data magnetic foliation and lineation for each of the sampled core sections, as well as statistical of the data on each core are summarized in Appendix 1. Values of Km, P%, L%, F%, T and the orientation of the foliation

and lineation averages for each of the 78 sites, as well as the statistical data for each site, are summarized in Appendix 2. Stereograms containing the orientation of k1, k2, k3 for each sample at individual sites can be found in Appendix 3.

A geographic database including the pluton boundary and location of sample sites was created in ArcView. The pluton boundary, based on Ernst et al. (2002) was hand drawn on USGS 7 ½ minute topographic map quadrangle sheets Mount Barcroft, White Mountain Peak and Juniper Flats. Sample sites were located on quadrangle maps during fieldwork. Composite USGS topographic maps with pluton boundary and sample sites were digitized and then brought into ArcView.

Histograms of magnetic scalar data (Km, P%, F%, L% and T) for each of the A an B core sections, at the 78 sites were plotted as bar diagrams. Contour maps of average values at each site for magnetic scalar parameters (Km, P%, F%, L%, and T) and directional foliation dip and lineation plunge were created using spline and 3rd order polynomial functions in ArcView.

Measurements of variation between the two samples (A and B cores) at each site for magnetic parameters (Km, P%, F%, L%, T, foliation dip, lineation plunge) were based on the difference between calculated averages of separate core sections from the A and B hand samples at each site. The degrees of variation between the A and B cores at each site were then also contoured using the program ArcView software package using spline and 4th order polynomial functions.

Spline versus polynomial contour functions

Both spline and polynomial 3rd and 4th order functions were used to contour individual magnetic parameters over the pluton. These two processes highlight very different trends in the data. The spline function is useful for identifying the degree of heterogeneity and variation between and among sites. The polynomial function illuminates general trends, downplaying the differences between adjacent sites (Burrough and McDonnell, 1998; Wechsler, 2000).

The spline function is a method of interpolation that fits a minimum curvature contour or surface, for values at sample sites, forcing it through each data point. Splines retain small-scale features and can be used as long as measurement errors are small. The polynomial function was used for fitting general trends to the data. The final surface is smooth but does not necessarily contour by going through values at sample sites. As the degree of polynomial function increases, the surface becomes more complex but may not generate an accurate surface (Burrough and McDonnell, 1998; Wechsler, 2000). For the Mount Barcroft pluton, 3^{rd} order polynomials were used to contour average values for magnetic parameters among the sites. Similarly, 4^{th} order polynomial functions were used to contour for variation of magnetic parameters of A and B core within sites.

Magnetic susceptibility (Km)

Typically susceptibility (Km) in ferromagnetic rocks is a measure of how much magnetite is present. Susceptibility values from the Mount Barcroft pluton range from a maximum 67.26×10^{-3} SI to a minimum of 0.14×10^{-3} SI with an average of 16.82×10^{-3} SI (Fig. 6a). These numbers are generally higher than most Km values for both Jurassic and Cretaceous plutons in the White-Inyo Range (Vines, 1999; Saint Blanquat, et al., 2001). The exception to this is the visibly petrographically zoned Eureka Valley-Joshua Flats-Beer Creek pluton, which has higher Km values over the more mafic facies (Morgan, 1998a).

Paramagnetic granites (magnetite-free granites) have a bulk susceptibility magnitude typically below 500×10^{-6} SI (0.5×10^{-3} SI) (Bouchez, 1997). The Mount Barcroft pluton has 59 core sections out of 655 total sections (9%) that have Km measurements in the paramagnetic range. Ferromagnetic granites that contain magnetite, tend to have susceptibility measurements three orders of magnitude larger than those for paramagnetic, biotite-containing granites (Bouchez, 1997). Magnetic susceptibilities of granitoids overall are bimodal, reflecting the

distribution of granites into a magnetite-series (ferromagnetic) and ilmenite-series (paramagnetic) (Ishihara, 1977).

The susceptibility histogram for the Mount Barcroft pluton is weakly bimodal with an isolated spike at 0-5.0 x 10^{-3} SI and a second, broad peak culminating at 15-20 x 10^{-3} SI (Fig. 6a). This bimodal distribution may, in part, be the result of the contribution of paramagnetic minerals to the low Km value spike.

Susceptibility is highly variable both across the pluton on the kilometer scale and within sites between A and B cores on the meter scale. Susceptibility, in general, is lower in the western part of the pluton and along the southeast margin. The spline contoured average location values, ranging from 0.2 – 64.48 x 10^{-3} SI, identify a number of sites and areas with some exceptionally high values adjacent to exceptionally low values (Fig. 6b) thus resulting in a complex pattern of "bulls eyes".

In contrast, the generalized trend surface formed by the 3rd order polynomial function indicates that high susceptibility values are located in the central part of the pluton paralleling the southeast margin of the pluton, with lower values to the west along the southeast margin (Fig. 6c).

Variation between the A and B cores at each of the sites (to be discussed in detail in a later section of this thesis) contoured by spline (Fig. 14a) and 4th order polynomial (Fig. 14b) functions range in value from 0-29.543 x 10^{-3} SI. The spline function distribution show low variation between A and B core samples at each site in the western part of the pluton, and within a north-south trending swath across the pluton to the east (Fig. 14a). The polynomial function indicates a high degree of variation to the east and in the northwest-central part of the pluton (Fig. 14b).

Magnetic minerals

Given the mineralogy and range in mean susceptibility (Fig. 8), the carriers of the AMS signature are probably both paramagnetic and ferromagnetic. Potential paramagnetic sources include biotite, amphibole, pyroxene and epidote, especially in the western part of the pluton. Ilmenite, other titanium oxides, and accessory tourmaline are also potential paramagnetic carriers. Magnetite is undoubtedly the principal ferromagnetic mineral. However, the spatial distribution and concentration of possible magnetite types (single-domain, pseudo-single-domain, multidomain) remains to be determined.

Aeromagnetic and gravity studies

Aeromagnetic data can indicate how much magnetite or iron is present in an area. A USGS (1983) survey identified a magnetic high coincident with the northernmost extremity of the Mount Barcroft pluton (Fig. 7). The magnetic high may be indicative of a highly magnetic pluton at depth. However, no corrections were made in the aeromagnetic data for elevation, and the magnetic high correlates with the high ridge crest of the White Mountains. Gravity data (corrected for elevation) compiled by Blakely and McKee (1985) indicate a gravity low to the north of the Barcroft Structural Break, which may be indicative of a different crustal block, associated with the northern White Mountains.

Susceptibility (Km) versus variation in susceptibility (KmCv)

Determination of the degree of susceptibility variation as the result of interaction between paramagnetic and ferromagnetic minerals can be achieved by plotting average site susceptibility (Km) against variation in sample site susceptibility (KmCv) (Fig. 9a). Mean susceptibility (Km) is defined as:

$$Km = \Sigma Km/\text{number of samples}$$

The susceptibility variation coefficient in percentage (KmCv) is defined as:

KmCv=100 x standard deviation of Km within a site/mean susceptibility

The plot of mean susceptibility (Km) versus the susceptibility variation coefficient (KmCv) can be an indicator of the presence of both paramagnetic and ferromagnetic minerals. There is a weak correlation between low mean susceptibility values and high susceptibility variation coefficients for the Mount Barcroft pluton (Fig. 9a), although this relationship is not conclusive.

Magnetic anisotropy (P%)

Anisotropy or P% is the degree of magnetic fabric strength and in some cases may be correlated with strain intensity (Bouchez, 1997). Anisotropy is calculated using two different methods: P% (P% = 100 [(k1/k3) – 1]) and P (P = k1/k3). For this study P% was employed. As indicated in the anisotropy histogram (Fig. 10a), for all core pieces, P% ranges from 0.01% to 19.49% (P= 1.0001 – 1.1949). Anisotropy values for single biotite grains, the primary carrier of magnetic susceptibility present in most paramagnetic granites, ranges from a totally random orientation of P% = 0% (P=1.0) and rarely exceeds P% = 10% (P=1.10) (Bouchez, 1997). Magnetite-bearing ferromagnetic granites have much higher anisotropy values that may exceed P%=60% (P=1.60).

For the Mount Barcroft pluton anisotropy, values for individual core pieces range from 0.02% –19.49%. Spikes occur in the anisotropy histogram in the 0%-1% and 9%-10% ranges, with a broad peak culminating between 3%-5% (Fig. 8a).

Average P% values for individual sites range from 0.02% - 12.14% (P=1.00002-1.1214) and were contoured using the spline and 3rd order polynomial functions (Fig. 8b, 8c). The spline function (Fig. 8b) indicates low P% to the west and along the long axis of the pluton. High P% values are located at sites to the southeast and in two isolated sites adjacent to the northwest pluton margin. The polynomial function map (Fig. 8c) suggests a series of north-south trending

domains oriented oblique to the southern pluton margin, with lower values to the west and higher values to the east. This domainal distribution of anisotropy magnitude agrees fairly well with the map distribution of outcrops in which macroscopic foliation is most clearly developed (Fig. 2b).

Variation between A and B cores at individual sites were contoured across the range of 0.003% -12.934 % using spline and 4^{th} order polynomial functions (Figs. 14c, 14d). The spline contour map reveals a 2-3 kilometer wide, north-northwest trending high situated in the eastern portion of the pluton, with a second high located along the mid-northwestern pluton margin (Fig. 14c). The polynomial contour map displays an arc shaped, low variability zone coincident with the pluton long axis, with high variability zones located along the southern, eastern and mid-northwest pluton margins (Fig. 14d).

Anisotropy (P%) versus susceptibility (Km)

Plotting anisotropy (P%) against susceptibility (Km) may provide a means to distinguish between modal ferromagnetic and paramagnetic minerals in a given pluton. A positive correlation of P% to Km indicates that both paramagnetic and ferromagnetic minerals are present (Rochette et al., 1992). An abrupt increase in total anisotropy suggests an anisotropic distribution of magnetite grains (Bouchez, 1997; Saint Blanquat and Tikoff, 1997). The plot of anisotropy versus susceptibility for the Mount Barcroft pluton has a positive correlation between the two parameters (Fig. 9b). In addition, an abrupt change in slope is present at lower susceptibility values below 500 x 10^{-6} SI (0.5 x 10^{-3} SI), which may be associated with paramagnetic minerals dominating the magnetic signature at specific sample sites (Bouchez, 1997).

Shape of the magnetic susceptibility ellipsoid – shape fabric (T)

Shape parameter T is defined as T = 2[(lnk2-lnk3)/(lnk1-lnk3)]-1 (Jelnik, 1981). T values of +1.0 indicate oblate magnetite fabrics and potential flattening strain. Values of -1.0 indicate prolate magnetic fabrics and potential constrictional strain. And T = 0 values are equivalent to

plane strain. T values for individual core pieces from across the pluton range in value from –0.91 to +0.93 (Fig. 10a). T shape values display a skewed to the right, bell-shaped distribution in the histogram, with greatest frequency of values ranging from +0.3 to +0.5 (Fig. 10a).

The spatial distribution of fabrics across the pluton was investigated by contouring average T values for each site (values ranging from –0.2 to +0.74) using spline and 3rd order polynomial functions (Fig. 10b, 10c). The spline function highlights a number of sinuous, prolate domains that appear to contain and/or separate oblate fields (Fig. 10b). Contours derived by the polynomial function for the most part parallel the southern pluton margin (Fig. 10c) with the exception of the +0.2 contour forming a northeast-trending double curve, oriented oblique to the southern pluton margin.

Variations of T shape between A and B cores for individual sites range from 0.007 to 1.22. Distribution of T variation between A and B cores were contoured using spline and 4th order polynomial functions (Figs.14e, 14f). The spline function indicates an "S" shaped pattern for higher amounts of variation with extremes along the southern, northwestern and western pluton margins. The polynomial function contours indicate high variation values in domains located adjacent to the northwest, northeast, southwest and southeast margins. The pluton interior is characterized by a lower variation in T (Fig. 14f).

Shape fabric (T) versus susceptibility (Km) and Anisotropy (P%)

Plotting T shape against susceptibility (Km) and against anisotropy (P%) has previously been used in AMS studies to correlate specific shape fabrics with either susceptibility or anisotropy. In the case of the Mount Barcroft pluton, these relationships are subtle at best. Plotting of T shape to susceptibility (Km) (Fig. 11a) indicates a slight propensity for oblate fabrics (flattening) at high susceptibility values, but this correlation is very weak. Plotting T shape against anisotropy (P%) (Fig. 11b) shows no convincing correlation.

Shape of the magnetic susceptibility ellipsoid - planer fabrics (F%)

F% is a shape parameter associated with the degree of planer anisotropy [F%=100(k2/k3)]. F% values for individual core pieces within the Mount Barcroft pluton range from 0% - 11.39% (Fig. 12a). The histogram of F % frequency for individual core pieces spikes in the 0% - 0.5% range, has a minor flat-topped peak between 1.5% and 2.5% and a ragged, tapering off of F% values to 11.39%.

Average F% values for individual sites range from 0.02% to 7.1 % and their map distribution was contoured using spline and 3rd order polynomial functions (Figs. 12b, 12c). Spline-based contour maps show higher values along the southern and northwestern pluton margins in the eastern two thirds of the pluton with a northwest trending, 2-3 kilometer wide domain of high F% values across the central portion of the pluton. Lower F% values are located to the west and along the mid-northwest pluton margin (Fig. 12b). Polynomial based contour maps indicate high F% values in the southeastern part of the pluton, with contour lines trending to the northeast, oblique to the southern pluton margin. Lowest F% values are located to the west where contour lines run north to south at high angle to the northern and southern pluton margins (Fig. 12c). There is a correlation between high F% values and the observed consistently NE trending macroscopic foliation in the NE part of the pluton (Figs. 12b, 12c), with the less, well-defined macroscopic foliation in the western part of the pluton coinciding with low F% values. A correlation exists between polynomial based contour maps of T shape and F% (Figs. 10 and 12) inasmuch as both indicate fabrics becoming increasingly oblate to the southeast. However, T shape contours are parallel to the pluton margins, whereas F% contours are oblique to the pluton margin.

Within-site F% variation between A and B cores range from 0.003% to 8.678% and were contoured using both spline and 4th order polynomial functions (Figs. 14g, 14h). For the spline function, the highest variation values are within sites adjacent to the northwestern and southern

pluton margins, and in a 2-3 kilometer wide, north-northwest trending domain located in the easternmost part of the pluton (Fig. 14g). Polynomial-based contours for F% within site variation display the highest degree of variation in the easternmost part of the pluton and along the mid-northwestern pluton margin. Lower variation values are located to the west and in the middle portion of the pluton (Fig. 14h).

Shape of the magnetic susceptibility ellipsoid – lineation fabric (L%)

L% is a shape parameter that indicates the degree of linear anisotropy (L%=100[k1/k2]) and for individual core pieces ranges from 0% -8.42% (Fig. 13a). The histogram of L% frequency for individual core pieces displays a peak at 0% to 0.5% and then steeply decreases to 8.42%.

L% averages for individual sites range from 0.01% - 6.52% and their map distribution was contoured using spline and 4^{th} order polynomial functions (Figs. 13b, 13c). Contouring based on spline function indicate high L% values along the eastern and northwestern margins, and along a northwest trending 2-3 kilometer wide domain cross-cutting the central part of the pluton (Fig.13b). The polynomial based function indicates higher L% values for the northeast to east part of the pluton (correlating with negative or prolate T values, (Fig. 10c), decreasing to low values in the west. Polynomial based L% contours in the western part of the pluton trend north-south at a high angle to the pluton margins. To the northeast, the contours are sinuous with "hinge surfaces" trending to the northeast (Fig 13c).

L% variations in individual sites between A and B core (Figs. 14i, 14j) are low in the western part of the pluton and along the central-western part of the pluton axis. Higher L% variation values are recorded in the eastern part of the pluton, and along the eastern part of the pluton, northern margin. Variation in L% between A and B core provide an explanation of why L% overall is higher in the east part of the pluton, coincident with average oblate T set of values.

Comparison of magnetic scalar parameters in Mount Barcroft pluton with other White-Inyo Range plutons

Magnetic scalar parameters within the Mount Barcroft pluton differ from previously recognized AMS systematics in the White-Inyo Range plutons. Correlations between different scalar parameters (Km, P%, T, F% and L%) in the Barcroft pluton are weak and highly suspect. Comparison of susceptibility (Km) to susceptibility variation (KmCv) and susceptibility (Km) to anisotropy (P%) in Figures 9a and 9b lack strong correlations. Comparison of T shape to susceptibility (Km) and T shape to anisotropy (P%) in Figures 9a and 9b, likewise, show no strong relationship.

Compared to the other Jurassic and Cretaceous plutons in the White-Inyo Range, the Mount Barcroft pluton displays a much more significant range of variability in AMS scalar parameters, both between and within sites. Significantly, compared to other plutons in the range (Table 1), anisotropy (P%) (Fig.8c) for the Mount Barcroft pluton is much lower, and displays no obvious systematic relationship to susceptibility (Km) (Fig. 6c). Average Km values for Jurassic plutons, in the White-Inyo Range are 2-4 times the values for those of Cretaceous plutons (Table 1). Anisotropy values (P%, P) have been used as an indicator of magmatic flow as opposed to solid-state deformation (St. Blanquat and Tikoff, 1997; Morgan et al., 2001). For ferromagnetic plutons in the Sierra Nevada, P% values of 9% were found to be an indication of magmatic flow, whereas in contrast, values of 16%-28% were considered to be an indication of solid-state deformation (Saint Blanquat and Tikoff, 1997; Saint Blanquat et al., 2001). The highest P% site average value for the Mount Barcroft pluton is 12.14%, with an average for all sites of 4.77%, suggesting a dominance of magmatic over solid-state processes. Similarly, the 165 Ma Santa Rita Flat pluton is characterized by an average P% of 5.6% (67 sites) and a maximum P% value of 9.7%, pointing to a magmatic origin (Vines, 1999; Vines and Law, 2000, 2001). In contrast, anisotropy values of greater than 40-50% have been recorded at individual sites in the 160-180 Ma Eureka Valley/Joshua Flat/Beer Creek composite pluton with an average P% across the entire

pluton of 17% (Morgan, 1998; Law, unpublished data). Similarly, the forcibly emplaced Papoose Flat pluton has P% values ranging from 0.8-66.8%, with an average P% value across the entire pluton (162 sites) of 19.1% (Saint Blanquat et al., 2001).

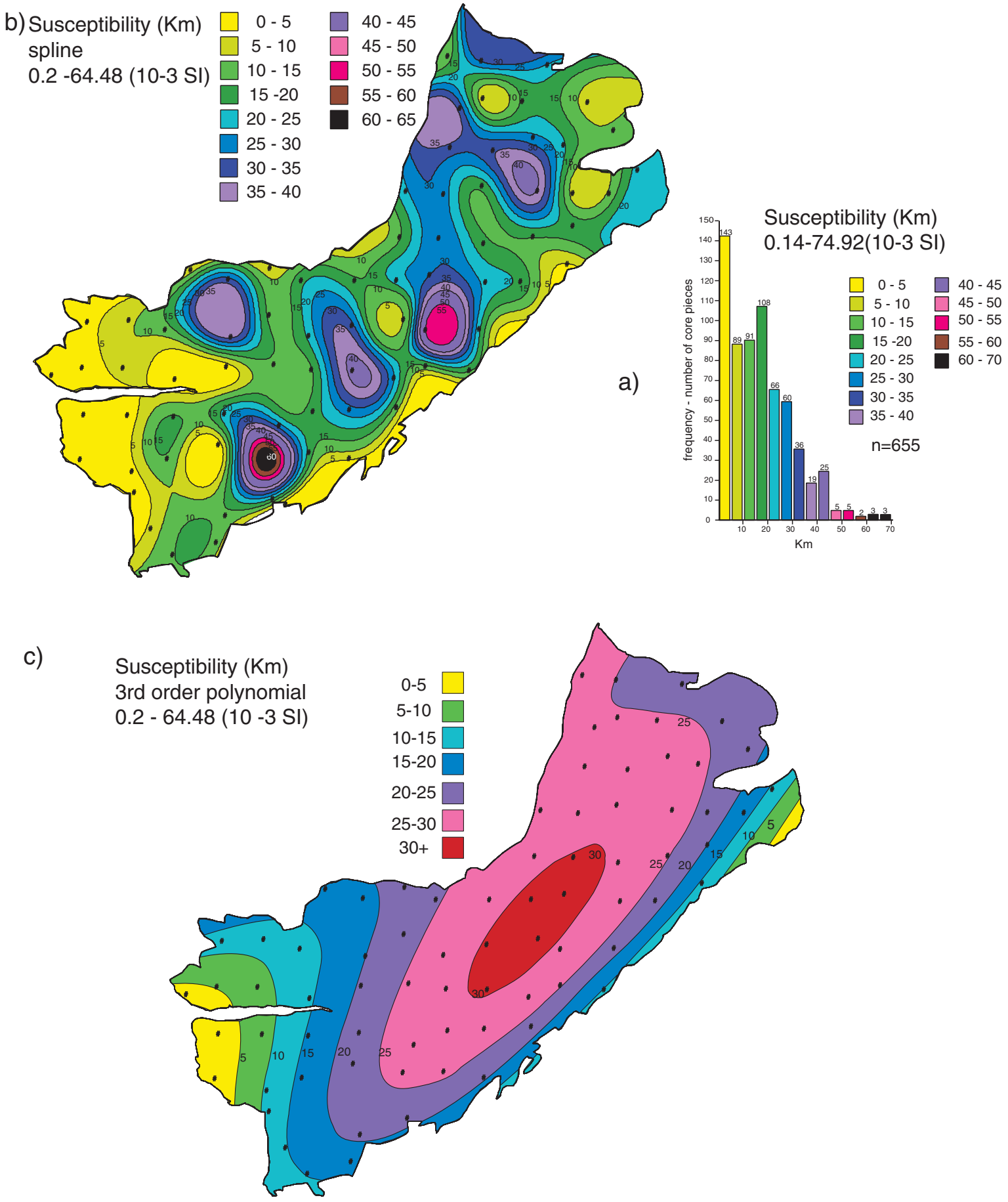

Figure 6: Susceptibility distribution (Km): a) susceptibility histogram for all core sections analyzed; b) created b y spline function; c) created by 3rd order polynomial function

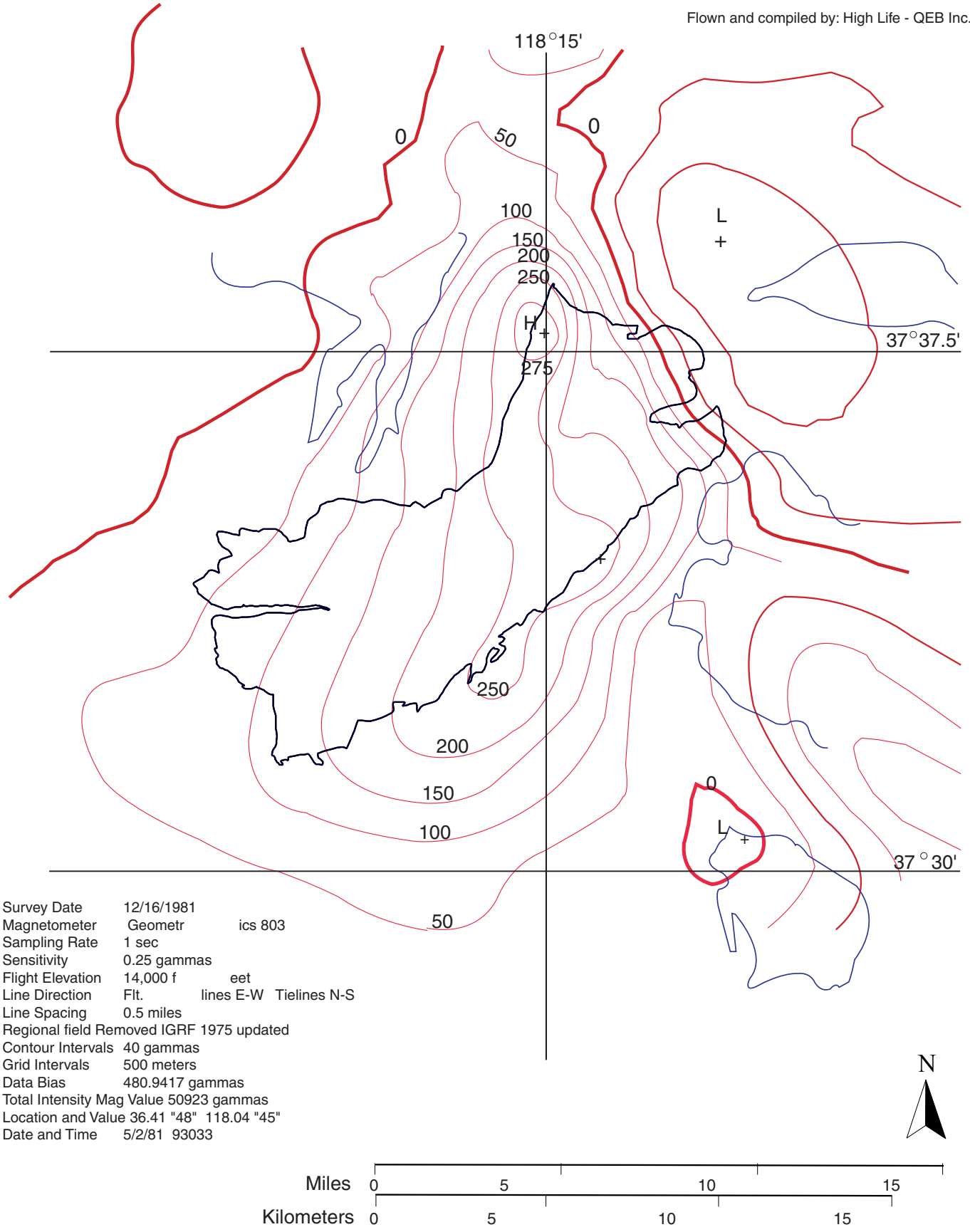

Figure 7: Aeromagnetic map of part of White Mountains surrounding Mount Barcroft pluton (adapted from U .S.G.S.1983 Open Report 656)

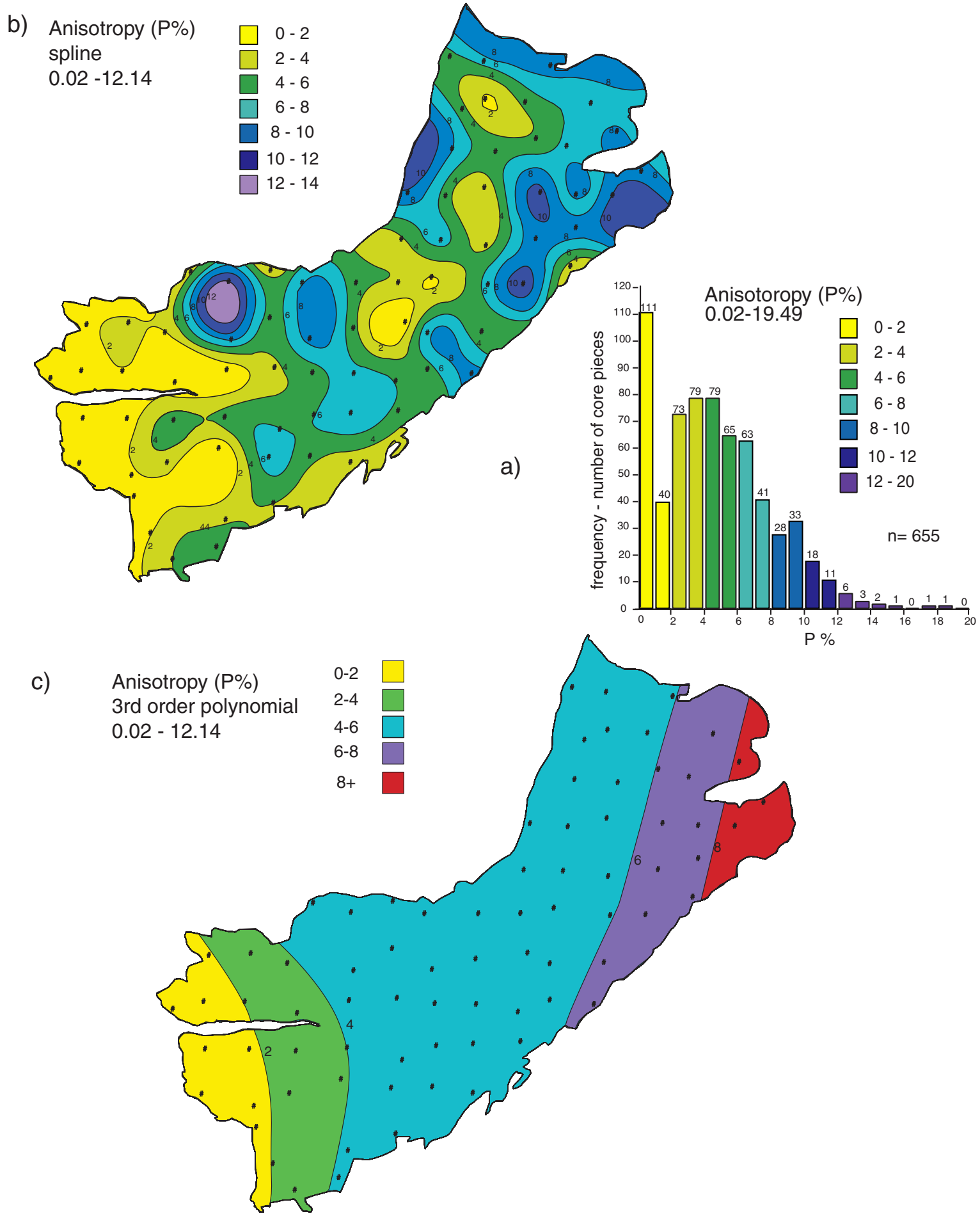

Figure 8: Anisotropy (P%): a) P% histogram; b) P% created by spline function; c) P% created by 3rd order polynomial

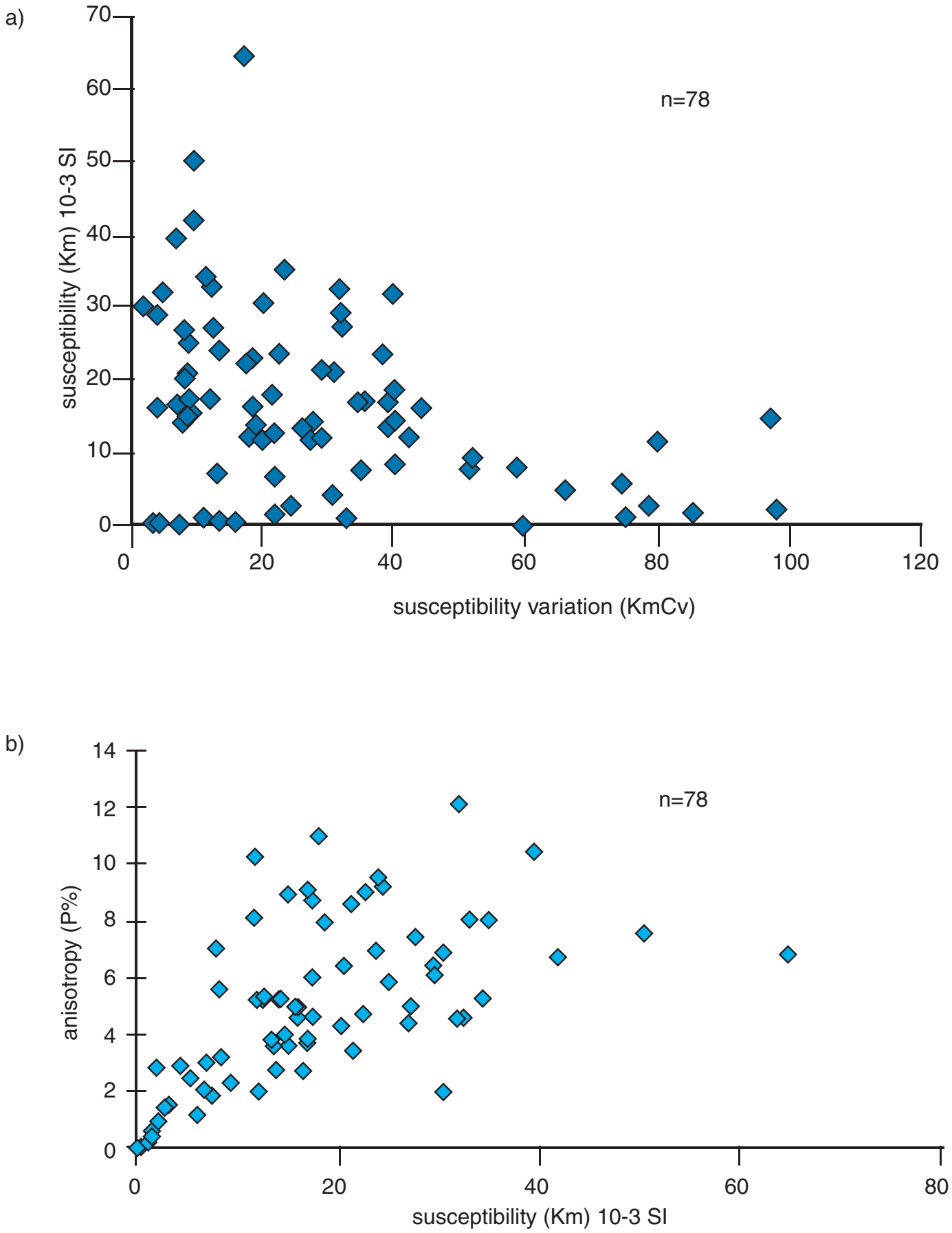

Figure 9:a) Susceptibility (Km) vs susceptibility variation (KmCv); b)susceptibility (Km) vs anisotropy (P%)

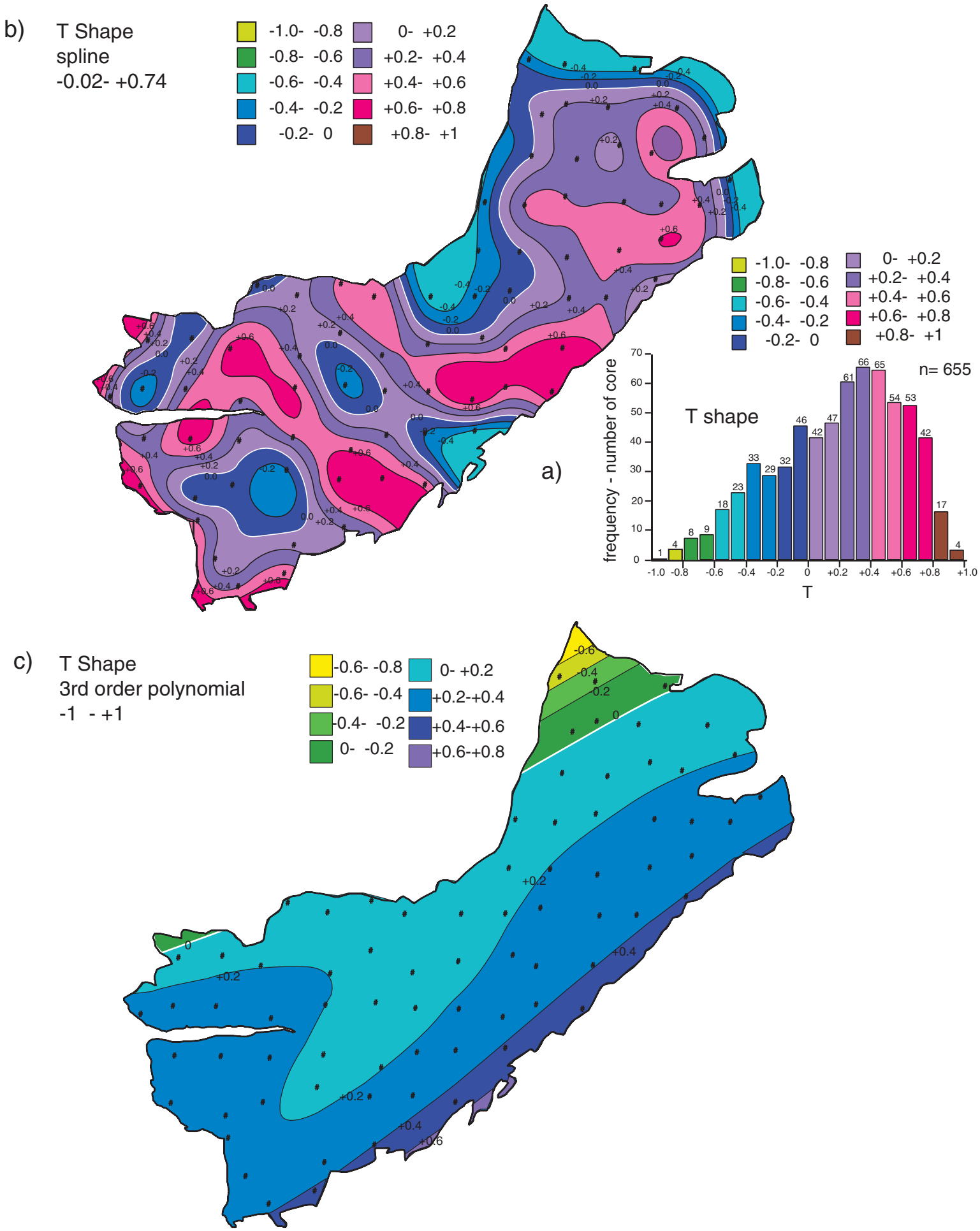

Figure 10: T Shape: a) T shape histogram; b) T shape spline created function; c) T shape created by 3rd order polynomial function

a)

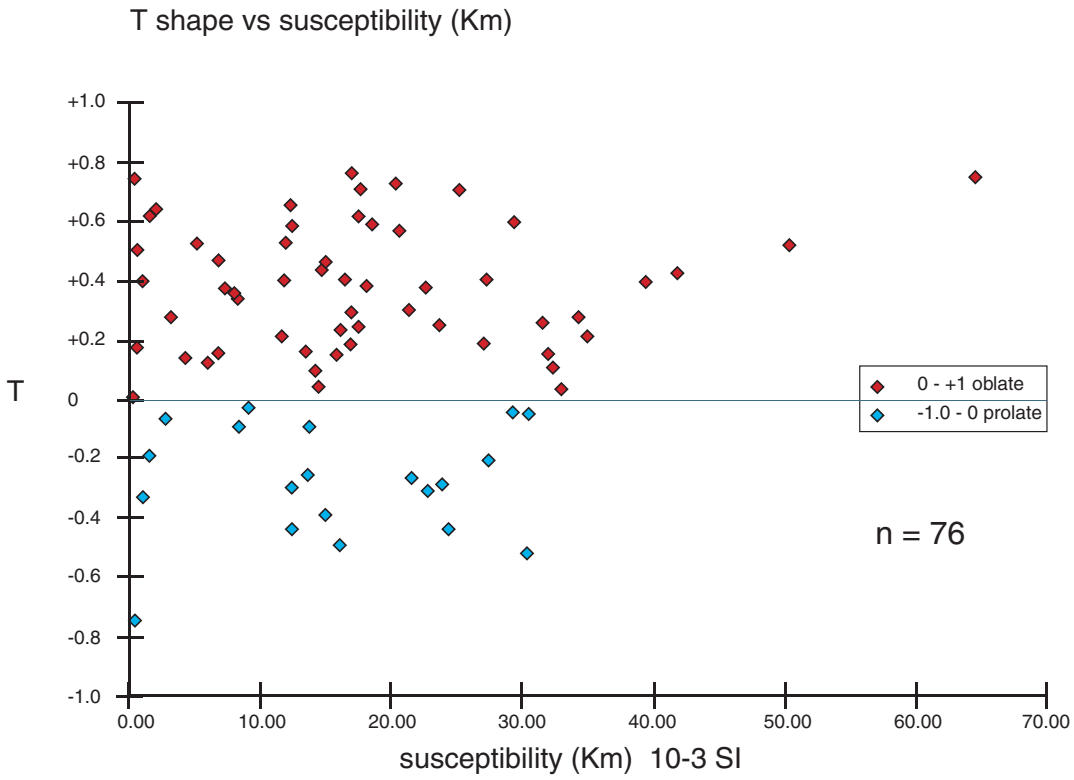

b)

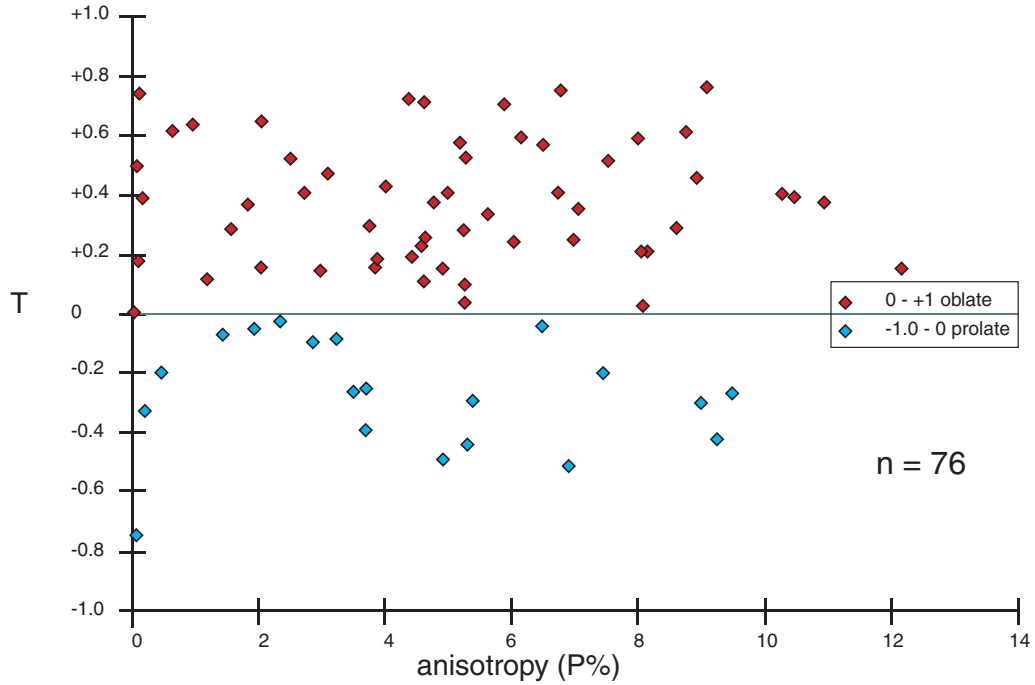

Figure 11: a) T shape vs susceptibility (Km); b) T shape vs anisotropy (P%)

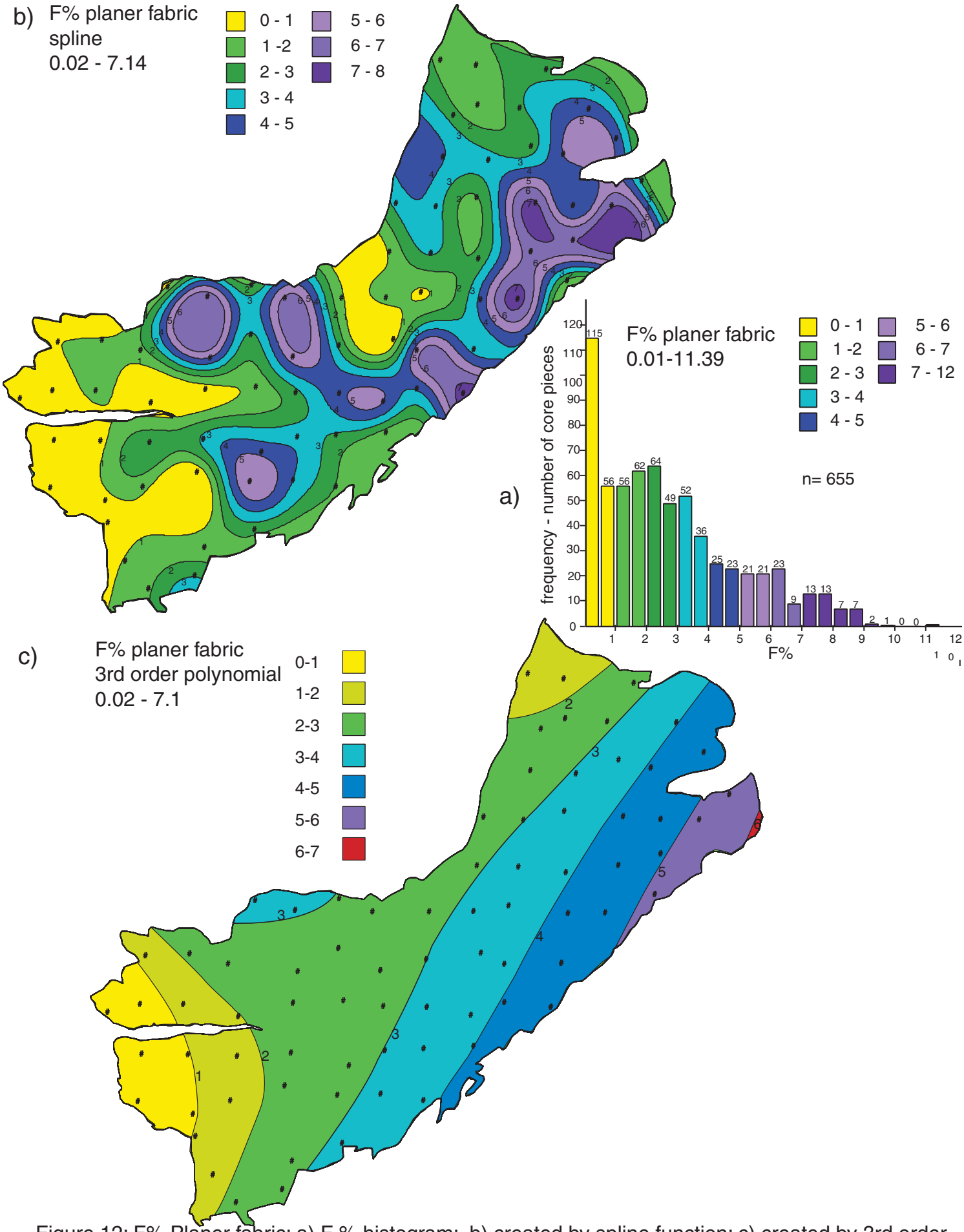

Figure 12: F% Planer fabric: a) F % histogram; b) created by spline function; c) created by 3rd order polynomial function

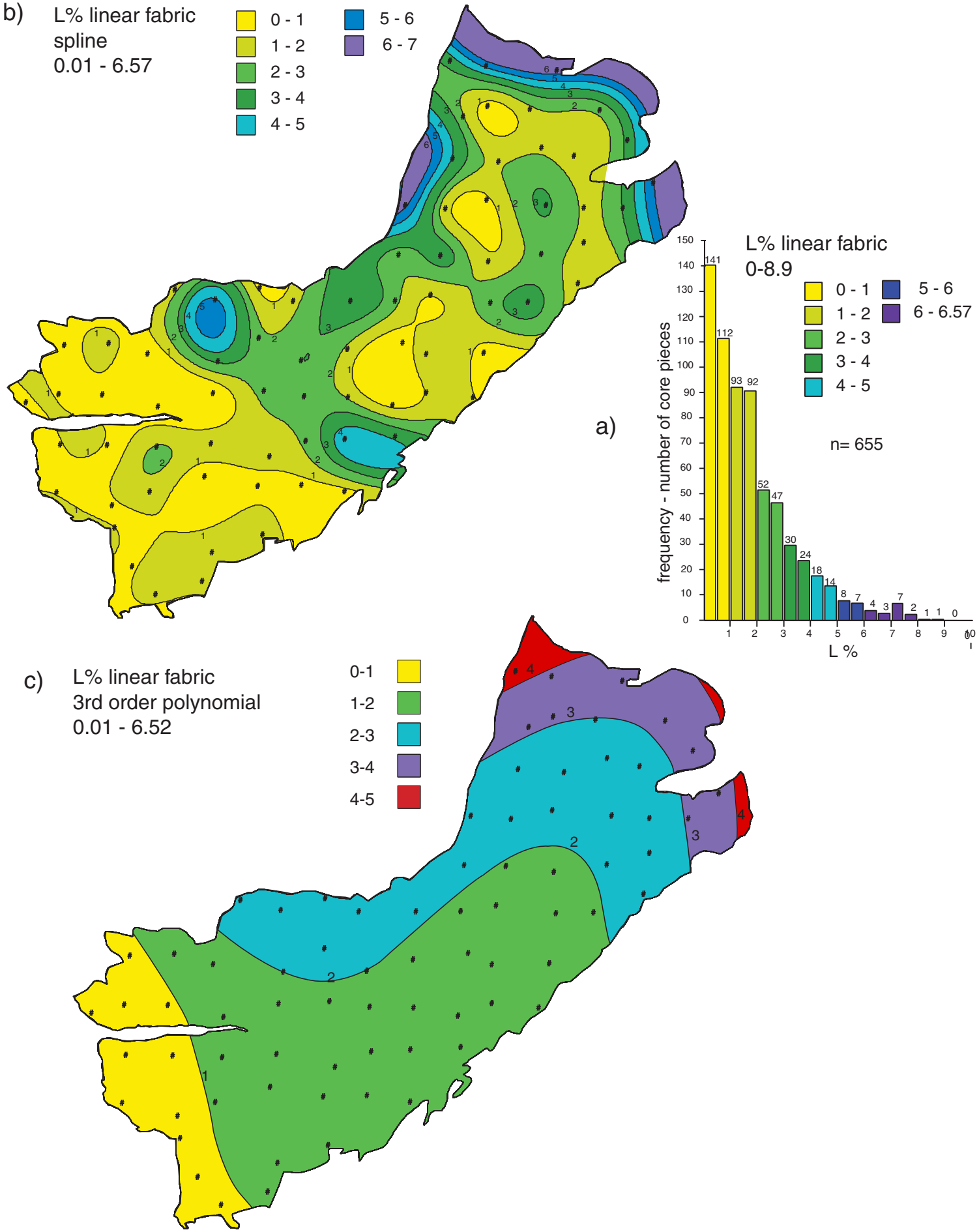

Figure 13: L% Linear fabric: a) L% histogram; b)L% contour created by spline function; c) L% contour created b y 3rd order polynomial function

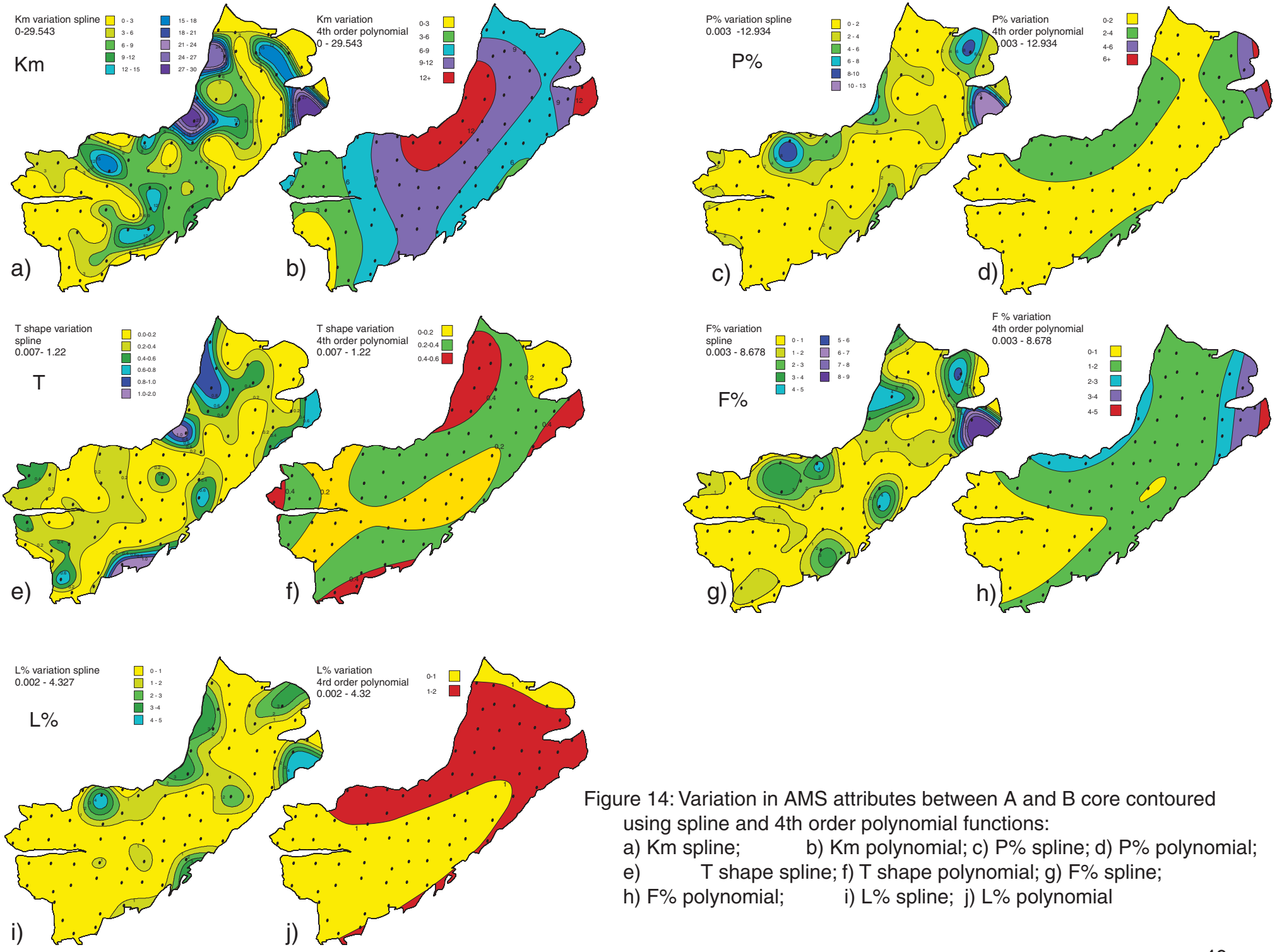

Figure 14: Variation in AMS attributes between A and B core contoured using spline and 4th order polynomial functions:
a) Km spline; b) Km polynomial; c) P% spline; d) P% polynomial; e) T shape spline; f) T shape polynomial; g) F% spline; h) F% polynomial; i) L% spline; j) L% polynomial

	Jurassic Plutons				**Cretaceous Plutons**	
	Barcroft	Sage Hen Flat	Santa Rita	Eureka Val./Joshua Flat/Beer Cr.	Papoose	Birch Creek
P% min	0.04	0.009	0.5	0.8	0.8	2.7
P% max	12.15	42.86	9.7	69.3	66.8	46.5
P % avg.	4.77	12.8	5.6	16.8	19.1	21
# of sites	78	51	64	319	102	72
Km min (10-3 SI)	0.2	0.09	1.2	0.0086	0.0538	0.127
Km max (10-3 SI)	64.48	42.86	49.37	94.71	30.588	10.801
Km avg (10-3 SI)	16.82	12.8	23.63	29	6.33	4.924
Cv Km min	2	3	5			4
Cv Km max	98	85	122			98
Cv Km avg	29	22	33			24
S(K) min (10-3 SI)	0.02	0.09	0.03			
S(K) max (10-3 SI)	14.8	42.86	16.86			
S(K) avg (10-3 SI)	3.82	12.8	2.73			
Cv (P%) min	0	5	0			
Cv (P%) max	6.41	53	50			
Cv (P%) avg	1.21	99	16			
site averages (A and B core) used						

Table 1:Comparison AMS parameters of Jurassic, Cretaceous White-Inyo Range plutons

Data: Santa Rita Flat (Vines 1999); Papoose Flat (St. Blanquat et al., 2001; remaining plutons, unpuplished data by R.D Law, S.S. Morgan and M. de St. Blanquat. 47

DIRECTIONAL MAGNETIC PARAMETERS – DATA REDUCTION AND ANALYSIS

Measured values of k1, k2, k3 for individual core pieces at each site are provided in Appendix 1. K1, K2, K3 are average measured values for individual sites and are tabulated in Appendix 2. These data were analyzed and statistically compared using the EXAMS program (Saint Blanquat, 1993) and then plotted on equal area, lower hemisphere stereonets (Appendix 3).

Identification of problem sites

Problem sites were identified where K1, K2 and K3 averages were not orthogonal of within 16 of the 78 total sites between the A and B cores (Fig. 15). Data from the problem sites are summarized in Appendix 4. For these sites, the orientations of K1, K2 and K3 were recalculated based on a case-by-case, visual inspection of stereonets. Initially, two courses of action were taken in order to have a single directional data measurement for foliation and lineation, at each site. Where variation between average K1, K2, and K3 of A and B core were small, principal directions were readjusted based on the susceptibility (Km), anisotropy (P%) and shape parameter (T). In the second case, where the differences in the steronets were not resolvable, a choice was made to select either the A or B core K1, K2, K3 averages or a hybrid was created. Selection between A or B core K1, K2, K3 averages was based on susceptibility (Km), anisotropy (P%), shape parameter (T) and consistency of fabric orientation between A and B cores in adjacent sites.

Problem sites within plutons are associated with large variation in directional AMS properties between A and B cores at individual sites. Of the sixteen problem sites identified, one had completely random distribution of K1, K2, K3, nine had distinctively different fabrics and six sites were distinguished by orientation mismatches between A and B cores to varying degrees.

Magnetic foliation

Stereoplots of foliation and lineation orientation averages for each site are shown in Figure 16. Poles to foliation indicate a "fold hinge" plunging 34° towards 314°. Two lineation maxima plunge at 54° towards 300°, and 58° towards 239°.

Magnetic foliation is determined by the plane containing K1 and K2 susceptibility axes, and has been used as a reliable proxy for foliation orientation in plutons. Figure 17a illustrates average magnetic foliation orientation measurements for individual sites. The foliation form lines are presented in Figure 17b. The magnetic foliation form lines define a northward plunging synform with a northwest dipping eastern limb, striking parallel to the southeast pluton margin. The western limb strikes north-south to southeast and is subvertical. In the western part of the pluton, foliation defines a northwest-trending antiformal structure. Foliation defines a synform in the eastern portion of the pluton. There is a broad correspondence between grain shape foliation noted in the field (Fig. 2b) and AMS foliation (Fig. 17b), particularly in the eastern part of the pluton.

Foliation dip ranges from 20° - 82°. Domainal variation in foliation dip was contoured using the spline function (Fig. 17c) and 3rd order polynomial function (Fig. 17d). The spline function contour map indicates steeper dips in the western part of the pluton and in isolated zones around the pluton margins (Fig. 17c). The polynomial function contour map indicates generally steeper dips to the west and at the northern and eastern margins of the pluton (Fig. 17d).

Variation in foliation dip between A and B cores at individual sites was contoured using spline and 4th order polynomial functions (Figs. 21a, 21b). A high degree of variation in foliation dip is centered along the central northwest and southern pluton margins and along the western margins. Also there is a north-trending domain of high variation in the eastern part of the pluton and an isolated high in the west-central part of the pluton (Fig. 21a). The polynomial function contours run parallel to the northwest and southeast pluton margins with higher variation values

along these margins. Minimum variation in foliation dip is recorded in the central part of the pluton.

The magnetic foliation map and spline contoured scalar AMS data are presented and compared in Figure 18. Visually, the strongest correlation exists between the magnetic foliation map and the spline-function T shape map (Figs. 18a, 18d). Additionally, the foliation map roughly correlates with the maps of planer fabric (F%) and linear fabric (L%) (Figs.18e, 18f). T shape, F%, L% all display northwest trending domains, which coincide with the western limb of the "synform" defined by the foliation. Susceptibility (Km) and anisotropy (P%) do not appear to correlate with the magnetic foliation map. The magnetic foliation map and 3rd order polynomial contoured, scalar AMS data are presented and compared in Figure 21. Susceptibility (Km) and T shape contours parallel the NE striking southern pluton margin, which broadly coincides with the NE trend of the directional data (Fig. 21). The antiformal foliation arch in the west part of the pluton is most clearly reflected in the anisotropy contour maps (P%, F%, L%).

Magnetic lineation

Macroscopic linear fabrics in granites are difficult to identify in outcrop. AMS analysis has proven to be one of the most useful procedures for identification of orientation and strength of linear fabrics. The k1 susceptibility axes define the magnetic lineation. Figure 22a illustrates average lineation trend and plunge at sites within the Mount Barcroft pluton. Lineation plunge varies from 4°- 68°.

Short yellow arrows represent sites with the steepest plunges from 60° - 90°; medium length red arrows represent plunges of 60°-30°; long, blue arrows represent plunges from 30°– 0°. Lineation trend appears to be random in orientation, although two distinct lineation clusters are noted on the stereonet (Fig. 16).

Domainal variation in lineation plunge was contoured using spline and 3rd order polynomial functions (Figs. 20b, 20c). The spline function map locates steep lineation plunges intermittently along the southeast and northwest pluton margins. A zone of steep plunge is also located in the west-central portion of the pluton. The 3rd order polynomial map indicates that low lineation plunge values are coincident with the central long axis of the pluton and along the western parts of the north and south pluton margins. Higher lineation plunges are also located in a domain in the west central portion of the pluton.

Variation in lineation plunge between A and B core were contoured using spline and 4th order polynomial functions (Figs. 21c, 21d). The spline function contour map indicates variation highs along the north, northwest, east and southeast pluton margins, and at isolated sites within the west-central and northeast parts of the pluton (Fig. 21c). The 4th order polynomial contour map indicates a northeast-trending variation high running across the central part of the pluton. A high degree of variation in lineation plunge is also apparent in the northeast part of the pluton (Fig. 21d).

White-Inyo Range plutons versus Mount Barcroft pluton magnetic directional parameters

Comparison of Mount Barcroft pluton magnetic directional parameters with other AMS studies carried out in the other White-Inyo Range plutons indicate that the Barcroft pluton is characterized by great variability between sites in terms of relative strength of magnetic scalar parameters (Km, P%, T, F% and L%), orientation mismatch, foliation strike and dip, and lineation trend and plunge. This makes comparison between the Mount Barcroft and other White-Inyo plutons difficult.

In most White-Inyo Range AMS studies, notably the Santa Rita pluton (Vines, 1999; Vines and Law, 2000), lineation is coincident with fold hinges defined by poles to foliation. The Mount Barcroft pluton does not exhibit this relationship, possibly due to the magnetic scalar and directional variations detected both within and between sites.

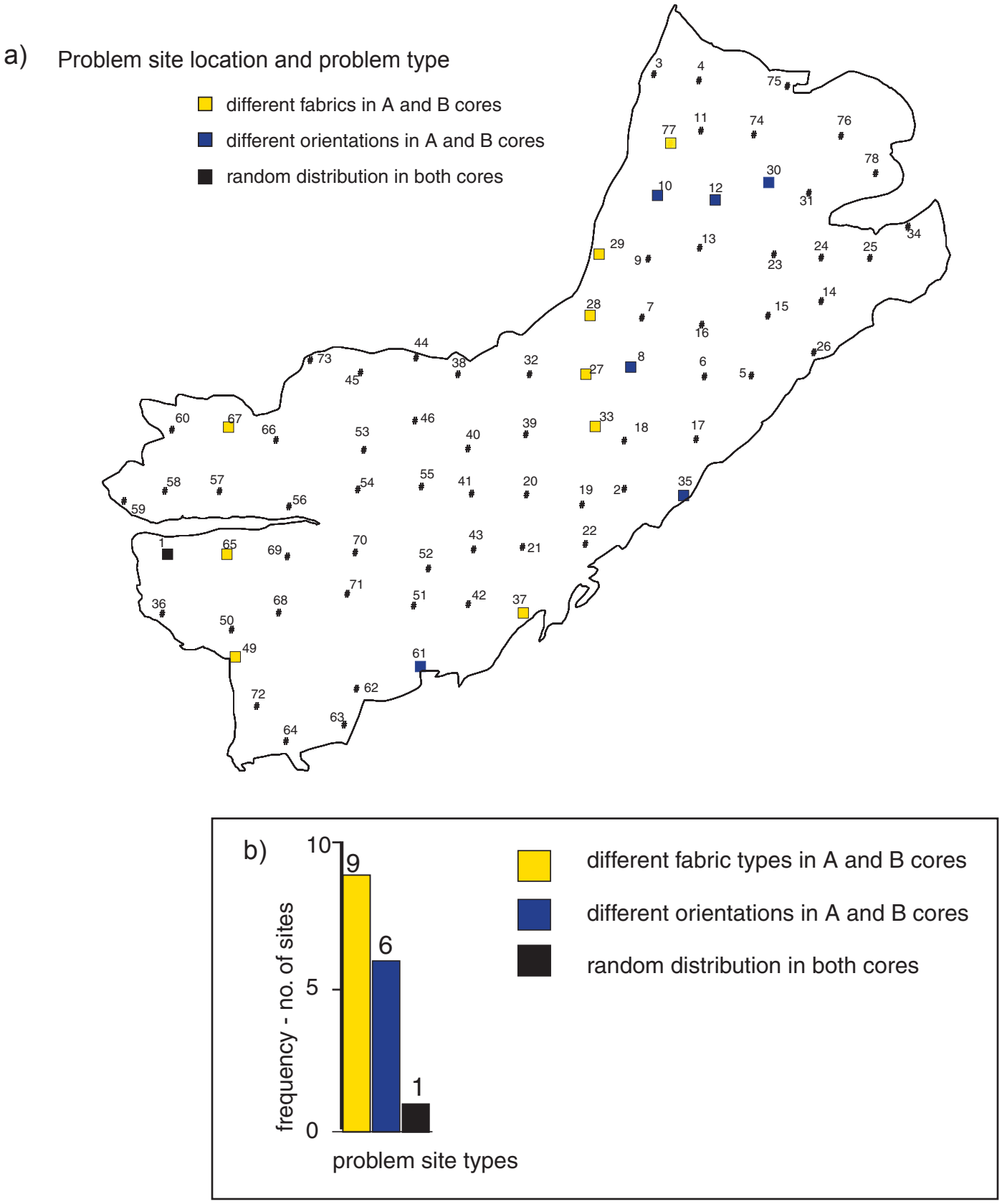

Figure 15: Problem sites: a) location of problem sites; b) histogram of type of problem site

a) AMS foliation

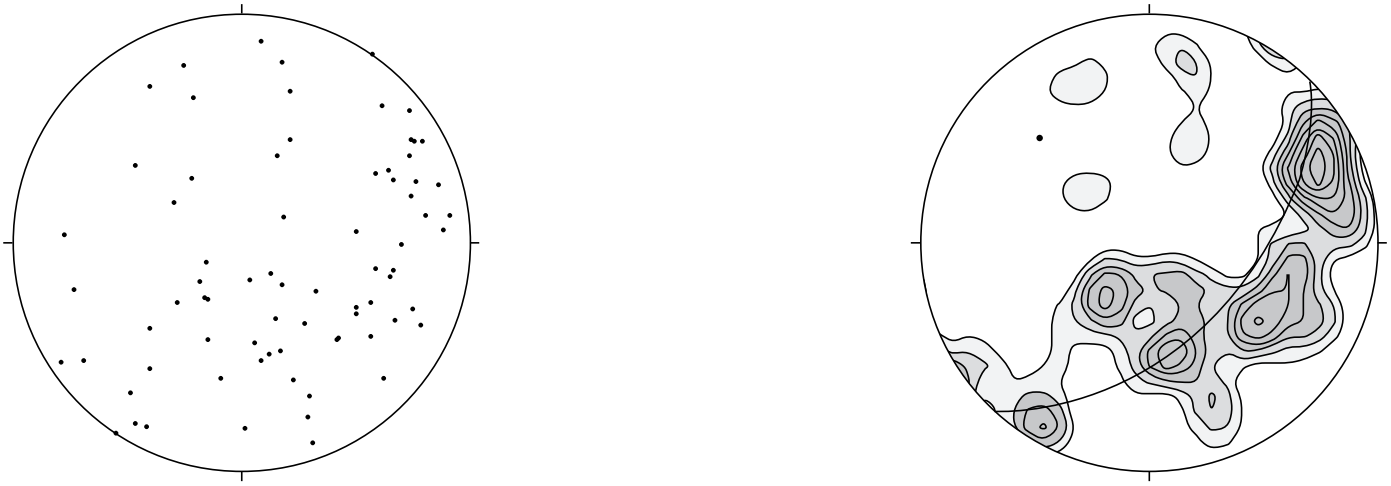

74 poles: 1.0, 1.5, 2.0, 2.5, 3.0, 3.5, 4.0, 4.5 times uniform

34/314

b) AMS lineation

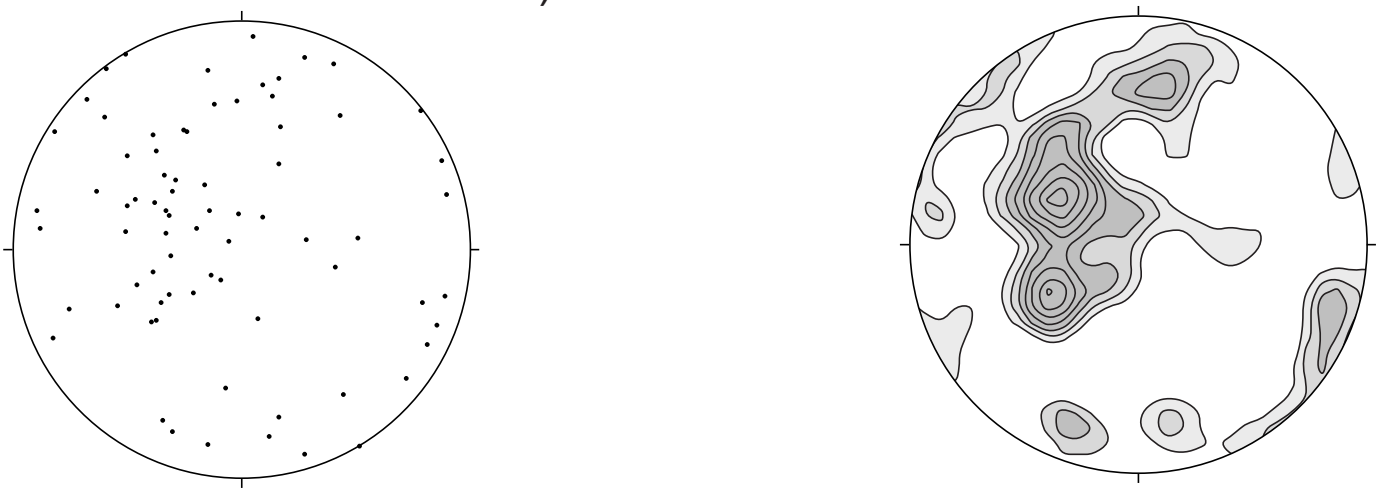

74 lineations: 1.0, 1.5, 2.0, 2.5, 3.0, 3.5, 4.0, 4.5 times uniform

300/58 and 239/54 and 006/34

Figure 16: Mount Barcroft pluton foliation and lineation data

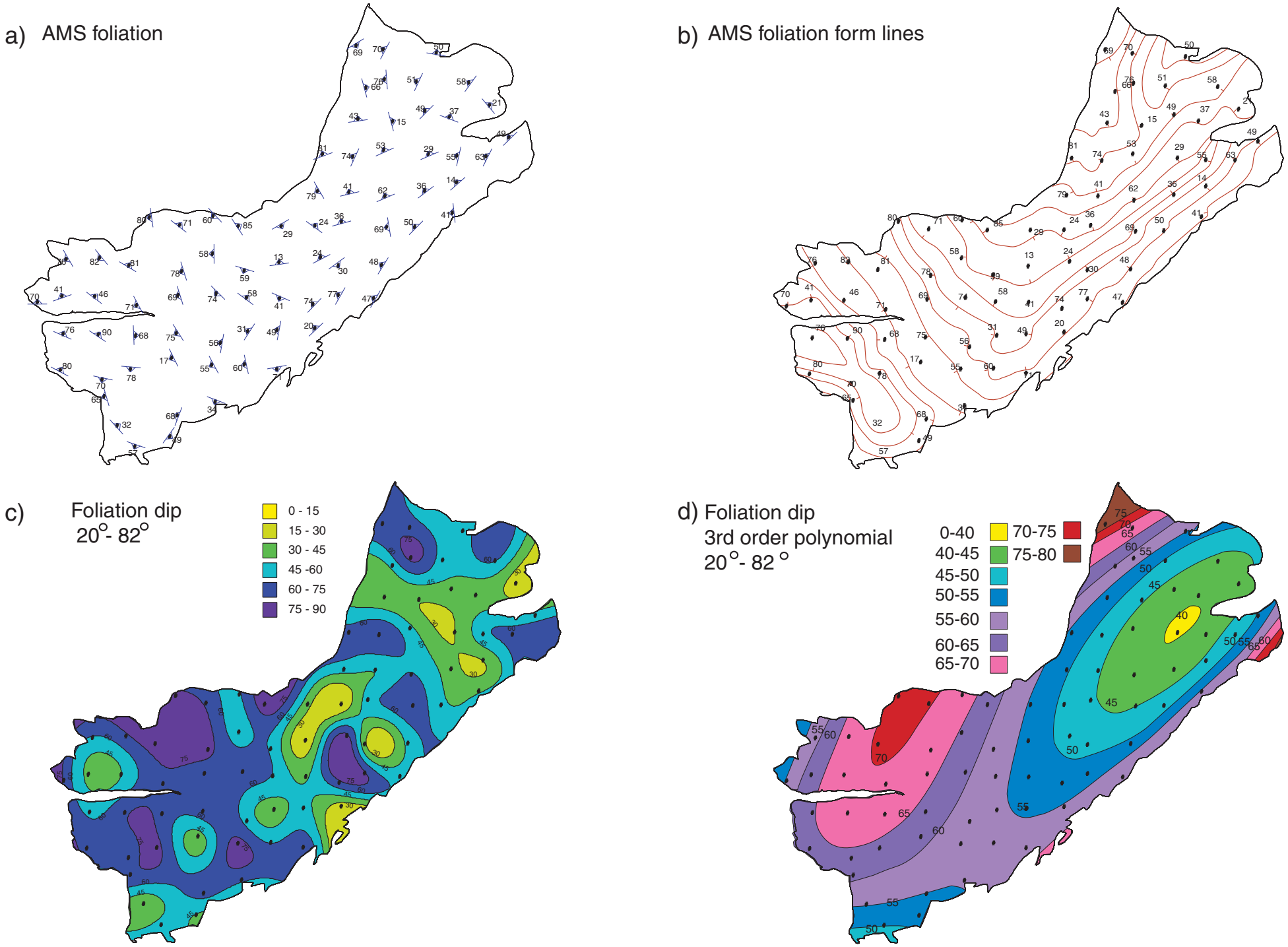

Figure 17: Magnetic foliation strike and dip: a) individual sites; b) magnetic foliation form lines; c) foliation dip created by spline function; d) f oliation dip created by 3rd order polynomial function

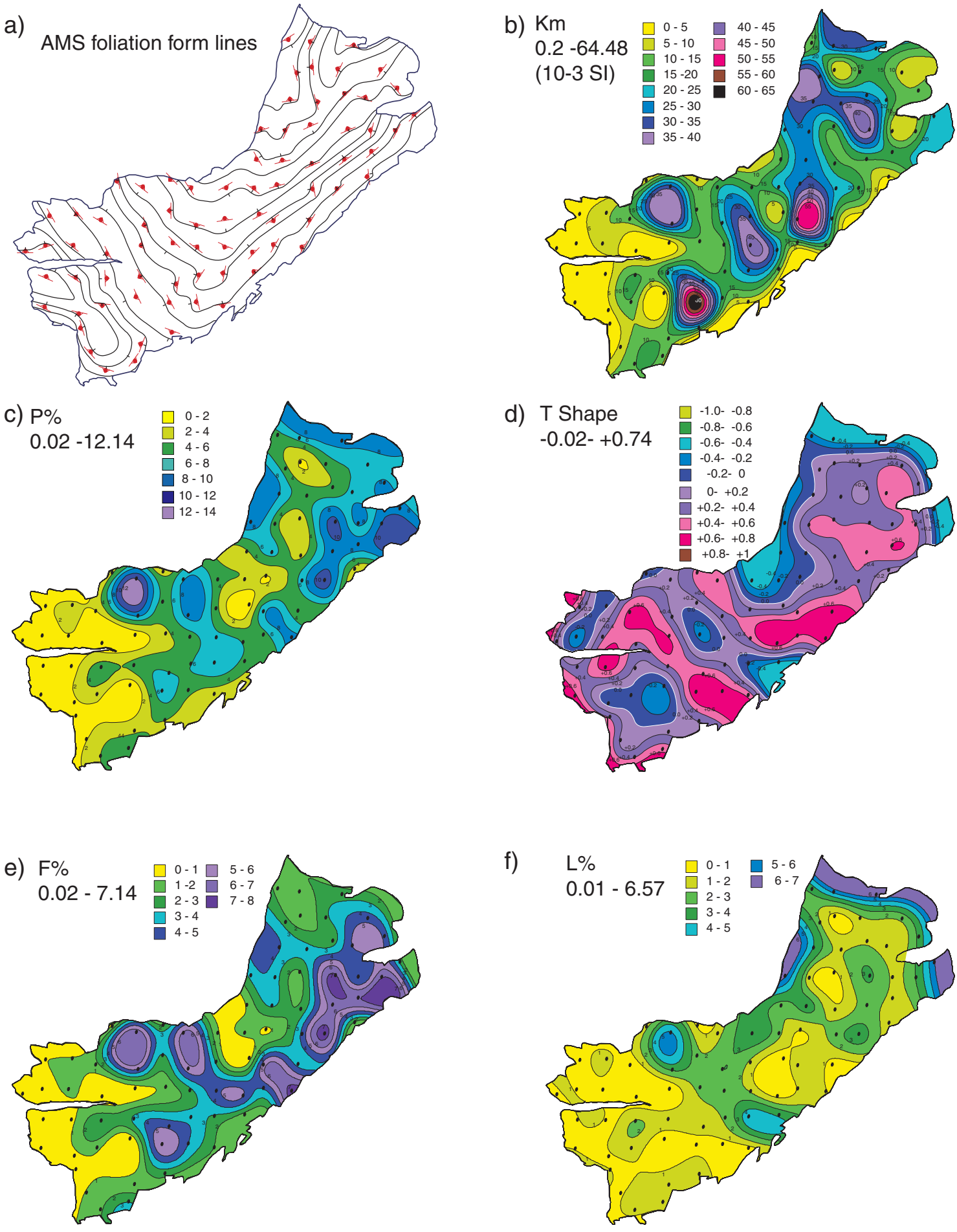

Figure 18: AMS foliation contour vs average magnetic parameters created by spline function: a) AMS foliation form lines; b) Km; c) P%; d) T shape; e) F%; f) L%

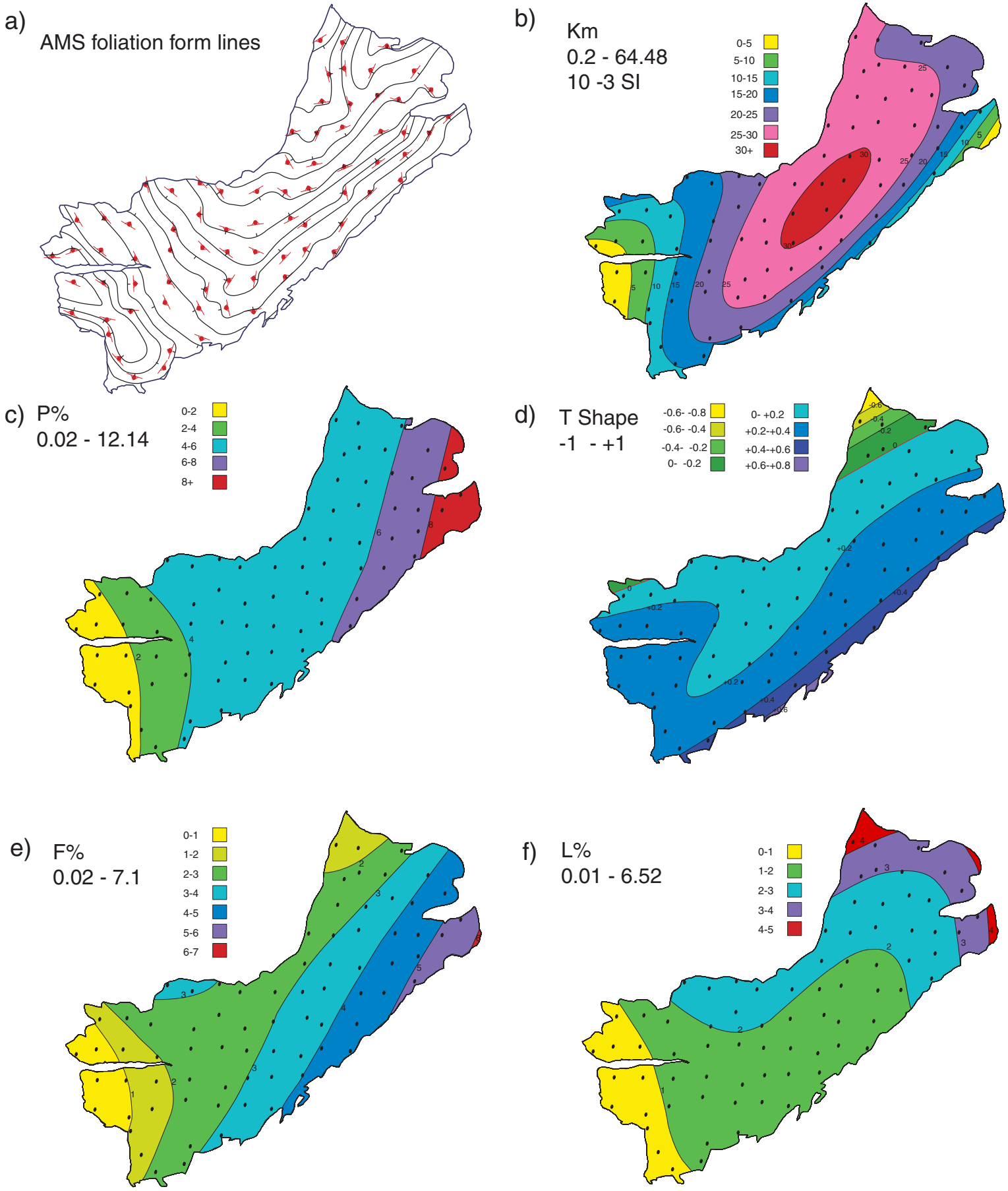

Figure 19: AMS foliation contour vs average magnetic parameters created by polynomial function: a) AMS foliation form lines; b) Km; c) P%; d) T shape; e) F%; f) L%

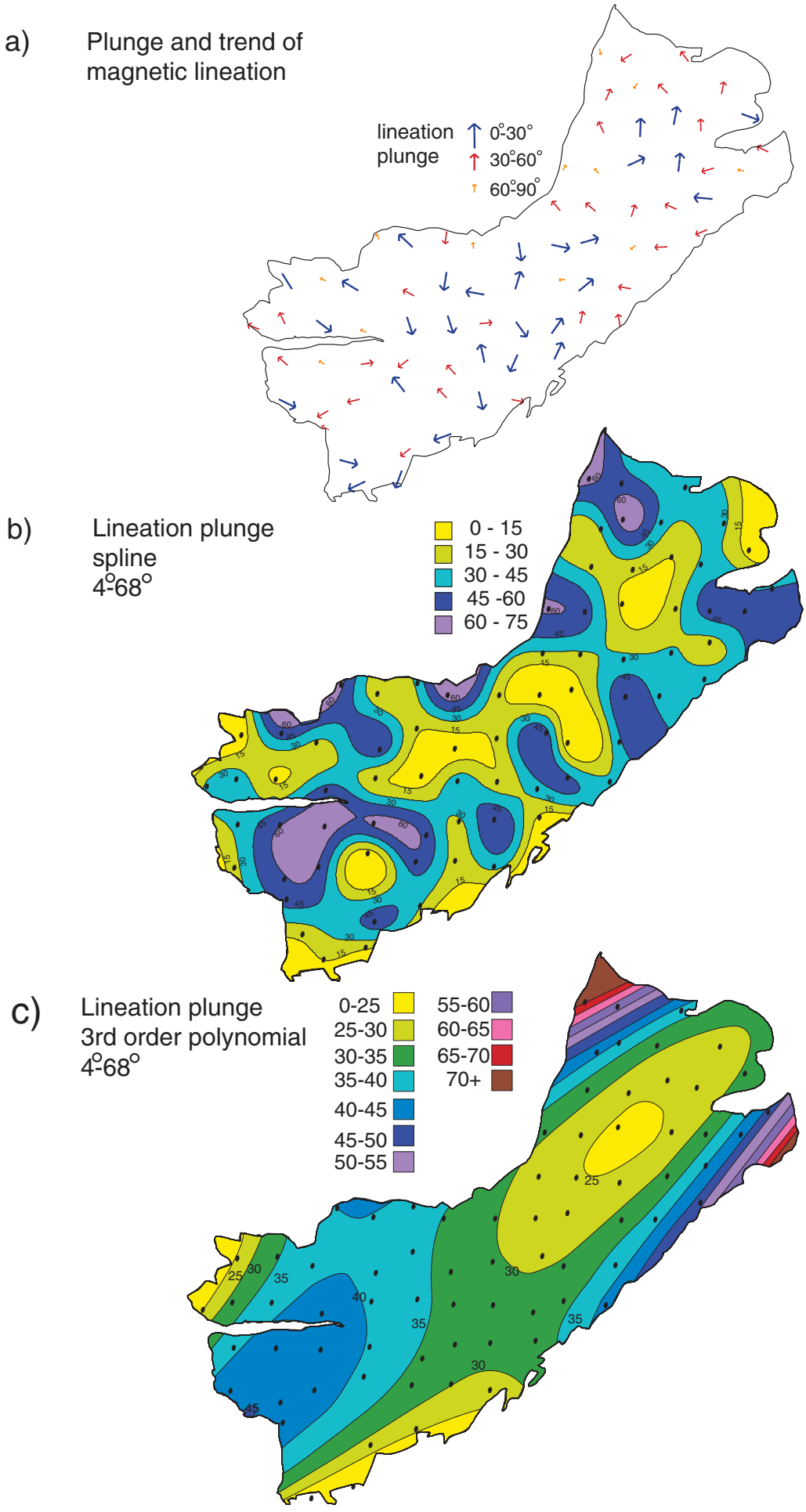

Figure 20: Magnetic lineation average: a) magnetic lineation plunge and trend; b) lineation plunge created by spline function; c) lineation plunge created by 3rd order polynomial function

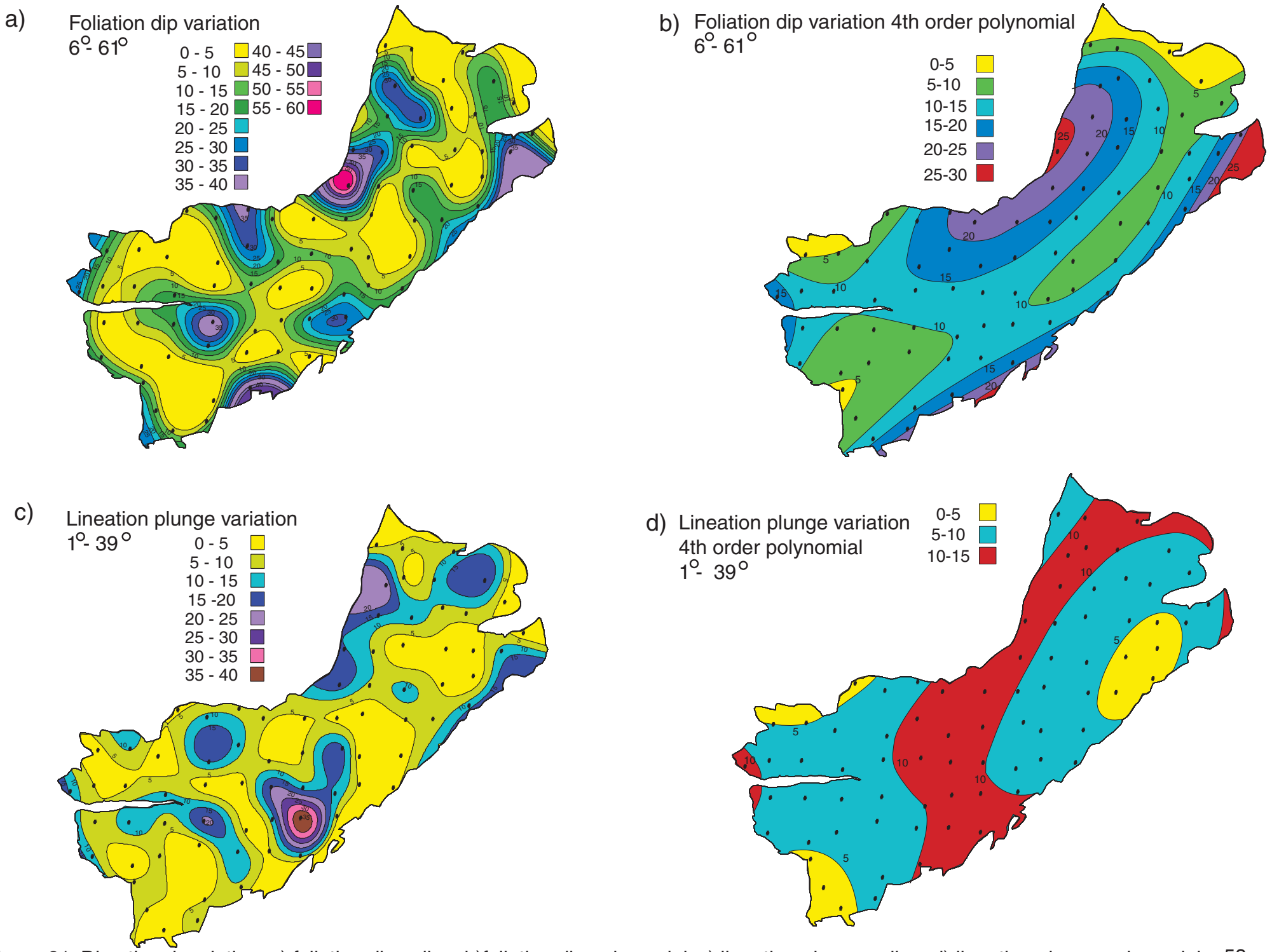

Figure 21: Directional variation: a) foliation dip spline: b)foliation dip polynomial; c) lineation plunge spline; d) lineation plunge polynomial

KILOMETER AND METER SCALE HETEROGENEITY

Heterogeneity of scalar and directional AMS parameters vary between sites and between A and B cores within individual sites. Variation across the Mount Barcroft pluton on the kilometer and meter scale does not appear to be systematically related to any particular scalar or directional magnetic parameter.

Heterogeneity of scalar parameters (Km, P%, T, F%, L%)

The map distribution of scalar and magnetic parameters does not seem to be controlled by any single factor. In most AMS based pluton studies, susceptibility (Km) and/or anisotropy (P%) govern the overall magnetic systematics. In the case of the Mount Barcroft pluton, a high degree of variation in scalar magnetic parameters across the pluton and between the A and B cores in individual sites is present. Heterogeneity on the kilometer and meter scale is probably controlled by a complex variation in minerals carrying the magnetic signature.

Susceptibility (Km) (Fig. 6a) does not seem to exert any control on degree of anisotropy (P%) (Fig. 8a), T shape (Fig. 10a), foliation anisotropy (F%)(Fig. 12a) or lineation anisotropy (L%) (Fig.13a). There is no obvious correspondence between sites based on susceptibility as related to the other scalar parameters, other than the exceptionally low values for magnetic susceptibility values in the western part of the pluton. The T shape parameter (Fig. 10a) does seem to correlate with anisotropy (P%) (Fig. 8a), foliation development (F%) (Fig. 12a) and lineation development (L%) (Fig. 13a), especially in the east to central portion of the pluton. Frequency histograms for susceptibility (Km) (Fig 6a), anisotropy (P%) (Fig. 8a) and foliation anisotropy (F%) (Fig. 12a) display a wide range of values not present in the linear anisotropy (L%) (Fig.13a) histogram. The initial low value peak in susceptibility (Fig. 6a) may, in part, be the expression of the paramagnetic mineral contribution to the over-all AMS magnetic signature.

Variation between A and B core data at specific sites, utilizing the spline function, readily illustrates many correlations between susceptibility (Km) (Fig. 14a) and other scalar parameters,

P%, F% and L% (Figs. 14c, 14g, 14i) and partially associated with T shape (Fig. 14e). Similar distributions of high variability values are indicated in the central to eastern sections of the pluton for Km, P%, F% and L%. The map distribution of high variability values for T shape (Fig. 14e) are indicated in domains adjacent to southern and western pluton contacts, and in coincident domains to Km high variation values along the northernmost, northwest pluton margin. The similarity in map distribution of many of the within-site magnetic parameters variation is puzzling. High within-site variation for magnetic susceptibility parameters both, between and within sites (Figs. 6, 14a, 14b) does not coincide with the distribution of directional parameters (problem sites, orientation, fabric type).

Variation between A and B core using the 4th order polynomial function, display similar distributions of high variation values for P%, F%, L% (all the anisotropy measures) within the domains along the eastern, southern and north-central pluton contacts (Fig. 14). Both susceptibility (Km) and T shape map distributions of variation between cores are less correlative with the anisotropy measures. High variation values for susceptibility lie in domains along eastern and northwest-central pluton margins with low variation values limited to the southwest pluton margin, but not extending up into the central part of the pluton (Fig. 14b). T shape map distributions of variation indicate high values along the southern, extreme west and northernmost northwest pluton margins. Lower T variation values are recorded along the northeast pluton margin and in a complicated "Y" shaped domain in the west-central part of the pluton (Fig. 14f). As a general rule, greater within-site variability values are recorded along the pluton margins, and a lower variability typifies the pluton interior.

Differences between A and B core fabric type and orientation

Different AMS fabric types and orientation in A and B cores at individual sites provides additional evidence for meter-scale heterogeneity across the Mount Barcroft pluton. Problem

sites identified early in the project (Fig. 15) were one of the first signs of complex magnetic mineral signatures.

AMS shape fabric categories

The shape fabrics of the Mount Barcroft pluton are variable both within and between sites. With further comparison of A and B cores at individual sites, it became evident that different shape fabrics and orientation are present. Sites were divided into eight different categories based on fabric types and strengths represented by A and B cores at individual sites (Fig. 22).

Type 1- Strong coincidence between principal susceptibility directions in A and B cores.

Type 2- Oblate susceptibility ellipsoid where k3 is coincident for both A and B cores.

Type 3- Prolate susceptibility ellipsoid where k1 is coincident for both A and B cores.

Type 4- Distinctively different ellipsoids shapes in A and B cores.

Type 5- Different ellipsoid shapes in A and B cores, but broad coincidence between k1, k2, k3 within A and B cores.

Type 6a- Different (minor) ellipsoid shapes in A and B cores, but moderate coincidence between k1, k2, k3 within A and B cores.

Type 6b- Random distribution of k1, k2, k3 in one core and either broad or weak coincidence between k1, k2, k3 within the other cores.

Type 7a- Similar susceptibility ellipsoid shapes in A and B cores with broad coincidence between k1, k2, k3 within A and B core.

Type 7b- Similar susceptibility ellipsoid shapes in A and B cores with one broad and one weak coincidence between k1, k2, k3 within A and B cores.

Type 8- Random principal directions in both A and B cores.

Based on histograms of identified fabric types (Figs. 22b, 23a) approximately 60% of the sites have distinguishably different fabrics in A and B cores (Types 4, 5, 6a, 6b). Fabric types are coded by color and mapped at sites in Figure 23b. The pluton-scale distribution of within site variability of mismatch between susceptibility ellipsoids in A versus B cores at individual sites is

indicated in Fig. 23c. The distribution of where similar fabrics are recorded at specific sites crudely approximates the fold shape of the magnetic foliation form-line map and associated dome in the western pluton section (c.f. Figs. 23c and 18a respectively).

Orientation mismatch between A and B cores

Orientation differences in k1, k2, k3 between A and B cores at individual sites were noted in the initial stages of this project as the problem sites (Fig. 15). During a later visual inspection of sample site stereoplots, orientation mismatch between the A and B cores was identified in 20 of the 76 sites. The distribution is mapped in Figure 24a where orientation mismatch ranges from 15° – 180°. A frequency histogram of the degree of orientation mismatch is presented in Figure 24b. 90° and 180° degree orientation mismatch between A and B cores can be attributed to errors in hand sample orientation, field measurements, incorrect measurement of core orientations and marking of cores in the lab prior to AMS measurements in Toulouse. Two of the sites have 90°orientation mismatch between A and B cores and three have 180° errors. Nine sites have approximate variation between A and B cores < 25°, three between 25°-50°, two between 50°-75° and one at 140°. Orientation errors of this nature cannot be so easily explained by human error. Possibly these variation are due to strong magnetic field discrepancies unrecognized at the outcrop, in hand samples and/or due to complex interaction of magnetic minerals or mineral alterations within the cores themselves.

Domain distribution of sites with probable orientation mismatches between A and B cores are mapped in Figure 24c. The distribution of orientation mismatch is apparent in two east-to-west-trending domains in the north and central sections of the pluton. Additionally, two small domains are evident in the south and west, close to the pluton contact.

Errors in orienting hand samples and cores could be the cause of angular mismatch between directional data in A and B cores. However, this cannot explain the differences in scalar parameters of Km, P%, T, F%, and L% between A and B cores.

Variation in opaque mineral grain shape

Reconnaissance mapping of opaque mineral shapes within thin sections of the Mount Barcroft pluton (Fig. 5b) indicate a degree of opaque shape variation across the pluton. As previously noted, four distinct types of opaque mineral grain shapes were identified. Obvious variations in opaque grain shape support the suggestion that magnetic mineral type is highly variable across the pluton. Opaque minerals are spatially associated with iron-rich silicates. The presence of four opaque mineral types strongly indicates that the local AMS fabric is the product of a complex magnetic signature.

Petrographic heterogeneity

Petrographic heterogeneity across the Mount Barcroft pluton is documented by previous studies (Ernst and Hall, 1987; Ernst et al., 1993; Ernst, 2000; 2002; Ernst et al., 2002). The Mount Barcroft pluton is composed of a complex suite of rock types ranging from metadiorite, gabbro/diorite, granodiorite, to rare alaskite, formed by fractional crystallization and mixing of high and low silica members (Ernst, 2002; Ernst et al., 2002, 2003). Contacts between rock types are gradational across the pluton and not readily distinguishable at outcrop. Based on the presence of inclusions, intrusive crosscutting relationships, and differing degrees of recrystallization, the gabbro/diorite and metadiorite phases are considered to represent the earliest stage of emplacement. Pulses of granodioritic magma were emplaced and crystallized during the cooling stages of pluton evolution, whereas rare, residual felsic alaskite aplite pods and stringers crystallized in the later stages of pluton cooling (Ernst et al., 2002; 2003).

In the Sierra Nevada batholith, two types of magmatic systems, heterogeneous and homogeneous, have been identified, based on correlation between isotopic and bulk rock compositions (Ernst et al., 2003). Homogeneous magma systems tend to dominate Cretaceous Sierran magmatism, and are characterized by a lack of correlation between isotopic compositions and bulk compositions. Homogeneous systems are interpreted as resulting from little or no assimilation or mixing with pre-Mesozoic crustal rocks. Widely ranging isotopic compositions that correlate with bulk rock compositions, characterize heterogeneous systems. Heterogeneous magmas are interpreted to be the result of significant mixing and assimilation with pre-Mesozoic crustal rocks. In the case of the Mount Barcroft pluton, variable isotopic composition data, associated with variable bulk rock compositions supports a pluton-wide heterogeneity of magnetic mineral types (Ernst et al., 2003).

Discrete magma pulses as an explanation of pluton heterogeneity

It is possible for both kilometer and meter scale heterogeneity of both scalar and directional magnetic parameters to be explained by injection of discrete pulses of magma over the time of emplacement (Fig. 25). In this model initial magma pulses of distinct composition with a specific magnetic mineralogy, and viscosity enter the magma chamber and assume a fabric (oblate, prolate, or grouped) (Fig. 25a). A second, later less, viscous magma pulse of different composition enters the chamber and is forced upward engulfing the previous pulses. This "squeeze play" of the younger magma pulse, results in flattening and formation of oblate fabrics of different orientation (Fig. 25b). The interaction of these small, discrete magma pulses during emplacement of the Mount Barcroft granodiorite could provide an explanation for the different fabrics types and orientations within sites on the meter scale (A and B cores) (Fig. 25c) and between sites on the kilometer scale.

The model of injection of discrete magma pulses over time of emplacement also accommodates variations within sites between the A and B cores, in terms of scalar data (Km,

P%, F%, L% and T); in addition to differences in documented petrographic heterogeneity, and opaque mineral grain shape across the pluton on the kilometer scale Mount Barcroft pluton. Compositional, and temporally discrete magma pulses would be supported by identification of a complex magnetic mineralogy of different magnetite species, variable distribution and concentration across the pluton on the meter and kilometer scale.

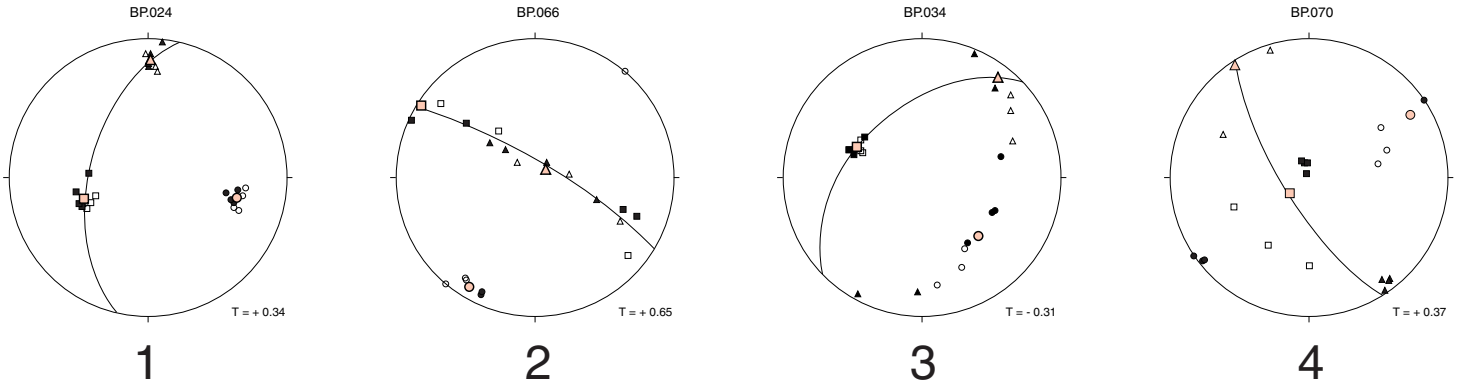

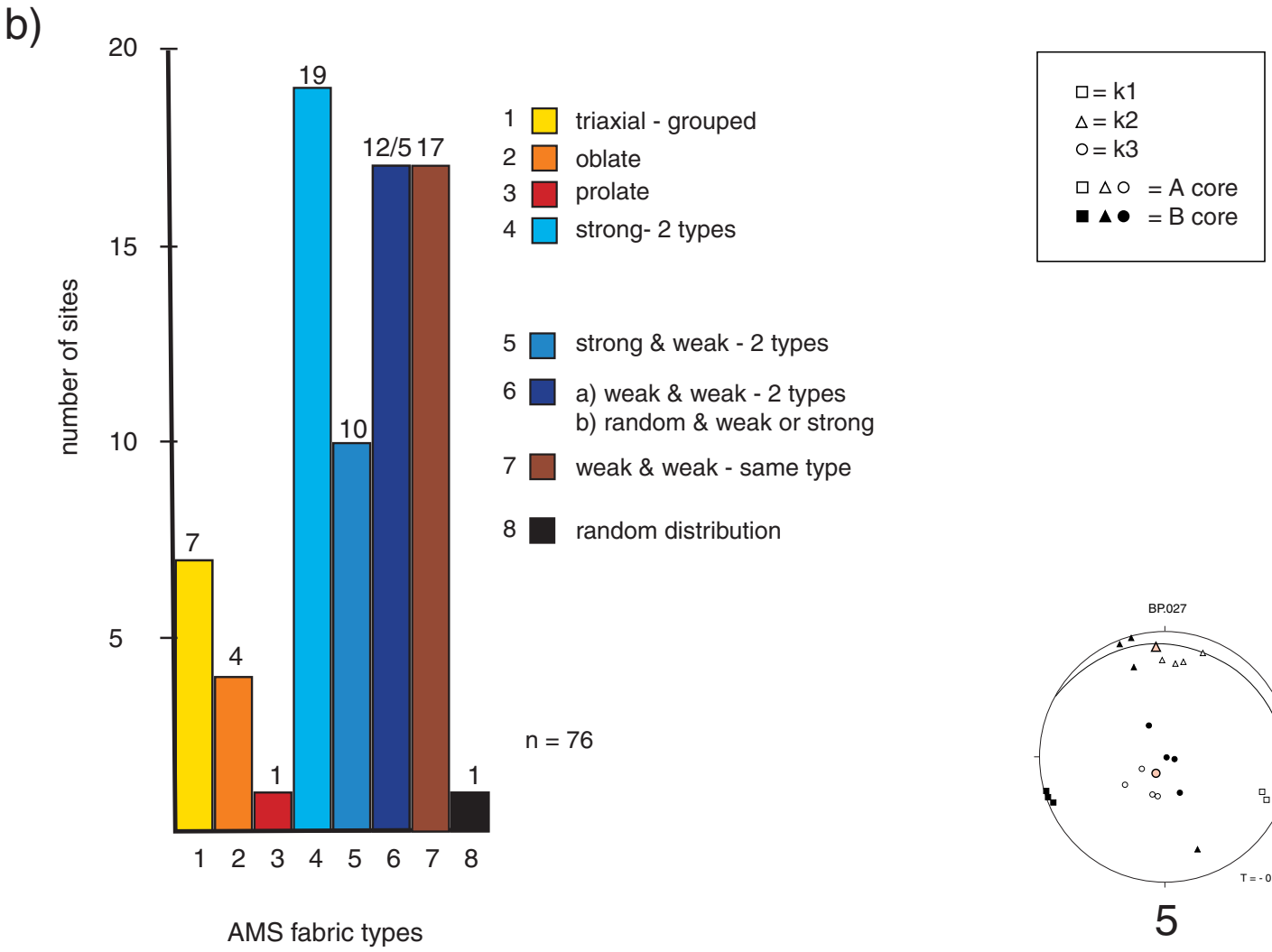

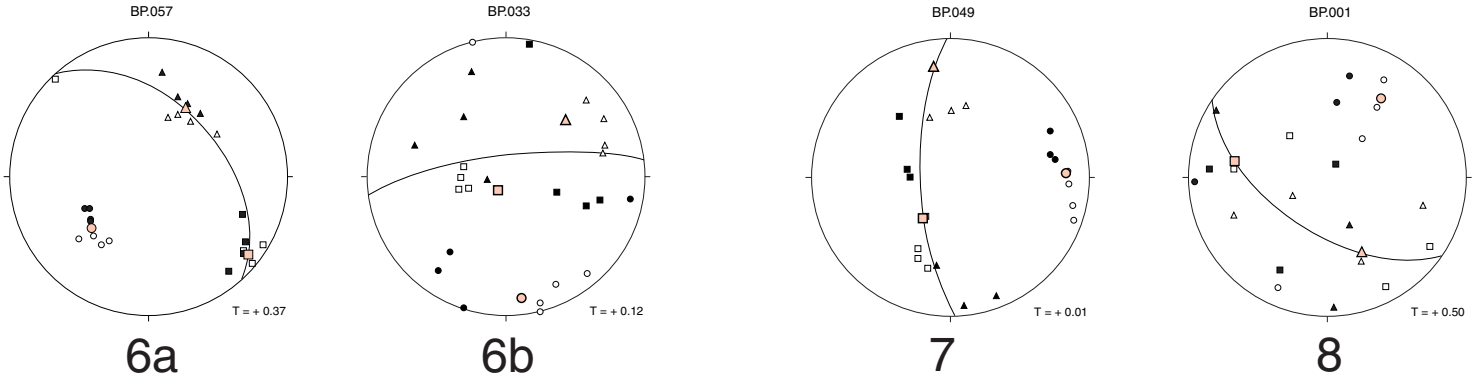

Figure 22: AMS fabric types: a)AMS fabrics types-comparison of A and B core; b) fabric type histogram

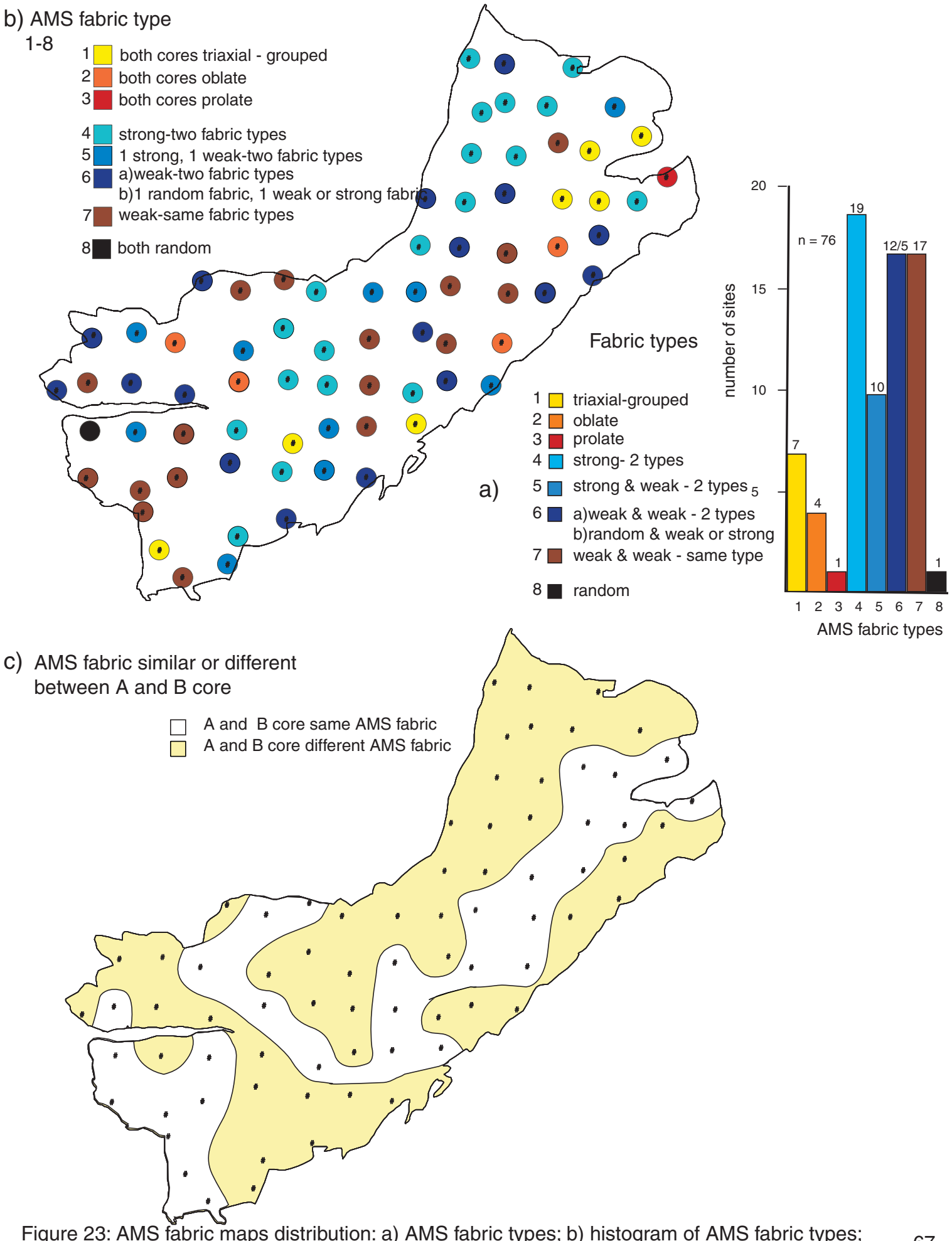

Figure 23: AMS fabric maps distribution: a) AMS fabric types; b) histogram of AMS fabric types; c) different fabrics in A and B cores

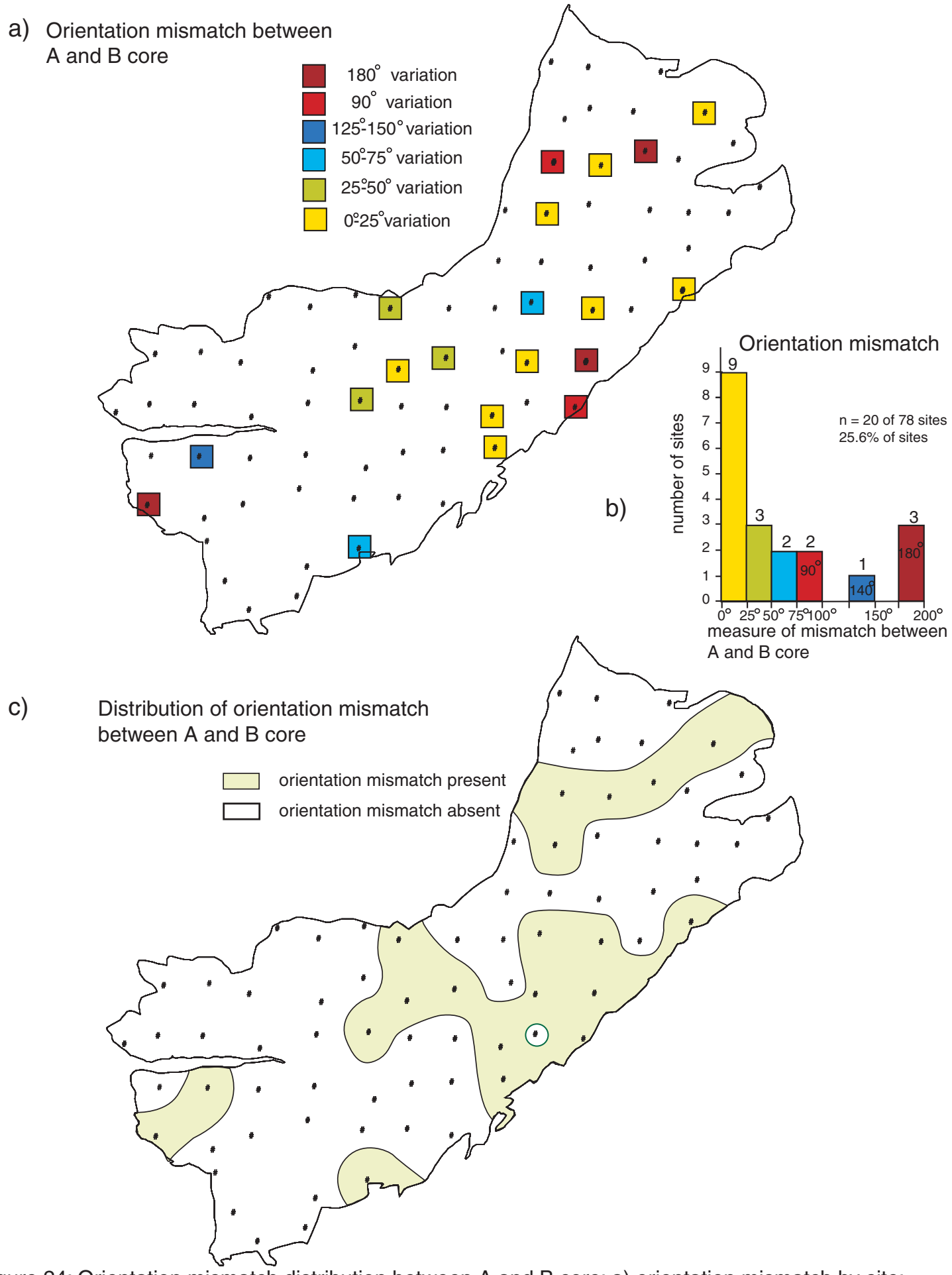

Figure 24: Orientation mismatch distribution between A and B core: a) orientation mismatch by site; b) histog ram; c) absence or presence of orientation mismatch

a) 1st magma pulses in chamber (more viscous), result in prolate fabric (scale in meters)

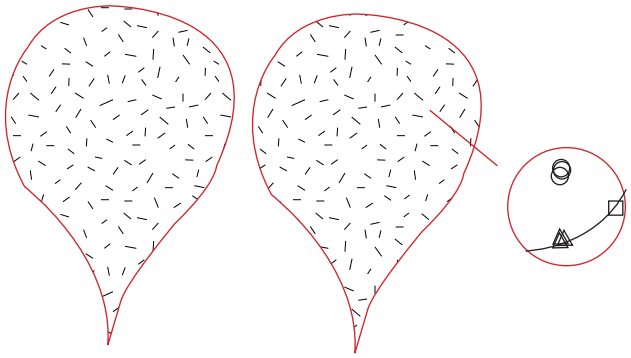

b) 2nd magma pulse (less viscous) intrudes and is forced to flow around inital pulses generating oblate f abrics of varying orientations

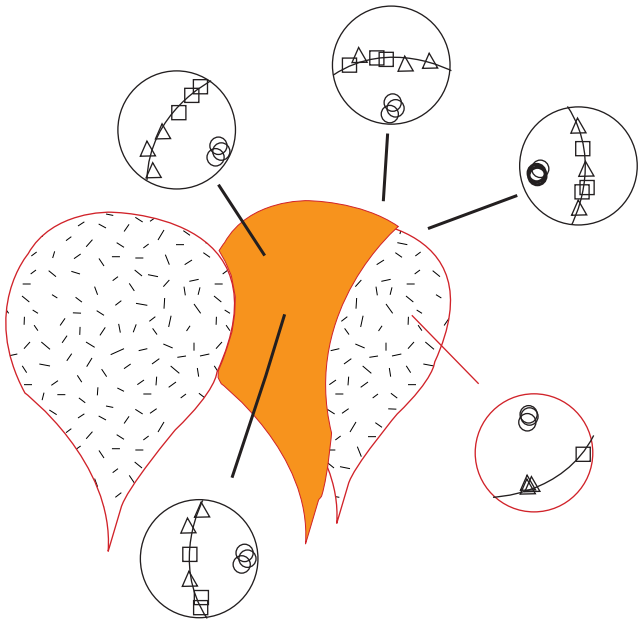

c) present day land surface with A and B core within an individual site (scale in meters)

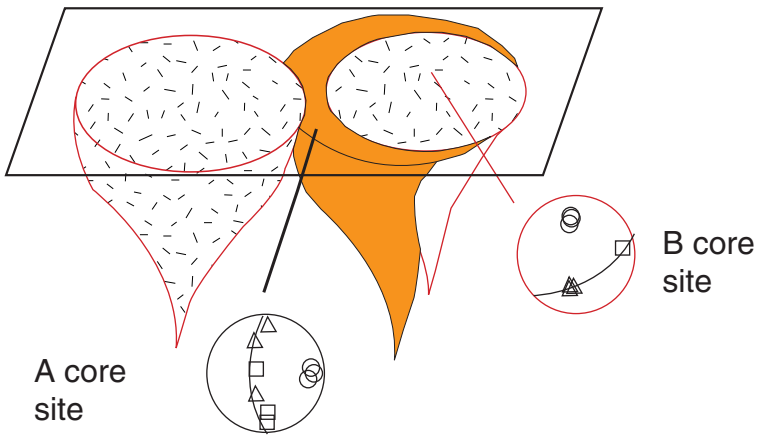

Figure 25: Possible explaination of variation in fabric type between A and B core at individual sites

ANOMOLOUS AMS FABRIC MAGNETIC MINERALOGY AND RECOGNITION

The AMS based technique of pluton analysis is founded on the assumption that fabrics are relatively homogeneous on the kilometer scale. Grain-shape fabrics are assumed to, and tend to be reflected in the AMS signature. Igneous rocks characterized by non-systematic heterogeneous magnetic signatures have been identified and studied (Rochette, et al., 1992; Borradaile, 2001). These studies have centered on the magnetic mineral dynamics, identified specific patterns associated with complex magnetic mineral interactions (Borradaile, 1988; Rochette et al., 1992; Borradaille and Henry, 1997; Rochette et al., 1999; Borradaile, 2001), and developed procedures to remove "noise" within the AMS signature (Rochette et al., 1992; Borradaile, 2001). Once normalized for the magnetic mineral species, and the spatial distribution of these minerals is identified, the filtered AMS data can be analyzed and interpreted.

Rocks containing more than one type of iron-bearing mineral result in complex AMS fabrics. Distribution, size and type of iron-bearing minerals in the rock can also result in distortion of the AMS fabric (Rochette et al., 1992; Borradaile and Henry, 1997). Interpreting AMS data requires identification and characterization of all the magnetic minerals contributing to the AMS signal.

An anomalous AMS signature in scalar and directional data sets has been documented and studied by numerous researchers working with variably deformed igneous rocks (Haragraves et al., 1991; Rochette et al., 1991; Benn et al., 1993; Ferre et al., 1999, 2002; Borradaile and Gauthier, 2003). The source of such anomalous data has been attributed to complex and/or variable magnetic mineral content, where some mineral species interact to disrupt and distort the magnetic signal. Anomalous magnetic susceptibility measurements in rocks are characterized by the presence of inverse and intermediate fabrics, which may be difficult to discern. Rochette and Rochette et al.

(1992, 1999) attribute variation in magnetic susceptibility characteristics to variation in matrix (typically paramagnetic) or ferromagnetic minerals. Variation in magnetic susceptibility may be attributed to the presence of more than one magnetic mineral and/or interaction between different magnetic mineral species (Rochette et al., 1992).

Single-domain, pseudo-single-domain and multidomain magnetite

Different species of magnetite can exert a potentially strong effect on magnetic susceptibility. Multidomain (MD), and single-domain (SD) and pseudo-single- domain (PSD) magnetite grains occur in igneous rocks. The magnetic susceptibility of coarse-grained granites tends to be dominated by multidomain magnetite behavior (Benn et al., 1993; Archanjo et al., 1995). The specific susceptibility ellipsoid for multidomain magnetite is proportional to the grain shape ratio (Uyeda et al., 1963)(Fig. 26). Therefore in granites containing exclusively multidomain magnetite, the shape fabric controls the magnetic fabric (Fig. 27). Multidomain magnetite tends to produce normal fabrics in accordance with the matrix silicate minerals (Fig. 27). Single-domain magnetite can produce anomalous magnetic ellipsoids to grain shape fabrics (Fig. 27) because they have minimal susceptibility along their grain shape long axis with maximum susceptibility along their grain shape short axis (Rochette et al., 1992)(Fig 26). Typically single domain magnetite are small grained while multidomain and pseudo-single-domain magnetite are larger grained. The limited size range of the single domain magnetite suggests that the magnetic signature is often carried by the pseudo-single-domain which contain imperfections in there crystal lattice which restrict/pin the creation/movement of domain walls (Tarling and Hrouda, 1993). Thus, the overall magnetic behavior of the large sized pseudo-single-domain magnetite is as single domain magnetite (Tarling and Hrouda, 1993).

Magnetic susceptibility magnitude and orientation can also be influenced by how closely the magnetite grains are spaced. Multidomain magnetite grains in close proximity to each other

seem to have the greatest influence on disruption of the AMS signal (Fig. 26). When grains are aligned with a space of less than two grain-diameters between adjacent grain centers, the susceptibility magnitude increases parallel to the alignment of the grains (Gregoire et al., 1995)(Fig. 26)(Fig. 27d). As a result, susceptibility, and K1 (magnetic lineation) values increase disproportionately to the other magnetic ellipsoid axis (K2 and K3)(Fig 27d).

Borradaile (2001) noted that for homogeneous magnetic fabrics that are well sampled, that the orientation and distribution of the principal magnetic ellipsoid axis should be orthoganol concentrations. In the event that this is not the case, and orthorhombic symmetry is lacking, then multiple or heterogeneous fabrics may be indicated. Distortion of the AMS signal may be the result of a small population of high susceptibility minerals that deflect the average away from the majority of the samples. Normalizing of the high susceptibility samples by bulk susceptibility overcomes this distortion of the overall signal (Fig. 28). However, the orientation of the high-susceptibility mineral may be indicative of an event of subfabric that may be of significance, and thus, not discarded (Borradaile, 2001).

It has been noted that the magnetic fields of magnetite inclusions within silicates may preferentially interact, increasing the bulk susceptibility magnitude. Conversely, magnetite inclusions within minerals, in a side-by-side configuration may lower susceptibility magnitude in the K1 direction (Archanjo and Bouchez, 1997; Bouchez, 1997). Depending on the type of magnetite forming the inclusions, this can further complicate the AMS signature (Borradaile and Werner, 1994).

Normal, inverse and intermediate magnetic fabrics

Matrix minerals, typically paramagnetic mafic silicates (such as tourmaline, cordierite, iron-bearing carbonate, goethite) can influence magnetic susceptibility behavior and produce inverse, as opposed to normal fabrics (Fig. 28) (Rochette et al., 1992). Crystallographic control of grain shape and susceptibility results in maximum susceptibility along the long dimension of

the mineral grain and minimum susceptibility along the short dimension of the grain. Based on this grain relationship, matrix minerals (biotite, pyroxene, amphibole) tend to have preferred orientation that results in what is defined as the "normal" characteristic magnetic fabric. Hematite, pyrrhotite, multidomain magnetite and related cubic iron oxides produce normal fabrics (Fig. 29a). Fabrics defined as "inverse" are often the result of a reversal of the maximum and minimum susceptibility axes for the iron-bearing mineral grain in reference to the grain shape ratio. Iron-bearing minerals where inverse fabrics are common include single-domain magnetite, carbonate, goethite, cordierite and tourmaline. Inverse fabrics have been clearly identified where grain shape fabric or other structural markers are obvious, and the magnetic fabric is rotated 90° to the known "normal" fabric (Fig. 29b). Apparently, the Mount Barcroft pluton has evidence for normal AMS fabrics. However what is not clear is to what degree inverse fabrics are present without knowledge of the magnetic minerals present, an observable grain shape fabric and/or lacking definite, proximal structural controls (pluton margins).

Although inverse fabrics may be attributed to the interaction between grains of a single mineral species, intermediate fabrics seem to require the mixing of different magnetic minerals (Rochette, et al., 1992). Intermediate fabrics are apparent when principal susceptibility directions of individual samples are interchanged with respect to the other samples within a given site (Fig. 29c). Alternatively, intermediate fabrics can result in cases where the intermediate magnetic susceptibility axis (k2) is perpendicular to the grain shape foliation plane (Rochette, et al., 1992). Single-domain magnetite in ferromagnetic granites and tourmaline, goethite, iron-bearing carbonate, or cordierite in paramagnetic granites may produce both inverse and intermediated fabrics.

Intermediate fabrics are typically associated with inverse fabrics, and are apparently associated with the interaction between two or more mineral species. In paramagnetic granites intermediate fabrics can be the result of interaction between biotite and amphibole. In

ferromagnetic granites the interaction of single-domain, pseudo-single-domain and multidomain magnetite can also produce intermediate fabrics.

Mount Barcroft pluton magnetic fabrics

The source of the AMS magnetic signature within the Mount Barcroft pluton was originally assumed to be relatively simple, based on previous AMS studies of Jurassic and Cretaceous plutons in the White-Inyo Range. In the White-Inyo Range plutons, magnetite (probably multidomain) is the primary source of magnetic signature (Morgan, 1998; Vines, 1999; Saint Blanquat et al., 2001). In the Mount Barcroft pluton this is probably not to be the case, given the highly heterogeneous and variable nature of the scalar and directional magnetic parameters on the kilometer and meter scale, and fabric type variation on the meter scale. Compared to other plutons in the White-Inyo Range, the minerals carrying the magnetic signature in the Mount Barcroft pluton are much more complicated in their type, distribution and interactions.

The Mount Barcroft pluton AMS directional parameters presented in the stereonets (Appendix 3 and 4), indicate a highly disrupted magnetic susceptibility signal both within and between sites. Intermediate fabrics, where swapping of principal ellipsoid axes exists between samples at sites, is observed in 21 of the 76 sites, randomly distributed across the pluton. Variation in shape fabric type and orientation between A and B core at individual sites may be the result of the interaction between single-domain, pseudo-single-domain and multidomain magnetite grains (Fig. 27). These magnetic effects could generate inverse fabrics and influence the formation of intermediate fabrics by interaction of both individual single-domain magnetite grains and multidomain magnetite grains.

Intermediate fabrics in the Mount Barcroft pluton could be produced by tourmaline, which has been documented as an accessory mineral in the pluton. However, unless tourmaline is present in modal percentages > 10 %, this is unlikely to result in the formation of inverse fabrics

(Ferre, personal communication, 3/2003). Inclusions within paramagnetic mafic silicates, such as pyroxene, amphibole and biotite have demonstratively disrupted the magnetic signature in some plutons (Borradaile and Werner, 1994: Lagroix and Borradaile, 2000). In the Mount Barcroft pluton, inclusions of needle-shaped opaque minerals aligned along basal cleavage planes of biotite have been identified in thin section. However it is unclear if the needle inclusions are magnetite or rutile, and therefore if they would have an impact on the AMS signature.

More significantly, the Mount Barcroft pluton probably contains considerable populations of both single-domain and multidomain magnetite. Numerous sample sites exist where opaque grains are present as small euhedral crystals associated with mafic silicates (especially in the western portion of the pluton) and may be single-domain magnetite grains. Possibly the inverse relationships and distribution effects are influencing the AMS signal at these sites. Multidomainal magnetite is probably characteristic of the large, interstitial "blobs" of opaque mineral grains identified at many sites, particularly in the eastern part of the pluton.

Mineral content is highly heterogeneous across the pluton, and opaque grain types vary widely between adjacent sites. These features are consistent with variation both within and between sites in magnetic susceptibility values, fabric type and orientation.

Alteration process influence on Mount Barcroft pluton scalar parameters

Further confounding the magnetic signature in the Mount Barcroft pluton are the generally low susceptibility values in the western part of the pluton (Figs. 6b, 6c). The alteration of Ca-plagioclase interacting with primary magnetite to produce epidote, may have caused this marked decrease in susceptibility. Possibly calcium (Ca) in the plagioclase and Fe^{3+} ions produced during the oxidation of magnetite to titanium oxides ilmenite and anatase (Dr. J. Craig, personal communication 7/2002) may have combined with excess silicon (Si) to form epidote. This reaction would result in lowering the susceptibility magnitude where alteration is present. The transformation of magnetite to titanium oxide would effectively lower the susceptibility to

the paramagnetic levels observed as well as reducing the signal strength of anisotropy (P%), shape factor (T), planer fabric (F%) and linear fabric (L%).

$2Fe_30_4 + 12CaAl + 12SiO_2 + 6\ H_20 + 02 = 3Ca_2FeAl_2Si_32Si_3O12(OH)$
magnetite + anorthite + quartz + water + oxygen = epidote (Robinson et al., 1985)

Alteration due to deuteric processes is indicated by the development of epidote from Ca-rich plagioclase as the pluton cooled through the sub-solidus and supports the proposed removal of Fe^{3+} from magnetite to form epidote.

Future research

Variation in scalar and directional AMS parameters, both within and between sites, and on the scale of individual core sample pieces, is most probably the result of a highly heterogeneous magnetic mineral assemblage. Additional work on the magnetic mineral content is required to determine the carriers, quantify their relative contributions, and spatially map their location (possibly on the meter scale within sites or the millimeter scale within core pieces). Until such work is completed, it is difficult to make strong conclusions concerning the relationships between the pluton margins and internal magnetic planer and linear fabrics.

Specifically what needs to be done includes the following: 1) Identification of the specific magnetic mineral species that are present in the pluton (rock heating and cooling experiments, magnetic remanance studies). These studies will help clarify the relative degree of mutidomain versus single-domain versus pseudo-single domain magnetite contributions to susceptibility, and more precisely distinguish the relative contributions of paramagnetic and ferromagnetic minerals. 2) Determine if the interaction between magnetite grains is occurring on a millimeter scale within cores. This can be achieved by taking all of the existing core pieces and running them through the AMS procedure again with cores rotated 180°. A different statistical output of the AMS analysis of the same core piece would indicate that clustering of magnetite grains is occurring, thus resulting in the alteration of the magnetic signal on the millimeter scale.

3) Normalizing samples by their bulk susceptibility in the event that different populations of magnetic minerals are present in the pluton, may assist in reducing the amount of deflection of the magnetic ellipsoid per core piece from the average (Fig. 28). 4) Previous petrographic work has been limited to determination of the primary and accessory minerals in the Mount Barcroft pluton, however, systematic analysis of the opaque minerals has not been undertaken to date. Future reflected light studies of opaque minerals to determine the range of oxide species and their distribution across the pluton, may help in clarifying the relative contributions of specific oxides to magnetic susceptibility both within and between sites. 5) Thin section analysis and comparison of opaque grain types, and degree of concentration within A and B cores at individual sites could assist in mapping the distribution of single domain, pseudo-single-domain and multidomain magnetite across the pluton. 6) Electron micro-probe work on inclusions within the mafic silicates is needed to determine if the inclusions are of magnetite, and if so what magnetite species, and if not what other paramagnetic oxides are present. This is particularly true for biotites containing needle-like inclusions (rutile or magnetite).

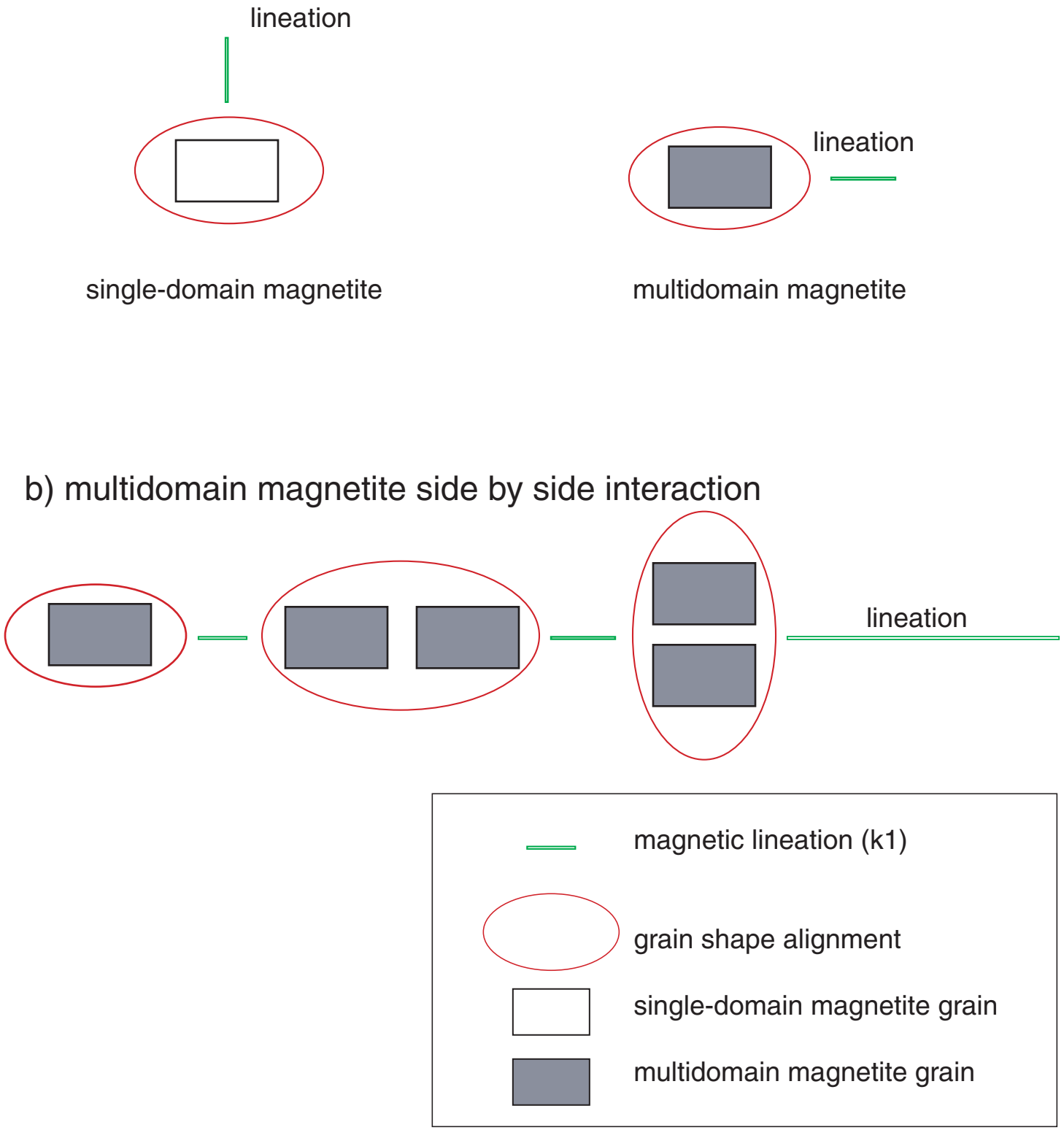

Figure 26: Single-domain and multidomainal magnetite grain shape to magnetic lineation (k1) relationship; adapted from Gregoire et al., 1995.

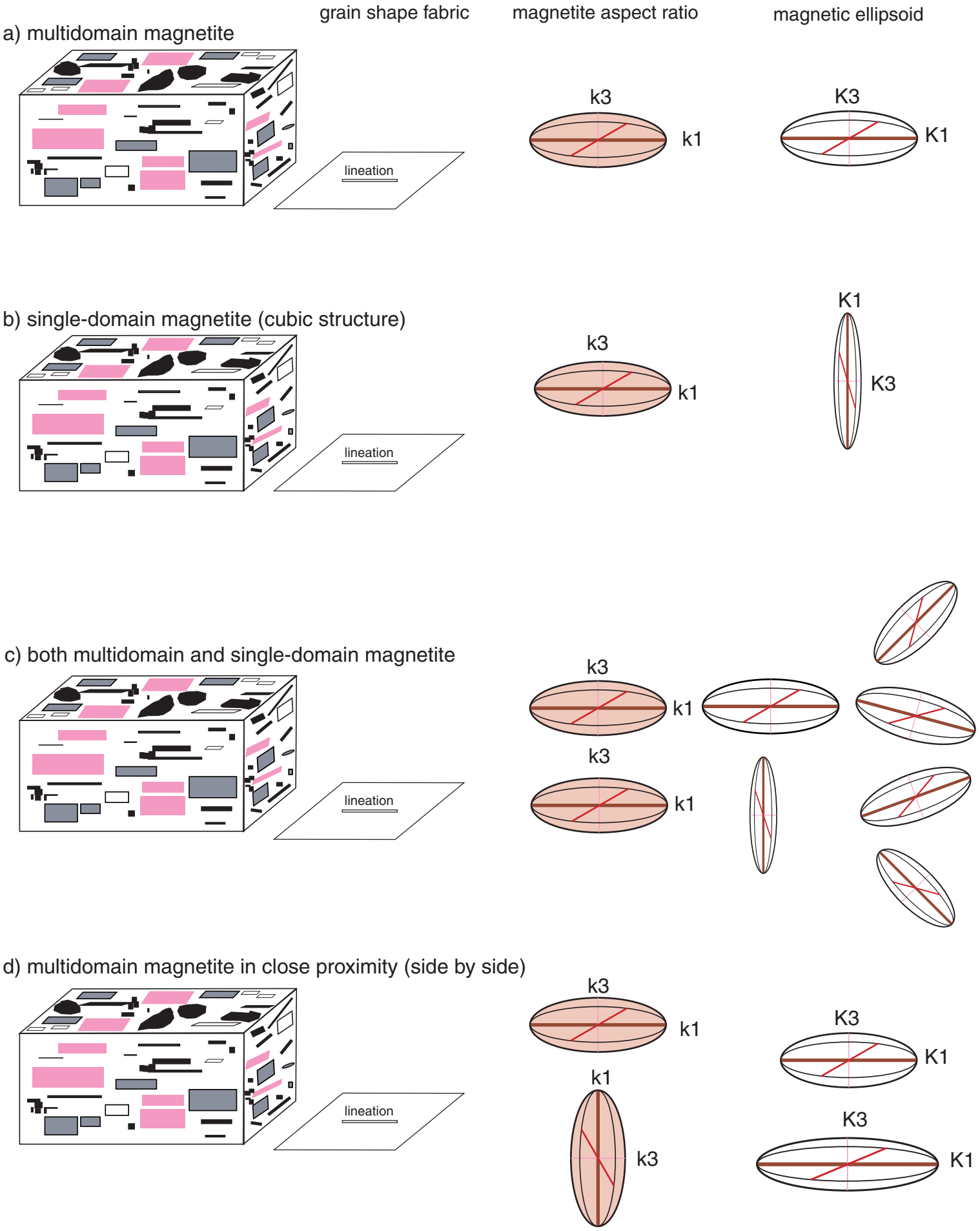

Figure 27: Relationships of same grain shape fabric to aspect ratio and magnetic ellipsiods for different populations of multidomain and single-domain magnetite

a) not normalized

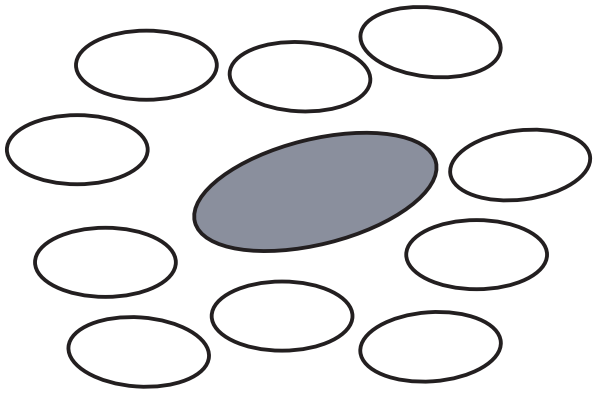

b) normalized

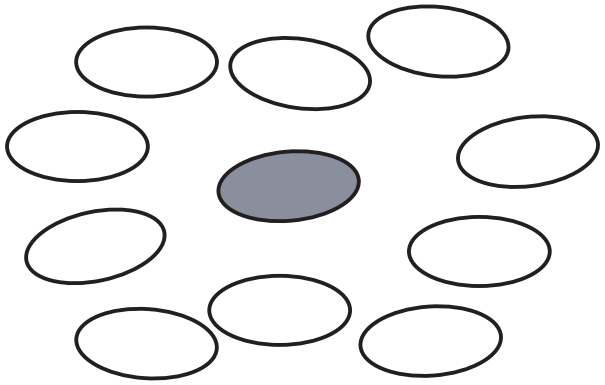

c) not normalized

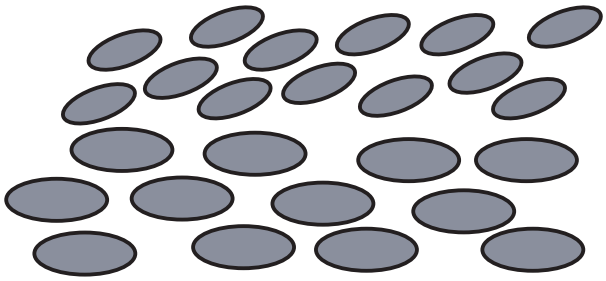

d) normalized

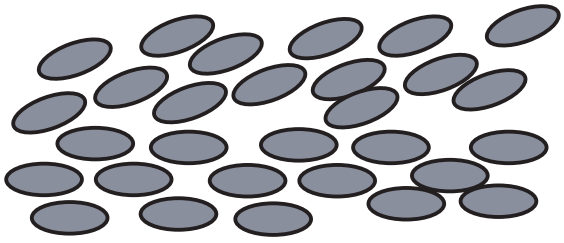

Figure 28: Effects of normalizing AMS magnitudes of samples to suppress the influence of high susceptibility subfabrics; adapted from Borradaile, 2001

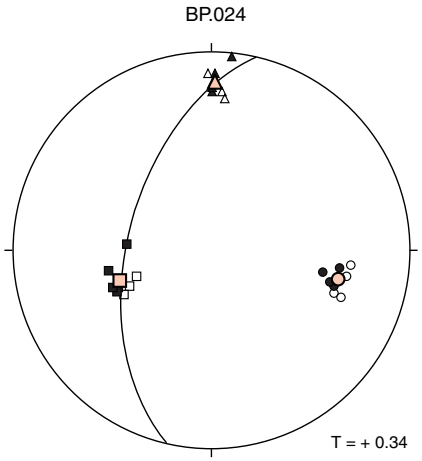

a) Normal fabrics

□ = k1

△ = k2

○ = k3

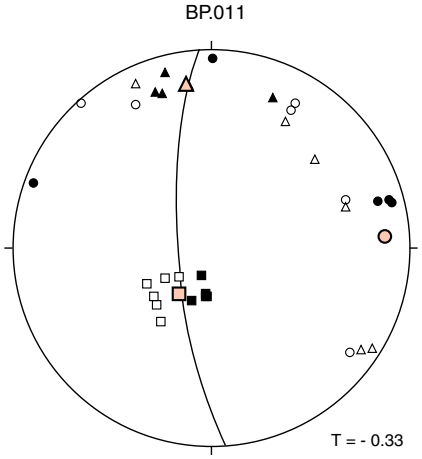

b) Possible inverse fabric at site where foliation is oblique to surrounding sites and pluton margin. Unresolvable unless mineralogy identified and structural controls present.

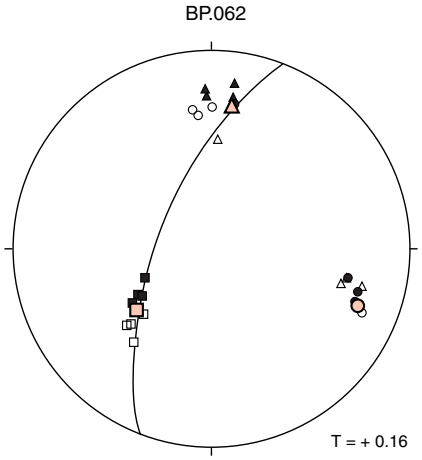

c) Intermediate fabrics where reversal of axis between A and B cores and within A core.

Figure 29 a) normal; b) inverse (possible); c) intermediate magnetic fabrics

GEOLOGICAL INTERPRETATION OF MICROSTRUCTURES AND MAGNETIC SUSCEPTIBILITY

Numerous petrographic, metamorphic, structural, and field mapping studies have contributed to our understanding of emplacement of the Mount Barcroft pluton, geometry of the Barcroft Structural Break, and the Phanerozoic deformational history of the northern White Mountains. The addition of AMS and microstructural analyses to the Mount Barcroft pluton further contributes to these studies. Specifically, microstructural analysis has assisted in determining the cooling history of the pluton and the AMS analysis may help us understand the nature and timing of emplacement.

Microstructures

Microstructural analysis indicates that the magnetic fabric in the Mount Barcroft pluton is due to magmatic processes with a minor overprint of solid-state deformation within individual mineral grains. In thin section, the pluton lacks grain shape fabric or imbrication. Solid-state deformation is limited to individual mineral grains with strain typically indicated by very limited intracrystalline plasticity. Most solid-state deformation seems to be associated with cooling stages of the pluton, and in highly specific cases with Cretaceous magmatism along the northeast contact with the McAfee Creek pluton and in association with Cretaceous intrusions within the Mount Barcroft pluton itself.

Anisotropy (P%) as an indicator of solid-state deformation versus magmatic flow

Anisotropy measures (P% and P) have been used to distinguish between magmatic flow and solid-state deformation (Blanquat and Tikoff, 1997; Saint Blanquat et al., 2001). Microstructural analyses and consistently low anisotropy values across the pluton indicates the dominance of magmatic flow rather than solid-state deformation as the dominant process resulting in the recorded AMS signature.

Recent work in the Sierra Nevada and the White-Inyo Range provide two examples of anisotropy values that indicate solid-state deformation. In the Rosy Finch shear zone in the Sierra Nevada (Blanquat and Tikoff, 1997), samples with primarily magmatic microstructures posses average anisotropy values of P % =9% (P= 1.09). Samples with high temperature and low to moderate temperature solid-state microstructures have P% = 16% (P=1.16) to P% = 28% (P= 1.28) respectively. A study of the Papoose Flat pluton in the Inyo Mountains (Saint Blanquat et al., 2001) (Fig. 1) found that a P% of 20% (P=1.20) is a reliable indicator of a significant amount of solid-state deformation (Table 1).

Anisotropy (P%) contour maps and solid-state microstructure distributions for the Mount Barcroft pluton show minimal correlation with each other (c.f. Figs. 3d, 8a, 8b). High to medium temperature solid-state microstructures (lobate quartz and feldspar, recrystallized quartz and feldspar) (Figs. 3c, 3d) roughly coincide with high P% domains indicated by the spline function contouring (Fig. 8a). None of the microstructure distribution maps agree with high P% domains indicated by the polynomial function contouring (Fig. 8c). P% values for the Mount Barcroft pluton with a maximum average within site of 12.14% are well below the published values for P% indicating solid-state deformation. This is consistent with the microstructural evidence supporting the conclusion that magmatic processes were of primary importance in controlling magnetic fabric development in the Mount Barcroft pluton.

Solid-state deformation with cooling

Temperatures within the Mount Barcroft pluton from the time of emplacement through cooling have been determined by analysis of clino-amphiboles (Ernst, 2002) and $^{18}O/^{16}O$ thermometry (Ernst and Rumble, 2003). According to Ernst (2002) emplacement and crystallization of the Mount Barcroft pluton occurred at 10-12 kilometers depth and temperature of 760°-650° C. The pluton cooled from 545° to 395°C, at depths less than ~10 kilometers, but averaged 525°-450°C at 3 to 4 kilometers.

During recrystallization of the Mount Barcroft pluton, sub-solidus, deuteric alteration also occurred (Ernst, 2002). Solid-state microstructures and Ca-plagioclase alteration can be associated with decreasing temperature during the cooling of the pluton from emplacement through the sub-solidus to total crystallization.

Documented high temperature solid-state microstructures include chessboard extinction in quartz, and recrystallization of feldspar which must have occurred in the initial stages of pluton cooling from temperatures>500° to 550°C. Medium temperature solid-state microstructures include lobate quartz and feldspar grain boundaries and myrmekite primarily produced as temperature decreased from 550° to 400°C (Ernst, 2002) probably in the documented range from 440°-495°C. Myrmekite also may have formed at lower temperatures due to replacement processes, following alteration of plagioclase to epidote. This late, low temperature myrmekite is well developed in the western portion of the pluton.

Myrmekite is considered to have two potential origins. Simpson and Wintsch (1989) considered that myrmekite formation is the result of applied stress along grain boundaries. Hibbard (1979) proposed a magmatic origin for myrmekite located along grain boundaries. In the case of the Mount Barcroft pluton, myrmekite is notably absent in many sites (Fig. 3b) where a high degree of alteration (Fig. 5a) of Ca-rich plagioclase to epidote is evident. Alteration of plagioclase is assumed to have occurred during post-crystallization cooling as grains are generally most altered at their cores with unaltered plagioclase forming diffuse, narrow rims. Because Hibbard's model attests that myrmekite forms synchronously with final euhedral growth of plagioclase, myrmekite formation in the Mount Barcroft pluton is probably the result of applied stress. Fractures and cracks within feldspars and quartz grains are barren rather than in-filled with crystallized melt, thereby arguing against Hibbard's model (Bouchez et al., 1992). In addition, Simpson and Wintsch's stress model is compatible with the microstructures observed in the pluton.

Low temperature solid-state microstructures including kinking of feldspars (Fig. 4d) and undulose extinction of quartz (Fig. 4c) are considered to have formed during the late, low temperature stage of pluton cooling (400°-300°C).

Brittle deformation of quartz and feldspar (Figs. 4a, 4b) could have occurred during any or all of the major deformational events recognized by Hanson (1986a; et al., 1987) in the northern White Mountains following emplacement and cooling. However, it seem probable that brittle deformation occurred during the final stage of west-directed deformation associated with last period of motion along the present-day, reverse fault systems (Sabies, Barcroft, Marmot) prior to Cretaceous magmatism.

Cretaceous magmatism may have influenced formation of specific microstructures at some localities. Emplacement of the Cretaceous McAfee Creek pluton may have resulted in the high temperature recrystallization of feldspar and quartz observed along the northeast pluton margin (Fig. 3d). Additionally, some domains of lobate quartz and feldspar coincide with intrusion of Cretaceous granitoids (Fig. 3c). In particular, the east-to-west-trending domains along the north-central pluton margin coincide with Cretaceous age intrusive bodies (Fig. 2a).

Scalar and directional magnetic susceptibility data

Domain mapping of the various AMS parameters by spline or polynomial factors indicate some degree of parallelism to both the northwest and southeast pluton margins and the general Barcroft Structural Break orientation. In addition, scalar map domains show a similar form to the north-plunging synform defined by the magnetic foliation form lines (Fig. 17b). Directional AMS parameters of foliation and lineation tend to indicate a synform plunging to the north.

Spline function contour maps of scalar magnetic parameters

Scalar magnetic parameters that have been contoured using the spline function show a number of similarities with the north plunging synform defined by magnetic foliation form lines

(Fig. 19b). T, F%, L% (Figs. 10b, 12b, 13b) all posses a distinctive northwest-trending 2-3 kilometer wide domainal distribution through the middle of the pluton. The eastern two thirds of the pluton show strong agreement between T shape domains (Fig.10b) and prolate/oblate fabrics indicated by L% and F% (Figs. 12b, 13b). The western part of the pluton, with low susceptibility values, displays a more ambiguous relationship between T shape domains and F% and L%. Susceptibility (Km) and anisotropy (P%) do not appear to have any influence on the development of the shape-related fabrics.

Polynomial function contour maps of scalar magnetic parameters

A general NE-SW trend is indicated by polynomial function contouring of all the main scalar parameters (Km, P%, T, F%, L%). Contours for Km (Fig. 6c) and T (Fig. 10c) are oriented parallel to the southern pluton margin, whereas contours for P% (Fig. 8c), F% (Fig. 12c), and L% (Fig. 13c) are oblique to the margin. The general fold shape indicated by the magnetic foliation form lines is most apparent in contour maps of the susceptibility (Km) and T shape (Figs. 6c, 10c), and to the least extent in L% (Fig. 13c). Finally, polynomial-based contour trend maps for P% and F% in the eastern part of the pluton are similar to the northeastern trend of the Barcroft Structural Break.

Polynomial-based contour maps for magnetic foliation dip and lineation plunge are very similar, particularly in the eastern part of the pluton (Figs. 17d, 20c). Contour trends for both foliation dip and lineation plunge are parallel to the southern margin in the eastern part of the pluton. To the west, the contours trend to the northeast in both maps and are generally coincident with the trend of the Barcroft Structural Break.

Directional magnetic parameters – foliation form line map

Some of the strongest evidence for a synformal structure within the Mount Barcroft pluton comes from magnetic susceptibility directional data. Hand drawn form lines of average

foliation strike, define an overturned synformal structure plunging moderately (approximately 60°) to the north (Figs. 16a, 17b). The eastern limb parallels the southern pluton margin, and the west-northwest trending overturned limb is perpendicular to the southern pluton margin. To the west, foliation form lines define an antiform plunging shallowly to the northwest parallel to the trend of the overturned limb.

Possible interpretations of magnetic scalar and directional parameters

Given the variability of the AMS signature both between and within sites, it is very difficult to draw geologic conclusions on such complex data. However, the scalar and directional data, as it is, indicates that the primary internal structure of the Mount Barcroft pluton is a large, north-westward plunging synform. Originally this synform may have been the result of magmatic flow within a fault-bounded magma chamber during emplacement.

Curvature of the foliation form lines could have developed in response to a number of magma chamber processes. 1) The curving foliation could be the result of flow perturbations in a planer magma channel where original pluton boundaries are reasonably intact. 2) Mapped pluton boundaries are actually faults cutting across an older internal fabric, where the curving foliation is either the result of flow within the original chamber, or the fabric was influenced by the pre-existing country rock structure. Proterozoic-Paleozoic rocks immediately to south of the Mount Barcroft pluton dip north and west and are located on the western limb of the White Mountain anticline. Geologic mapping indicates that this westward dipping limb contain numerous minor, open folds which may have had an influence on the magma flow as it entered the chamber between Paleozoic and Mesozoic rocks.

The Barcroft, and Sabies faults to the northwest (Hanson, 1986a) and Marmot fault (Ernst and Hall, 1987; Ernst et al., 1993) to the southeast (Fig. 30), impact the magnetic parameter maps differently. The Barcroft and Sabies faults are primarily, steeply dipping, west directed reverse faults that appear to truncate the original northwest pluton margin (Hanson, 1986a). Additionally,

the Barcroft and Sabies faults appear to cut the scalar and directional AMS structures. The Marmot fault, is roughly parallel to the southeast pluton margin, and tends to parallel most of the contours of scalar and directional magnetic data, using 3rd order polynomial function contour. Exceptions to this are P%, F%, and L% maps where contours tend to align with the northern extension of the Barcroft Structural Break.

POSSIBLE HISTORY OF FORMATION OF THE BARCROFT STRUCTURAL BREAK AND MOUNT BARCROFT PLUTON

A great deal of previous geologic research has been focused on the northern White Mountains and the Barcroft Structural Break. Previous mapping (Krauskopf, 1971; Crowder and Sheridan, 1972; Crowder et al., 1973; Robinson and Crowder, 1973; Hanson, 1986 a, b; Ernst and Hall, 1987; Ernst et al., 1993, 2002), petrographic work on the pluton and Mesozoic metasediments and metavolcanics (Anderson, 1937; Emerson, 1966; Crowder and Ross, 1972; Fates, 1985, Hanson, 1986a,b; Ernst, 2000; 2002; Ernst et al., 2002, 2003) and geochronological studies (Crowder et al., 1973; Stern et al., 1981; Hanson, 1986a; Coleman et al., 2003) have resulted in the massing of a tremendous amount of data. Based upon previous mapping and geological studies, in addition to this AMS and microstructural study of the Mount Barcroft pluton, what follows is an attempt to provide a reasonable historical context for formation of the Barcroft Structural Break and emplacement of the Mount Barcroft pluton.

Formation of the Barcroft Structural Break

The establishment of the Barcroft Structural Break was probably the result of transtension, producing a series of large, rotated and down-dropped blocks in the northern White Mountains, following deposition of bimodal Triassic volcanics, but prior to Jurassic plutonism and final Mesozoic volcanic activity. Evidence for normal and wrench style faulting includes the system of east-west trending normal faults to the south of the Barcroft Structural Break, and the juxtaposition of different Proterozoic-Paleozoic rocks exposed in the northern White Mountains.

It seems highly improbable that the Mount Barcroft pluton emplaced along a high angle reverse fault due to the vertical to steeply southeast dipping pluton margins. Andersonian mechanics predicts that steep to subvertical faults are the result of strike-slip, normal or wrench motion. Reverse faults rarely achieve angles over 35^0. Steeper dips can be achieved when pore fluid pressures are high, thus reducing differential stress. It was initially speculated that the

movement of magmas along the Break in conjunction with faulting could have resulted in high angle reverse faults (Sibson, 1985). It is postulated that the initial formation of the Barcroft Stuctural Break was the result a complicated fault structure of strike-slip, normal and wrench faults that juxtaposed crustal blocks in response to trantensional stress.

Normal faults in the Proterozoic-Paleozoic section to the south of the Barcroft Structural Break are expressed in two ways. These include the steeply dipping Marmot and Lamb faults striking east-west (Ernst and Hall, 1987; Ernst et al., 1993) (Fig. 30). The Marmot fault is presently a sub-vertical thrust fault and is partially coincident with the southern margin of the Mount Barcroft pluton (Ernst and Hall, 1987; Ernst et al., 1993). The Lamb fault lies further to the south, paralleling the Marmot fault and may be associated with a correlative fault on the east side of the White Mountains. This structure was later truncated by the Cottonwood and McAfee Creek plutons (Krauskopf, 1971). A second set of normal faults is associated with a discrete section of folded Precambrian rocks (Wyman Argillite and Reed Dolomite) located to the east, along strike of the Mount Barcroft pluton long axis. It is speculated, that following emplacement of the Mount Barcroft pluton, that the Marmot fault to the southeast was reactivated as a reverse fault. The Sabies, Barcroft, and Millner faults to the northwest may have been formed and/or reactivated as reverse and strike-slip faults, respectively, in the Cretaceous.

Three different crustal blocks can be identified in the northern White Mountains based on their associations with Proterozoic-Paleozoic sedimentary rocks (Fig. 30). East of the Barcroft Structural Break, a faulted block of folded Precambrian sedimentary rocks (Wyman and Reed formations)(Krauskopf, 1971) represents the first block. A second block composed of relatively undeformed Precambrian sedimentary rock (Wyman Formation) is located immediately to the north of the first block (Robinson and Crowder, 1973). These two blocks to the east of the Barcroft Break may form a faulted northern extension of the White Mountain anticline.

The largest of the three identifiable crustal blocks is located northwest of the Barcroft Structural Break and is somewhat obscured by Cretaceous deformation and plutonism (Crowder

et al., 1972; Robinson and Crowder, 1973) (Fig. 30). The Paleozoic rocks in this block are marbles assumed to belong to the Poleta formation, and siliciclastic rocks assumed to be Harkless formation (both Lower Cambrian) (Crowder et al., 1972; Robinson and Crowder, 1973). Outcrops of Ordovician age rocks (Palmetto formation) occur in the extreme northeast part of the range, possibly indicating either a single or possibly a series of down-dropped blocks.

Additional evidence for this large, down-dropped fault block is provided by the presence of Mesozoic metavolcanics and metasediments located at similar or deeper structural levels to Precambrian-Paleozoic rocks to the north of the Mount Barcroft pluton. This down-dropped block may have provided a depositional basin for the second younger generation of the Inyo Mountain Volcanic Complex of Mesozoic age associated with volcanic arc development (Dunne and Walker, 1993; Dunne et al., 1998). In addition, the problematic 154 Ma U/Pb dates for the ash flow tuff (Hanson, 1986a) could be contemporaneous with this second Mesozoic volcanic event, resulting in the younger deposits of the Inyo Mountain Volcanic Complex.

Although highly speculative, it is possible that a fourth fault bound, down-dropped block was situated along the initial Barcroft Structural Break itself, thereby providing space for emplacement of the Mount Barcroft pluton in Jurassic times (Fig. 31). This contention is supported by the dike-like shape of the pluton in map view, the presence of a possible pendant of carbonate and felsic volcanic rock, of probable Mesozoic age, located in the northeast part of the Mount Barcroft pluton (Hanson, 1986a), the Marmot fault that parallels the southern pluton margin, and association with the Barcroft Structural Break.

Jurassic magmatism

The Barcroft Structural Break primarily controlled emplacement of the Mount Barcroft pluton. The initial Barcroft Structural Break provided a conduit for magma to reach the upper crust, and be emplaced. Juxtaposed crustal blocks of folded Proterozoic-Paleozoic rock are

associated with initial formation of the Barcroft Structural Break. These blocks, in addition to the noticeable tabular shape of the pluton in map view are indicative of a fault or fault block origin.

Emplacement of the Mount Barcroft pluton into a down-dropped block between the Proterozoic and Paleoazoic section and the lower Mesozoic metavolcanic section, is supported by the presence of the assumed Mesozoic age pendant mapped within the body of the pluton. The pendant is composed of felsic metavolcanic and carbonate and is located in the northeast part of the Mount Barcroft pluton (Hanson, 1986a). This quartz-bearing, carbonate rock did not metamorphose to wollastinite even though temperatures reached the equivalent of greenschist facies, supporting a pendant as opposed to xenolith origin. This lack of high-grade contact metamorphism may have been due to an extreme thermal gradient of more than 100°C per kilometer and is consistent with shallow emplacement (Hanson, 1986a) where the roof of the pluton, in part, was formed of relatively cool metavolcanic rocks.

I speculate, that the mode of emplacement for the Mount Barcroft pluton was via magma flow into a space provided by a down-dropped crustal block along the Barcroft Stuctural Break. The emplacing magma could have intruded between the Mesozoic and Proterozoic-Paleozoic assemblages (Fig. 31). However what is clear is that the Barcroft Structural Break provided conduits for Jurassic age magmas to reach the upper crust. The Mount Barcroft and Cabin Creek plutons are the only Jurassic age plutons remaining exposed along the Barcroft Structural Break. Characteristics shared by both plutons are their dark gray coloration, relative abundance of biotite and hornblende, and distinct clotted grouping of the mafic minerals. These common features may indicate that these two plutons originated from the same magma chamber at depth (Krauskopf, 1965, 1971).

Deformation between Jurassic and Cretaceous magamtism

Following faulting along the initial Barcroft Structural Break, possibly concurrent with Jurassic plutonism, deposition of the younger generation of the Mesozoic metavolcanics,

metasediments and volcanics may have occurred. A possible time lag between formation of the Mount Barcroft pluton and Mesozoic volcanism is indicated by a gap in U/Pb zircon dates between the cooling age for the Mount Barcroft pluton (165 Ma) and ages of samples taken from the Mesozoic rocks (Hanson et al., 1987). U/Pb zircon dates for an ash flow tuff and hypabyssal plug samples taken from the same mapped unit within the Mesozoic section yielded dates of 154 Ma (concordant) and 137 Ma (highly discordant) respectively. The 154 Ma age is compatible with deposition of the ash flow tuff into a space provided by a down-dropped block following faulting and emplacement of the Mount Barcroft pluton. The 137 Ma discordant age for the hypabyssal plug has been explained by entrainment of Proterozoic zircons into a Cretaceous magma (Hanson et al., 1987). The source for the hypabyssal magma was most probably to the north of the Barcroft Structural Break and associated with the Pellisier Flat pluton. There is little evidence of magmas intruding upward along, or across the Barcroft Structural Break and through the Mesozoic metavolcanics during Cretaceous magmatism.

Hanson (1986a) identified two deformational events in the Mesozoic metasediments and metavolcanics, which predate doming and final deformation during Cretaceous magmatism. Initially, deformation was east directed followed by a second more significant period of westward directed motion. Mesozoic metasediments and metavolcanics were transported to the west, forming westward-verging fold structures (Hanson, 1986a; Hanson et al., 1987). It is possible that earlier normal faults were reactivated as steeply, southeast dipping reverse faults during the last period of west directed motion in the Cretaceous.

Cretaceous magmatism

The Barcroft Structural Break was not utilized as a conduit to the upper crust by Cretaceous magmas and may have actually acted as a barrier to magma transport. The Boundary Peak pluton, which lies along the eastern flank of the White Mountains, is the only example of Cretaceous or Jurassic age magma intruding across the Barcroft Structural Break (Fig. 30). More

typically Cretaceous age plutons, such as Leidy Creek to the south and Pellisier to the north, seem to originate within their respective fault blocks and assume a finger-like pattern as they project into and towards the Barcroft Structural Break.

Future research

Field mapping and further geochronological studies are needed to more clearly constrain the timing of geologic events in the northern White Mountains. Petrographic, and further AMS studies of other Jurassic and Cretaceous age plutons and Mesozoic volcanics, metavolcanics and metasediments in the northern White Mountains are also required to determine the magnetic affinities of possibly related magmas along, and to the north, of the Barcroft Structural Break. Possibly magmas generated beneath the northern White Mountains and the Barcroft Structural Break are the result of different processes from those generated beneath the remainder of the White-Inyo Range and possibly the Sierra Nevada Mountains. Additional analysis of Mesozoic metavolcanics and metasediments may help to establish if these are extrusive equivalents of nearby plutons, and if so, which ones.

Magmatic mixing zones identified within the Mount Barcroft pluton are puzzling, and their relationship to emplacement remains unclear. Further analysis of these zones is needed to determine possible relationships with the "undifferentiated granites" mapped by Hanson (1986a) and the "migmatites" mapped by Crowder and Ross (1973). The "undifferentiated granites" are significant as they may represent the only remaining example of original emplacement relationships along the northwest margin of the Mount Barcroft pluton, given the later truncation by the Sabies and Barcroft faults.

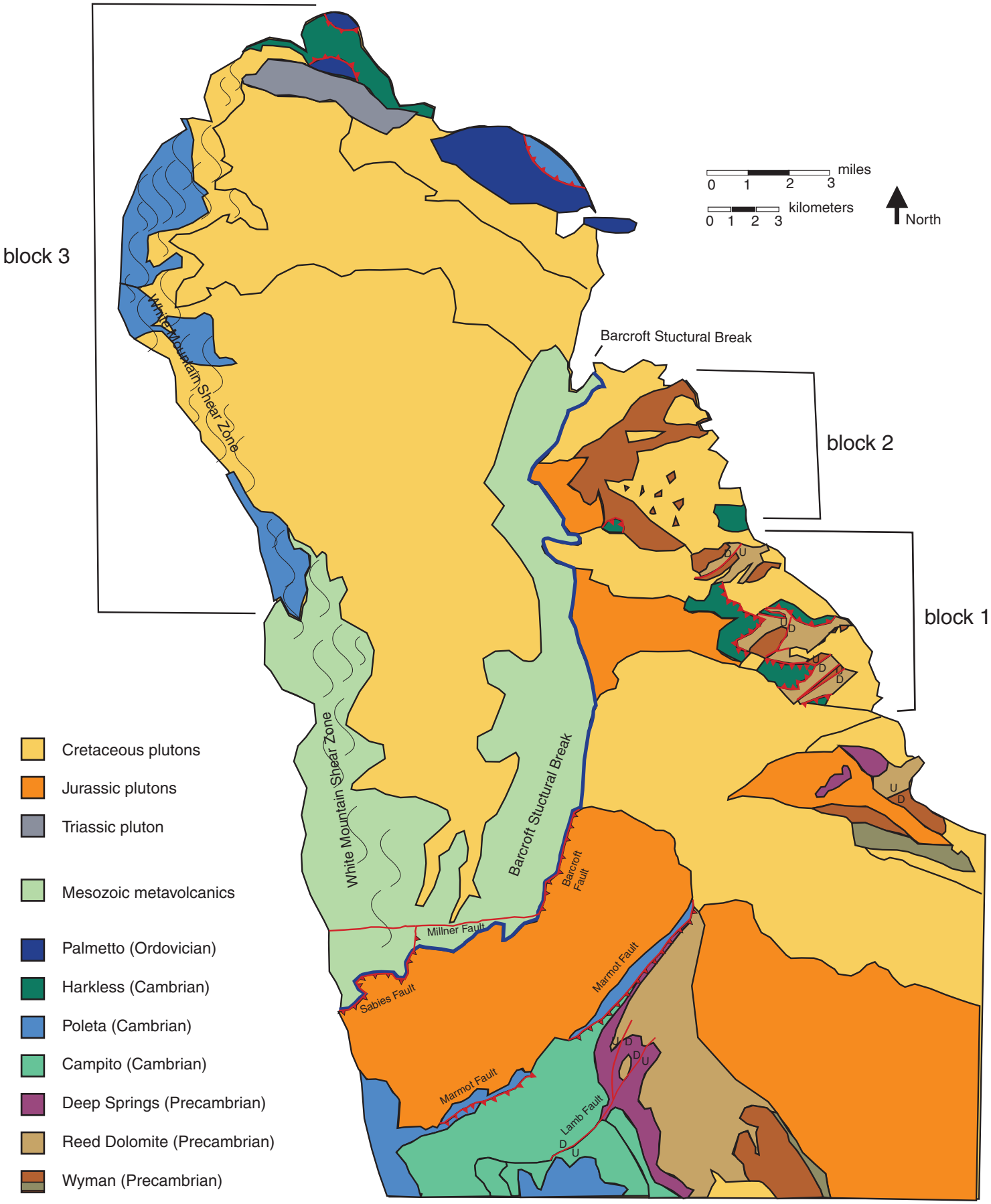

Figure 30: Map of northern White Mountains; adapted from: Krauskopf,1971; Crowder et al., 1972; Crowder and Sheridan,1972; Robinson and Crowder, 1973; Hanson, 1986a; Ernst and Hall, 1987; Ernst et al., 2002.

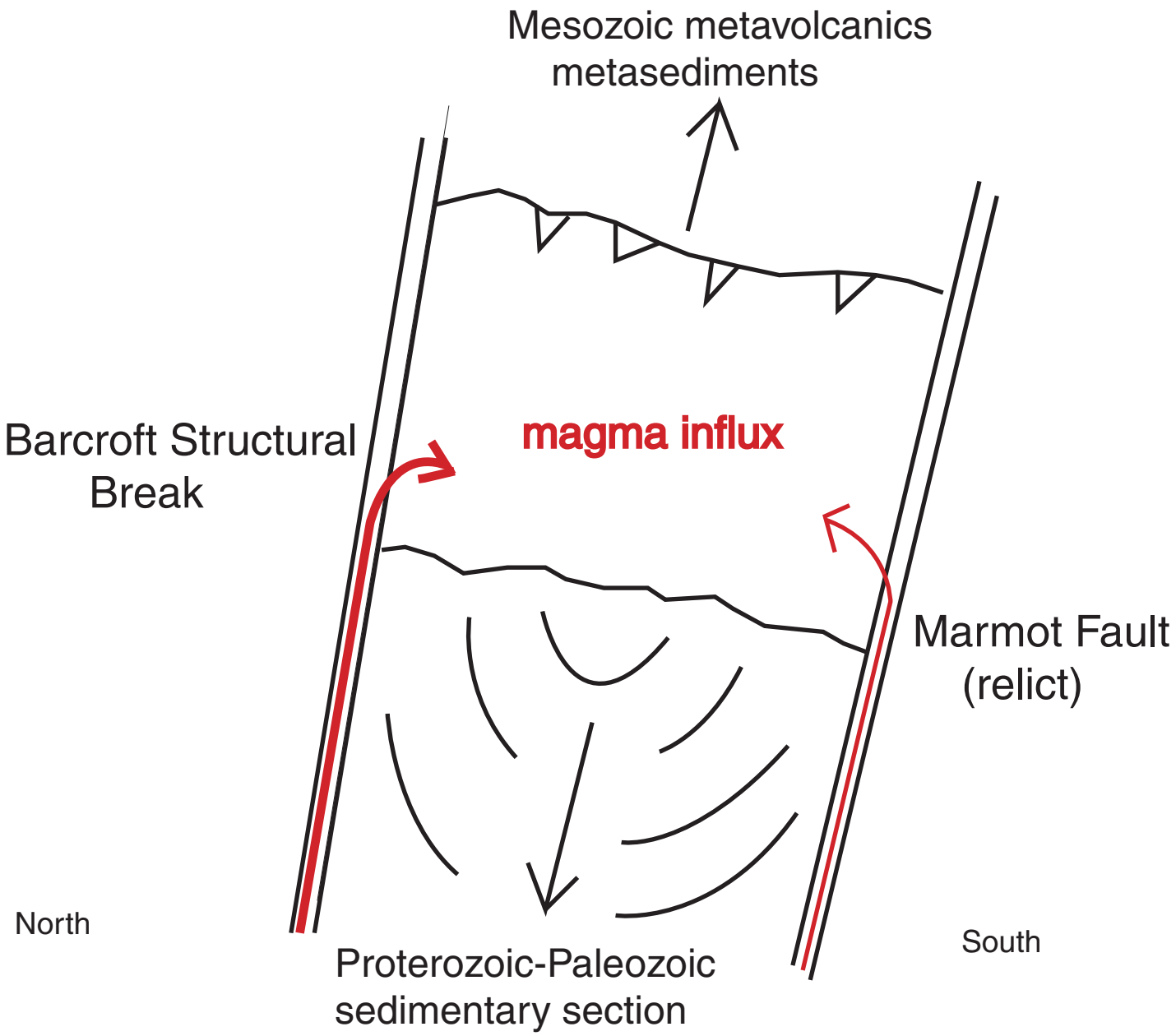

Figure 31: Mount Barcroft pluton possible emplacement model

SUMMARY

The Mount Barcroft pluton was emplaced along the Barcroft Structural Break separating Mesozoic metavolcanics and metasediments to the north from folded Proterozoic-Paleozoic sedimentary rocks to the south. The Barcroft Structural Break was probably originally a composite extensional structure composed of steeply dipping faults, bounding large down-dropped blocks of folded Proterozoic-Paleozoic sedimentary rock, capped by bimodal volcanics. These faults provided the conduits for magma to move into the upper crust during Jurassic plutonism in the northern White Mountains.

The Mount Barcroft pluton displays significant differences to Jurassic plutons of similar age, located to the south of the Barcroft Structural Break. Given its unique emplacement setting, and heterogeneous nature of its AMS signature, petrology and opaque mineral grain type, the Mount Barcroft pluton may have originated from a separate magma chamber associated with the northern White Mountains and Barcroft Structural Break.

In summary:

1) The Mount Barcroft pluton's scalar and directional AMS parameters are highly heterogeneous on both kilometer and meter scale.

2) Heterogeneity in the AMS signature is supported by previous petrographic and isotopic work, variation in fabric type and orientation between A and B cores, and by identification of different opaque mineral grain-shape types.

3) Variability on all scales in the AMS signature is probably the result of a highly complex ferromagnetic mineral assemblage.

4) Although variability in AMS scalar data can be explained by a complex magnetic mineralogy, it is difficult to determine a mechanism for variations directional orientation and magnetic fabric type on the meter scale.

5) The Mount Barcroft pluton AMS signature is significantly different compared to data previously obtained from Jurassic plutons in the White-Inyo Range and Sierra Batholith, and may

be indicative of a previously unrecognized magma source associated with the northern White Mountains and initial formation of the Barcroft Structural Break.

6) The Mount Barcroft pluton was probably emplaced following normal/wrench faulting associated with initial formation Barcroft Structural Break.

REFERENCES

Anderson, G.H., (1937) Granitization, albitization and related phenomena in the northern Inyo Range of California-Nevada. Geological Society of America Bulletin, v. 48, p.1-74.

Archanjo, C. J., and Bouchez, J.L. (1997) Magnetic fabrics and microstructures of the post-collisional aegirine-augite syenite Triunfo Pluton, Northeast Brazil. Journal of Structural Geology, v. 19, p. 849-860.

Archanjo, C. J., Launeau, P., and Bouchez, J.L., (1995) Magnetic fabric versus magnetite and biotite shape fabrics of the magnetite-bearing granite pluton of Gameleiras (Northeast Brazil). Physical Earth Planet International, v. 89, p. 63-75.

Barton, M.D., and Hanson, B., (1989) Magmatism and the development of low-pressure metamorphic belts: Implications for the western United States and thermal modeling. Geological Society of America Bulletin, v. 101, p. 1051-1065.

Bateman, P.C., (1992) Plutonism in the central part of the Sierra Nevada Batolith, California. United States Geological Survey Professional Paper 1483, 186p.

Benn, K., Rochette, J.L., Bouchez, J.L., and Hattori, K, (1993) Magnetic susceptibility, magnetic mineralogy and magnetic fabrics in a late Archean granitoid-gneiss belt. Precambrian Research, v. 63, p. 59-81.

Blakely, R.J., and McKee, E.H., (1985) Subsurface structural features of the Saline Range and adjacent regions of eastern California as interpreted from isostatic residual gravity anomalies. Geology, v. 13 p. 781-785.

Blenkinsop, T., (2000) Deformation Microstructures and Mechanisms in Minerals and Rocks. Kluwer Academic Publishers, pp. 105.

Borradaile G.J., (1988) Anisotropy of magnetic susceptibility: Rock composition versus strain. Tectonophysics, v. 156, p. 1-20.

Borradaile G.J., (1991) Correlation of strain with anisotropy of magnetic susceptibility. Pure and Applied Geophysics, v. 135, p. 15-29.

Borradaile, G.J., (2001) Magnetic fabrics and petrofabrics: their orientation distributions and Anisotropies. Journal of Structural Geology, v. 23, p. 1581-1596.

Borradaile, G.J., and Gauthier, D., (2003) Interpreting anomalous magnetic fabrics in opiolite dikes. Journal of Structural Geology, v. 25, p. 171-182.

Borradaile, G.J., and Henry, B., (1997) Tectonic application of magnetic susceptibility and its anisotropy. Earth Science Reviews, v. 42, p. 49-93.

Borradaile, G.J., Werner, T., (1994) Magnetic anisotropy of some phyllosilicates. Tectonophysics, v. 235, p. 233-248.

Bouchez, J.-L., (1997) Granite is never isotropic: an introduction to AMS studies of granitic rocks. In *Granite: From Segregation of Melt to Emplacement Fabrics,* eds. J.L. Bouchez, D.H.W. Hutton and W.E. Stephens, pp. 95-112. Kluwer Academic Publishers.

Bouchez, J. L., Delas, C., Gleizes, G., Nedelec, A. and Cuney, M., (1992) Submagmatic microfractures in granite. Geology, v. 20, 35-38.

Bouchez, J.L., and Gleizes, G., (1995) Two-stage deformation of the Mont-Louis Andorra granite pluton (Variscan Pyrenees) inferred from magnetic susceptibility anisotropy. Journal of Geological Society of London, v. 152, p. 669-679.

Burrough, P. A., and McDonnell, R.A., (1998) Principles of Geographical Information Systems. Oxford University Press, New York.

Chen, J. H., and Moore, J.G., (1982) Uranium lead isotopic ages from the Sierra Nevada batholith California. Journal of Geophysical Research, v. 87, p. 4766-4784.

Chen, J. H., (1977) Uranium-lead isotopic ages from the southern Sierra Nevada batholith and adjacent areas, California. Ph.D. Thesis, University of California Santa Barbara, 138 p..

Coleman D. S., Briggs, S., Glazner, A.F., and Northrup, C.J., (2003) Timing of plutonism and deformation in the White Mountains of eastern California, in press, Geological Society of America Bulletin, v. 115, p. 48-57.

Corbett, K.P., Wrucke, C.T., and Nelsonb, C.A. (1988) Structure and tectonic history of the Last Chance thrust system, Inyo Mountains and Last Chance Range, California. In Weide, D.L., and Faber, M.L., eds., This extended land: Geological journeys in the southern Basin and Range. Geological Society of America Annual Meeting, Cordilleran Section, Las Vegas, NV, 1988, Field Trip Guidebook, p.269-262.

Crowder, D.F., McKee, E.H., Ross, D.C., and Krauskopf, K.B., (1973) Granitic rocks of the White Mountain area, California-Nevada: Age and regional significance Geological Society of America Bulletin 84, p. 285-296.

Crowder, D.F., Robinson, P.T., and Harris, D.L., (1972) Geological map of Benton Quadrangle, Mono County, California and Esmerelda and Mineral Counties, Nevada. U. S. Geological Survey Geologic Quadrangle Map GQ-1012, scale 1:62,500.

Crowder, D.F., and Ross, D.C., (1972) Permian (?) to Jurassic (?) metavolcanics and related rocks that mark a major structural break in the Northern White Mountains, California-Nevada. U.S. Geological Survey Professional Paper: 0800-B, pp. B-195-B-203.

Crowder, D.F., and Ross, D.C., (1973) Petrography of some granitic bodies: Northern White Mountains, California-Nevada. U.S. Geological Survey Professional Paper: P 0775, pp. 28.

Crowder, D.F., and Sheridan, M.F., (1972) Geologic map of the White Mountain Peak Quadrangle, California. U. S. Geological Survey Geologic Quadrangle Map GQ-1012, scale 1:62,500.

Curtis, G.H., Evernden, J. F., and Lipson, J., (1958) Age determination of some granitic rocks in California by potassium-argon method. California Division of Mines Special Report 54, 16p.

Diggles, M.F., Blacely, R.J., Schmach, S.W., Rains, R.L., Lipton, D.A., Winters, R.A., and Iverson, R.L., (1983) Mineral resource potential of the White Mountain and Birch Creek roadless areas, White Mountains, California and Nevada. U. S. Geological Survey miscellaneous Field Studies Map, MF-1361-D, 25 p., scale 1: 62,500.

Dollase, W.A., (1994) Minerals of the White Mountains. In Crooked Creek Guidebook, C.A. Hall Jr. and B. Widawski eds., University of California, p. 39-52.

Dunne, G.C., Garvey, T.P., Osborne, M., Schneidereit, D., Walker, J.D., (1998) Geology of the Inyo mountain volcanic complex: Implications for Jurassic paleogeography of the Sierran magmatic arc in eastern California. Geological Society of America Bulletin, v. 110, p. 1376-1397.

Dunne, G.C., Gulliver, R.M, and Sylvester, A.G., (1978) Mesozoic evolution of the White, Inyo, Argus and Slate ranges, Eastern California: in Mesozoic Paleogeography of the Western U.S., Howell, D.G., and McDougal, K.A. eds., p. 189-207, Society of Economic Paleontologists and Mineralogists, Pacific Section, Pacific Coast Paleogeography Symposium, 2.

Dunne, G.C., and Walker J.D., (1993) Age of Jurassic volcanism and tectonism, southern Owens Valley region, east-central California, Geological Society of America Bulletin, v.105, p. 1223-1230.

Emerson, D.O., (1966) Granitic rocks of the Mount Barcroft Quadrangle, Inyo Batholith, California-Nevada. Geological Society of America Bulletin, v. 77, p. 127-152.

Ernst, W.G., (1996) Petrochemical study of regional contact metamorphism in metaclastic strata of the central White-Inyo Range, Eastern California, Geological Society of America Bulletin, v. 108, n. 2, p. 1528-1548.

Ernst, W.G. (2000) Petrochemistry of the Barcroft plutonic complex, White mountains, east-central California. Geological Society of America Abstracts with Programs 32 (7) p.47.
Ernst, W.G. (2002) Paragenesis and thermobarometry of Ca-clinoamphiboles in the Barcroft Granodiorite pluton, central White Mountains, eastern California. American Mineralolgist, v. 87, p 478-490.

Ernst, W.G., Coleman, D. S., and Van de Ven, C., (2003) Petrochemistry of granitic rocks in the Mount Barcroft area, Implications for arc evolution, Central White Mountains, easternmost California, Geological Society of America Bulletin, v.115, n.4, p. 499-512.

Ernst, W.G., and Hall, C.A., (1987) Geology of the north Barcroft-Blanco Mountain Area, Eastern California. Geological Society of America Map and Chart Series MCH006, scale 1: 24,000.

Ernst, W.G. Jones, R.E., and Van de Ven C., (2002) Geological Map of Mount Barcroft Complex, central White Mountains, eastern California: Structure, mineral parageneses, and tectonic evolution. California Division of Mines and Geology, Map Sheet 15, scale 1:24,000, accompanying text 88 p.

Ernst, W.G., Nelson, C.A., and Hall, C.A., (1993) Geology and metamorphic assemblages of Precambrian and Cambrian rocks of the central White-Inyo Range eastern California. California Department of Conservation, Division of Mines and Geology, map sheet 46.

Ernst, W.G., and Rumble, D. III (2003) Oxygen isotopic study of Late Mesozoic cooling on the Mount Barcroft area, central White Mountains, eastern California. Contributions to Mineralogy and Petrology, v. 144, n. 6, p. 639-651.

Fates, D.G., (1985) Mesozoic (?) metavocaniclastic rocks, northern White Mountains, California: Structural style, lithology, petrology, depositional setting and paleogeographic significance, [M.S. Thesis]: Los Angeles, University of California, 225 p.

Fates, D.G., and Hanson, R.B., (1985) Mesozoic (?) metavolcaniclastic rocks, northern White Mountains, California, lithology, depositional setting, and paleogeographic Significance. Geological Society of America Abstract with Programs 17, (6), p. 354-355.

Ferre, E.C., Wilson, J., Gleizes, G. (1999) Magnetic susceptibility and AMS of the Bushveld alkaline granites, South Africa. Tectonophysics, v. 307, n. 1-2, p. 113-133.

Ferre, E.C., Bordarier, C., and Marsh, J.S., (2002) Magma flow inferred from AMS fabrics in a layered mafic sill, Insizwa, South Africa. Tectonophysics, v. 354, p. 1-23.

Gillespie, J.G., Jr., (1979) U-Pb and Pb-Pb ages of primary and detrital zircons from the White Mountains eastern California. Geological Society of America Abstracts with Programs 11, p.79.

Gregoire, V., Saint Blanquat, M., Nedelec, A., & Bouchez, J.L., (1995) Shape anisotropy versus magnetic interactions of magnetite grains; experiments and applications to AMS in granitic rocks. Geophysical Research Letters, v. 22, (20), p. 2765-2768.

Hanson, R.B., (1986a), Geology of Mesozoic metavolcanics and metasedimentary rocks, northern White-Inyo Mountains, California. [Ph.D. Dissertation]: Los Angeles, University of California, 231p.

Hanson, R.B., (1986b), Stratigraphy and paleogeographic significance of the Mesozoic metasedimentary rocks northern White Mountains, California, in Hall, C.A., and Young, D.V., eds., Natural history of the White-Inyo Range, eastern California and western Nevada and high altitude Physiology. Los Angeles, University of California White Mountain Research Station Symposium, v.1, p. 37-46.

Hanson R. B., Saleeby, J.B., (1986) Mesozoic metavolcanica and metasedimentary rocks, Northern White Mountains, California; U/Pb age, stratigraphy, and timing of westward-vergent structures. Geological Society of America with Programs 18 (2) p. 113.

Hanson, R.B., Saleeby, J.B., and Fates, D.G., (1987) Age and tectonic setting of Mesozoic metavolcanics and metasedimentary rocks, Northern White Mountains, California. Geology, v. 15, p. 1074-1078.

Hargraves, R.B.D., Johnson, D., and Chen C.Y., (1991) Distribution anisotropy: The cause of AMS in igneous rocks. Geophysical Research Letters, v. 18, p. 2193-2196.

Hibbard, M. J., (1979) Myrmekites as a marker between preaqueous and post aqueous phase saturation in granitic systems. Geological Society of America Bulletin: v. 90, p. 1047-1062.

Ishihara, S., (1977) The magnetite series and ilmenite series granitic rocks. Mining Geologist, v. 27, p. 293-305

Jelinek, V., (1981) Characterization of the magnetic fabric of rocks. Tectonophysics v. 79, p. 63-67.

Jover, O., Rochette, P., Lorand, J.P., Naeder, M., and Bouchez, J.L., (1989) Magnetic mineralogy of some granites from the French Massif Central: Origin of their low-field susceptibility. Physics of Earth Planet and Interiors v. 55, p.79-92.

Kistler, R.W., and Peterman, Z.E., (1978) Reconstruction of crustal blocks of California on the basis of initial strontium isotopic compositions of Mesozoic granitic rocks. U.S. Geological Survey Professional Paper 1071, 17p.

Kistler, R. W., Bateman, P. C., and Brannock, W.W., (1965) Isotopic ages of minerals from granitic rocts of the central Sierra Nevada, California. Geological Society of America Bulletin, v. 76, n. 2, p. 155-164.

Krauskopf, K.B., (1965) A tale of ten plutons. Geological Society of America Bulletin, v. 79, p. 1-18.

Krauskopf, K. B., (1971) Geologic map of the Mount Barcroft quadrangle, California-Nevada. U. S. Geological Survey Geologic Quadrangle Map, GQ-960, scale 1:62,500.

Krauskopf, K.B., (1997) Ten plutons revisited; a retrospective view. International Geology Review, v. 39, p. 766-767.

Lagroix, F., and Borradaile, G.J., (2000) Magnetic fabric interpretation complicated by inclusions in mafic silicates. Tectonophysics, v. 325, p. 207-255.

McKee, E.H., and Conrad, J.E., (1996), A tale of ten plutons – Revisited age of granitic rocks in the White Mountains, California and Nevada. Geological Society of America Bulletin, v. 108, p. 1515-1527.

McKee, E.H., Diggles, M.F., Donahoe, J.L., and Elliot, G.S. (1982) Geologic map of the White Mountain wilderness and roadless areas California and Nevada, U.S. Geological Society miscellaneous, field studies Map MF-1361-A, scale 1:62,500.

McKee, E.H., and Nash, D.B., (1967) Potassium argon ages of granitic rocks in the Inyo Batholith, east-central California. Geological Society of America Bulletin, v. 78, p. 669-680.

Morgan, S. S., (1998a) Pluton emplacement, aureole deformation and metamorphism, and regional deformation within the White-Inyo Range of eastern California {Ph. D. thesis]: Virginia Polytechnic Institute and State University, 172 p.

Morgan, S. S., and Law, R. D., (1998) an overview of Paleozoic-Mesozoic age structures in the central White Inyo Range, eastern California. International Geology Review, v. 40, p. 245-256.

Nelson, C.A., 1962 Lower Cambrian – Precambrian succession, White-Inyo Mountains, California. Geological Society of America Bulletin, v. 73, p. 139-144.

Nelson, C.A., Hall, C.A., and Ernst, W.G., (1991), Geologic history of the White-Inyo Range. In Hall, C.A., Jr. ed., Natural history of the White-Inyo Range, California, University of California Natural History Guides, v. 55, p. 42-74.

Passchier, C.W., and Trouw, R.A.J., (1996) Microtectonics. Springer-Verlag, pp. 250.

Ratajeski, K., Glazner, A.F., and Miller, B. V., 2001, Geology and geochemistry of mafic to felsic plutonic rocks in the Cretaceous intrusive suite of Yosemite Valley, California. Geological Society of America Bulletin, v.113, p. 1486-1502.

Roubigou, V. (1984) Metamorphism of the Cambrian Campito Formation, White-Inyo Mountains, eastern California. [M.S.thesis], University of California, Los Angeles, 101 p.

Roubigou, V. (1986) Metamorphism in the Cambrian Campito Formation, White-Inyo Mountains. In Hall, C.A., and Young, D.V., eds., Natural history of the White-Inyo Range, eastern California and western Nevada and high altitude physiology: Los Angeles, University of California White Mountain Research Station Symposium, v.1, p.27-36.

Robinson, E.S., Poland, R.V., Glover, L. III., and Speer, J.A., (1985) Some effects of regional metamorphism and geological structure on magnetic anomalies over the Carolina Slate Belt near Roxboro, North Carolina. In: The utility of regional gravity and magnetic anomoly maps. Hinze, W.J. ed., Society of Exploration Geophysicist, p. 320-324.

Robinson, P.T., and Crowder, D. F., (1973) Geological map of the Davis Mountain Quadrangle, Esmeralda and Mineral Counties, Nevada and Mono County California. U. S. Geological Society Geologic Quadrangle Map GQ-1012, scale 1:62,500.

Rochette, P., (1987) Magnetic susceptibility of the rock matrix related to magnetic fabric studies. Journal of Structural Geology, v. 9, (8), p. 1015-1020.

Rochette, P., Aubourg, C., and Perrin, M., (1999) Is this magnetic fabric normal? A review of case studies in volcanic formations. Tectonophysics, v. 307, p. 219-234.

Rochette, P., Jackson, M., and Aubourg., (1992) Rock magnatism and the interpretation of anisotropy of magnetic susceptibility. Reviews of Geophysics, v. 30, p. 209-226.

Saint Blanquat, M., (1993) EXAMS: an Excel macro for automatic computing of AMS data, unpublished program, University of Toulouse.

Saint Blanquat, M. and Tikoff, B. (1997) Development of magmatic to solid-state fabrics during syntectonic emplacement of the Mono Creek granite, Sierra Nevada Batholith . In *Granite: From Segregation of Melt to Emplacement Fabrics,* eds J.L. Bouchez, D.H.W. Hutton and W.E. Stephens, pp. 231-252. Kluwer Academic Publishers.

Saint Blanquat, M., Law, R.D., Bouchez, J.L., and Morgan, S.S., (2001) Internal structure and emplacement of the Papoose Flat pluton: an integrated structural, pertographic and magnetic susceptibility study. Geological Society of America Bulletin 113, 976-995; GSA Data Repository item 2001078, 18 p.

Sibson, R. H., (1985) A note on fault reactivation. Journal of Structural Geology, v. 7, n. 6, p. 751-754.

Simpson, C., and Wintsch, R.P., (1989) Evidence for deformation-induced K-feldspar replacement by myrmekite. Journal Metamorphic Petrology, v. 7, p. 261-275.

Sorensen, S.S., Dunne, G.C., Hanson, R.B., Barton, M.D., Becker, J., Tobisch, O.T., and Fiske, R.S. (1998) From Jurassic shores to Cretaceous Plutons: geochemical evidence for paleoalteration environments of metavolcanic rock eastern California. Geological Society of America Bulletin, v. 110, p. 326-343

Stern, T.W., Bateman, P.C., Morgan, B.A., Newell, M.F., and Peck, D.L., (1981), Isotopic U-Pb ages of zircon from granitiods of the Central Sierra Nevada California. U.S. Geological Survey Professional Paper 1185, 17p.

Stevens, C.H., and Greene, D.C. (1999) Stratigraphy, depositional history, and tectonic evolution of Paleozoic and Mesozoic margin rocks in roof pendants of the eastern Sierra Nevada, California. Geological Society of America Bulletin, v. 11, p. 919-933

Stevens, C.H., and Olson, R.C., (1972) Nature and significance of the Inyo thrust fault, eastern California. Geological Society of America Bulletin, v. 83, p. 3761-3768.

Stevens, C.H., Stone, P., Dunne, G.C., Greene, D.C., Walker, J.D., and Swanson, B.J., (1997) Paleozoic and Mesozoic evolution of east-central California. International Geology Review, v. 39, p. 788-829

Stewart, J., Ross, P., Nelson, C.A., and Burchfiel, D. (1966), Last Chance Thrust, a major fault in the eastern part of Inyo County. U.S. Geological Survey Professional Paper 550-D.

Streckeisen, A., 1976, To each plutonic rock its proper name. Earth Science Reviews, v. 12, p. 1-33.

Stockli, D. F., Dumitru, T. A., McWilliams, M. O., and Farley, K. A., (2003) Cenozoic tectonic evolution of the White Mountains, California and Nevada. Geological Society of America Bulletin, v. 115, n.7, p. 788-816.

Sullivan, W.A., (2003) Geometry, kinematics and age of the northern half of the White Mountain Shear Zone, eastern California and Nevada. [M.S. thesis] Virginia Polytechnic Institute and State University, 52 p.

Sylvester, A. G. and Babcock, J. W., (1975) Significance of multiphase folding in the White-Inyo Range, eastern California (abstracts). Geological Society of America Abstracts with Program, v. 7, p. 1289.

Sylvester, A.G., Miller, C.F., and Nelson, C.A., (1978), Monazites of the White-InyoRange, California and their relation to the calc-alkalic Sierra Nevada batholith, Geological Society of America Bulletin, v. 89, p. 1677-1687.

Tarling, D.H., and Hrouda, F., (1993), The magnetic anisotropy of rocks. Chapman and Hall, pp.217.

Tobisch, O.T., and Cruden, A.R., (1995) Fracture-controlled magma conduits in an obliquely convergent continental magmatic arc. Geology, v. 23, p. 941-944.

United States Geological Survey (1983) Aeromagnetic map. of part of the White and Inyo Mountains, California and Nevada. U. S. Geological Society Open File Report 656.

Uyeda, S., Fuller, M.D., Belshe, J. C., and Girdler, R.W., (1963) Anisotropy of magnetic susceptibility of rocks and minerals, Journal of Geophysical Research, v. 68, 279-291.

Vines, J. A., (1999) Emplacement of the Santa Rita Flat pluton and kinematic analysis of cross cutting shear zones, eastern California. [M.S. thesis] Virginia Polytechnic Institute and State University, 89 p.

Vines, J. A., and Law, R.D. (2000) Emplacement of the Santa Rita Flat pluton as a pluton scale saddle reef. Geology, v. 28, n. 12, p. 1115-1118.

Vines, J. A., and Law, R.D. (2001) Emplacement of the Santa Rita Flat pluton-scale saddle reef: Discussion and Reply. Geology 29, 1157-1158.

Walker, J.D., Martin, M.W., Bartley, J. M., and Coleman, D. S., (1990) Timing and kinematics of deformation in the Cronese Hills, California, and implications for Mesozoic structure of the southwestern Cordillera.Geology, v. 18, p. 554-557.

Wechsler, S.P. (2000), Water resource management and GIS modeling research: Effect of Digital Elevation Models (DEM) uncertainty on topographic parameters, DEM scale and terrain evaluation. Retrieved February 20, 2003 from California State University Long Beach Web site:
http//www.csulb.edu/~wechsler/Dissertation/ch2_/litrev_webdoc